

IMPROVING THE CHARACTERISTICS OF WATER-BASED
DRILLING FLUIDS USING NANOPARTICLES

A Dissertation

by

OMAR SAAD AHMED MAHMOUD

Submitted to the Office of Graduate and Professional Studies of
Texas A&M University
in partial fulfillment of the requirements for the degree of

DOCTOR OF PHILOSOPHY

Chair of Committee,	Hisham A. Nasr-El-Din
Committee Members,	Jerome Schubert
	Berna Hascakir
	Mahmoud El-Halwagi
Head of Department,	A. Daniel Hill

December 2017

Major Subject: Petroleum Engineering

Copyright 2017 Omar Saad Ahmed Mahmoud

ABSTRACT

The capabilities of different types of nanoparticles (NPs) had been exploited to develop a water-based drilling fluid having better characteristics for harsh drilling conditions. More specifically, the objectives of this work are to: 1) investigate the effectiveness of using different oxide NPs: ferric oxide (of sizes <50 nm), magnetic iron oxide (of average particle size 50 –100 nm), silica NPs (size =12 nm), and zinc oxide NPs (of sizes <100 nm) on the rheological properties and filter cake characteristics of Ca-bentonite-based drilling fluid at downhole conditions, 2) conduct a sensitivity analysis of the rheological properties of these drilling fluids and investigate the effect of charge potential, 3) determine the optimum concentration of NPs, and 4) evaluate the effect of different drilling fluid additives on the performance of NPs/Ca-bentonite fluids by formulating and testing a complete bentonite-based drilling fluid formula.

A reduction of 43% in the fluid loss volume was achieved when using 0.5 wt% of ferric oxide NPs with 7 wt% Ca-bentonite suspension compared to that without NPs. However, using silica or zinc oxide NPs at different concentrations resulted in an increase in the fluid loss volume and filter cake thickness. The inductively coupled plasma (ICP) analysis of the filtrate fluids and the scanning electron microscopy-energy dispersive spectroscopy (SEM-EDS) of the filter cakes revealed the replacement of the cations dissociated from the Ca-bentonite by ferric oxide NPs at the investigated conditions, which promoted the formation of rigid clay platelet structure. Furthermore, using 0.5 wt% of NPs provided less agglomeration, as shown by the SEM images, and less filter cake

permeability. Moreover, the produced filter cake consisted of two layers, as indicated by the computed-tomography (CT) scan. Increasing the concentration of NPs resulted in an increase in the fluid loss and filter cake thickness. At high NP concentration (2.5 wt%), a new layer of the agglomerated NPs generated in the filter cake close to the surface of formation, which adversely affected the cake characteristics. The ferric oxide and magnetic iron oxide NPs/Ca-bentonite fluids were found to have stable rheological properties at different NP concentrations and temperatures (up to 200°F). Additionally, thermally aging these fluids at 350°F for 16 hours showed minor changes in their rheological properties, which confirmed their applicability in drilling downhole environments.

The ferric oxide NPs improved the filter cake and filtration properties of Ca-bentonite-based drilling fluids in the presence of polymer and other additives under both static and dynamic filtration (at 100 rpm). The best filter cake characteristics were obtained when using a NP concentration of 0.3-0.5 wt%. Furthermore, the formulated NPs/Ca-bentonite-based drilling fluids could withstand downhole conditions up to 500 psi and 350°F and produced a filter cake that has 0.151-in. thickness, 6.9 ml filtrate loss volume, and 0.428 μ d permeability at this conditions. Moreover, it was noticed that the ultrasonication for at least one hour and bentonite hydration for 16 hours are recommended for better preparation of the formulated ferric oxide NPs/Ca-bentonite-based drilling fluid.

DEDICATION

TO THE SOUL OF MY FATHER, MY MOTHER, MY WIFE, AND MY KIDS

(SAAD, AHMED, AND MAHMOUD)

ACKNOWLEDGEMENTS

I would like to thank my committee chair, Dr. Hisham A. Nasr-El-Din, for his continuous encouragement, guidance and support throughout my time at Texas A&M University. I would like to extend my appreciation to Dr. Jerome J. Schubert, Dr. Berna Hascakir, and Dr. Mahmoud M. El-Halwagi for serving as committee members. Thanks also go to my friends and colleagues in our research group and the department faculty and staff for making my time at Texas A&M University a great experience. Ms. Gia Alexander is acknowledged for editorial assistance and proofreading parts of this work. I also want to extend my gratitude to the Qatar National Research Fund, QNRF (a member of the Qatar Foundation) for funding this research. Dr. Vassilios C. Kelessidis and Mr. Zisis Vryzas of the Department of Petroleum Engineering, Texas A&M University at Qatar, are acknowledged for their encouragement and support throughout the time of this research work.

Finally, I wish to express my love and gratitude to my beloved family; my parents (the soul of my father, and my mother), my wife, and my kids; for their encouragement, patient, understanding, and endless love.

CONTRIBUTORS AND FUNDING SOURCES

Contributors

This work was supervised by a dissertation committee consisting of Professor Hisham A. Nasr-El-Din, Associate Professor Jerome J. Schubert, Assistant Professor Berna Hascakir of the Department of Petroleum Engineering and Professor Mahmoud El-Halwagi of the Department of Chemical Engineering.

All of the work conducted for the dissertation was completed by the student, under the advisement of Professor Hisham A. Nasr-El-Din of the Department of Petroleum Engineering.

Funding Sources

This work was made possible in part by Qatar National Research Fund, QNRF (a member of the Qatar Foundation) under the NPRP Grant Number 6-127-2-050.

NOMENCLATURE

A	= Cross-sectional area of the filter core disk, in. ²
ASCH	= Aluminosilicate clay hybrid
API	= American Petroleum Institute
CMC	= Carboxymethyl cellulose
CNC	= Cellulose nano-crystals
CT	= Computed tomography
CTN	= Computed tomography number
f_{sc}	= Volume fraction of the solids in the filter cake
f_{sm}	= Volume fraction of solids in the drilling fluid
HP/HT	= High-pressure/high-temperature
ICP-OES	= Inductively coupled plasma-optical emission spectrometry
ICH	= Iron oxide clay hybrid
GO	= Graphene oxide
K	= Consistency index, lbf. s ⁿ /100 ft ²
k_c	= Permeability of the filter cake, d
k_m	= Permeability of the filter medium, d
LCM	= Lost circulation material
LP/LT	= Low-pressure/low-temperature
L_c	= Thickness of the filter cake, in.
L_m	= Thickness of the filter medium, in.

MFC	= Microfibrillated cellulose
MWCNTs	= Multi-walled carbon nano-tubes
n	= Flow behavior index (dimensionless)
NWBM	= Nano-fluid/water-based drilling muds
NP	= Nanoparticle
PAC	= Polyanionic cellulose
PALS	= Phase analysis light scattering
Pal	= Palygorskite
PAM	= Polyacrylamide
q	= Filtrate fluid rate, ml/ in. ² .s
ROP	= Rate of penetration
R^2	= Regression coefficient (dimensionless)
SDFL	= Nano-silica composite with core-shell structure
SEM-EDS	= Scanning electron microscopy-energy dispersive spectrometry
t	= Time of filtration, s
V_f	= Cumulative filtrate volume, ft ³
XG	= Xanthan gum
XRD	= X-ray diffraction
XRF	= X-ray fluorescence
ZnO-Am	= Zinc oxide NP-acrylamide composite
Δp_c	= Pressure drop across the filter cake, psi
Δp_m	= Pressure drop across the filter medium, psi

Δp_t	= Total pressure drop, psi
μ	= Viscosity of the filtrate, cp
μ_p	= Plastic viscosity, cp
$\sum Q^2$	= Sum of square errors, (lbf/100 ft ²) ²
τ	= Shear stress, lbf/100 ft ²
τ_o	= Yield stress, lbf/100 ft ²
$\dot{\gamma}$	= Shear rate, s ⁻¹
ζ	= Zeta potential, mV

TABLE OF CONTENTS

	Page
ABSTRACT	ii
DEDICATION	iv
ACKNOWLEDGEMENTS	v
CONTRIBUTORS AND FUNDING SOURCES.....	vi
NOMENCLATURE.....	vii
TABLE OF CONTENTS	x
LIST OF FIGURES.....	xiii
LIST OF TABLES	xix
CHAPTER I INTRODUCTION AND LITERATURE REVIEW”	1
Introduction.....	1
Drilling Fluid.....	3
Applications of Nanoparticles in the Drilling Fluid Technology.....	8
Rheological Property and Fluid Loss Controller.....	10
Wellbore Strengthening and Shale Stability agents	25
Research Objectives	29
CHAPTER II EXPERIMENTAL SETUP AND MATERIALS.....	31
Introduction.....	31
Materials.....	31
Bentonite	31
Nanoparticles.....	34
Drilling Fluid Additives	36
Core Outcrops and Deionized Water.....	36
Zeta Potential Measurements	37
Rheological Measurements	40
NPs/Ca-Bentonite Suspensions	40
Fully Formulated Drilling Fluid	42
Filtration Loss Measurements	43

NPs/Ca-Bentonite Suspension.....	43
Fully Formulated Drilling Fluid.....	46
CHAPTER III USING NANOPARTICLES TO DEVELOP MODIFIED CA-BENTONITE FLUIDS	48
Introduction.....	48
Zeta Potential Analysis.....	50
Bentonite.....	50
Nanoparticles.....	51
Rheological Analysis.....	53
Ca-Bentonite Base Fluid.....	54
NPs/Ca-Bentonite Fluids.....	56
Effect of Aging.....	61
Filtration Loss Analysis.....	62
Filter Press Results.....	62
CT Scan Analysis of the Filter Cake.....	66
SEM-EDS Analysis of the Filter Cake.....	70
Filter Cake Permeability.....	72
Elemental Analysis of Filtrate Fluid.....	76
Effect of Filtration Temperature and Pressure.....	77
Formation Damage Analysis.....	78
Conclusions.....	85
CHAPTER IV CHARACTERIZATION OF THE FILTER CAKE GENERATED BY NANOPARTICLE/CA-BENTONITE-BASED DRILLING FLUID	87
Introduction.....	87
Properties of the Drilling Fluid.....	88
Filter Press Measurements and Analysis.....	90
Effect of Nanoparticle Concentration.....	92
Effect of Filtration Temperature and Pressure.....	98
Effect of Dynamic Filtration.....	101
Effect of Drilling Fluid Preparation Method.....	104
Conclusions.....	109
CHAPTER V CONCLUSIONS AND RECOMMENDATIONS	111
REFERENCES	116
APPENDIX A DEHYDRATION OF CA-BENTONITE SUSPENSIONS	132
APPENDIX B DETAILED RHEOLOGICAL MEASUREMENT RESULTS	137

APPENDIX C DETAILED FLUID LOSS RESULTS OF NPS/CA-BENTONITE
SUSPENSIONS 149

APPENDIX D DETAILED FLUID LOSS RESULTS OF FULLY FORMULATED
DRILLING FLUID 154

LIST OF FIGURES

	Page
Fig. I- 1—Structure of montmorillonite (Grim 1968).....	5
Fig. I- 2—Filtrate fluid invasion through the deposited filter cake and porous formation during drilling (Civan 1994).	7
Fig. I- 3—Formation of the filter cake while filtrate fluid invasion (Civan 1994).	7
Fig. I- 4—Scale of particle-size (Cai et al. 2012).	9
Fig. I- 5—Surface-area-to-volume ratio of nanoparticles (El-Diasty and Aly 2015)	9
Fig. I- 6—SEM images of Pal: (a) regular Pal (needle like clusters), and (b) uniformly dispersed Pal NPs (Abdo and Haneef 2013).....	16
Fig. I- 7—Images of the generated filter cakes (Contreras et al. 2014).	18
Fig. I- 8—SEM images of the filter cakes after LP/LT filter press experiments for different samples with the corresponding illustrations of bentonite clay platelet interaction (Barry et al. 2015).	20
Fig. I- 9—SEM images of: (a) pure polyacrylamide (PAM), and (b) TiO ₂ /polyacrylamide (TiO ₂ /PAM) nano-composite (Sadeghalvaad and Sabbaghi 2015).	21
Fig. I- 10—SEM images of: (a) NPs plugging different pore throats, (b) aggregated particles plugging a pore throat (Sensoy et al. 2009).....	25
Fig. II- 1— Spectrum XRD of bentonite.....	33
Fig. II- 2—Particle-size distribution of bentonite.	33
Fig. II- 3—Scanning electron microscopy image of bentonite (X500-50 μm).....	34
Fig. II- 4— Scanning electron microscopy image of ferric oxide NPs (X200-200 μm).	35
Fig. II- 5—Brookhaven Zeta Potential Analyzer (ZetaPALS).	38
Fig. II- 6—OFITE Multi Mixer (11,000 RPM).	39

Fig. II- 7—Model 150 VT Ultrasonic Homogenizer.	39
Fig. II- 8—Grace M3600 Viscometer.	40
Fig. II- 9—Aging Cell and Teflon Liner.	42
Fig. II- 10—OFITE Dynamic HP/HT Filter Press.	46
Fig. III- 1— Rheograms of the base fluid (7 wt% bentonite) at different temperatures.	55
Fig. III- 2— Rheograms of the fluid containing 0.5 wt% of ferric oxide NPs at different temperatures.	57
Fig. III- 3— Rheograms of the fluid containing different concentrations of ferric oxide NPs at 140°F.	58
Fig. III- 4— Rheograms of the fluid containing 0.5 wt% of silica NPs at different temperatures.	59
Fig. III- 5— Rheograms of fluid containing different concentrations of silica NPs at 140°F.	60
Fig. III- 6—The change of apparent viscosity with shear rate for the fluids having: (a) different ferric oxide NP concentrations at 140°F, (b) a silica NP concentration of 0.5 wt% at different temperatures.	61
Fig. III- 7—Cumulative filtrate volume (30 minutes) and filter cake thickness for the cakes having different NP concentrations formed under static filtrations at 250°F and 300 psi differential pressure.	66
Fig. III- 8—CT scan images of the filter cakes having ferric oxide NPs under static conditions at 250°F and 300 psi differential pressure, (a) with 0.5 wt%, and (b) with 2.5 wt% of NPs.	67
Fig. III- 9—CTNs through the filter cake of the samples that have different nanoparticle concentrations under static conditions at a differential pressure of 300 psi and a temperature of 250°F: (a) 0.0 wt%, (b) 0.5 wt% ferric oxide, (c) 1.5 wt% ferric oxide, (d) 2.5 wt% ferric oxide, (e) 0.5 wt% silica, and (f) 1.5 wt% silica nanoparticles.	68
Fig. III- 10—3D CT scan cross-section of the filter cake having 2.5 wt% of ferric oxide NPs.	69
Fig. III- 11— CT scan images through the filter cake in the direction of fluid flow for the sample that has 2.5 wt% magnetic iron oxide Fe ₃ O ₄	

nanoparticles under static conditions at 250°F and a differential pressure of 300 psi.	71
Fig. III- 12— CTN profile through the filter cake in the direction of fluid flow for the sample that has 2.5 wt% magnetic iron oxide Fe ₃ O ₄ nanoparticles under static conditions at 250°F and a differential pressure of 300 psi.	72
Fig. III- 13—SEM images (X1000-30 μm) of the dried filter cake surface for samples having different concentrations ferric oxide NPs: (a) 0.0 wt%, (b) 0.5 wt%, (c) 1.5 wt%, and (d) 2.5 wt% of NPs. The images show that adding 0.5 wt% to the base fluid results in less agglomeration (shown as red circles) and less porous surface compared to the filter cakes containing higher NP concentration or that for the base fluid.	73
Fig. III- 14—EDS elemental analysis of the surface of the bottom layer of the filter cakes as a function of nanoparticle concentration.	74
Fig. III- 15—SEM images: (a) for the surface of the third layer (agglomerated ferric oxide NP layer) formed in the filter cake containing 2.5 wt% of ferric oxide NPs (X500-50 μm), and (b) for the surface of the filter cake containing 0.5 wt% of silica NPs (X1000-30 μm). Both images show highly porous/permeable microstructure. Image (b) shows different clay-platelet structure compared to the filter cakes containing ferric oxide NPs (SEM images in Fig. III-13).	74
Fig. III- 16—Cumulative filtrate volume (for 30 min.) as a function of square root of time for the fluids containing different concentrations of ferric oxide NPs at 250°F and 300 psi differential pressure.	75
Fig. III- 17—Viscosity of the filtrate fluid against temperature for the base fluid.	76
Fig. III- 18— ICP-OES analysis of the filtrate fluids for the samples having different ferric oxide NP concentrations at 300 psi and 250°F.	77
Fig. III- 19—CT scan image of the filter cake and core disk in the direction of fluid flow.	79
Fig. III- 20—CTN profile through the core disk (in the direction of fluid flow) used for running the experiment of the sample having 0.5 wt% of zinc oxide NPs.	81

Fig. III- 21—Porosity profile through the core disk (in the direction of fluid flow) used for running the experiment of the sample having 0.5 wt% of zinc oxide NPs.....	81
Fig. III- 22—CTN profile through the core disk (in the direction of fluid flow) used for running the experiment of the sample having 1.5 wt% of magnetic iron oxide Fe ₃ O ₄ NPs.	82
Fig. III- 23—Porosity profile through the core disk (in the direction of fluid flow) used for running the experiment of the sample having 1.5 wt% of magnetic iron oxide Fe ₃ O ₄ NPs.	83
Fig. III- 24—CTN profile through the core disk (in the direction of fluid flow) used for running the experiment of the sample having 2.5 wt% of magnetic iron oxide Fe ₃ O ₄ NPs.	84
Fig. III- 25—CTN profile through the core disk (in the direction of fluid flow) used for running the experiment of the sample having 2.5 wt% of magnetic iron oxide Fe ₃ O ₄ NPs.	84
Fig. IV- 1— Particle-size distribution of solids in the drilling fluid.....	89
Fig. IV- 2— Cumulative filtrate volume (30 minutes) and filter cake thickness for the filter cakes having different concentrations of ferric oxide NPs formed under static filtration at 250°F and 300 psi differential pressure.	92
Fig. IV- 3— CT scan images of the filter cakes having different concentrations of ferric oxide NPs formed under static filtration at 250°F and 300 psi differential pressure: (a) with 0.0 wt%, (b) with 0.3 wt%, (c) with 0.5 wt%, and (b) with 1.0 wt% of NPs.	94
Fig. IV- 4— Average CTNs throughout the filter cakes having different concentrations of ferric oxide NPs generated under static filtration at 250°F and 300 psi differential pressure.	94
Fig. IV- 5—SEM images (X100-300 μm) of the top surface of the dried filter cakes having different concentrations of ferric oxide NPs formed under static filtration at 250°F and 300 psi differential pressure: (a) with 0.0 wt%, and (b) with 0.5 wt% of NPs. The images show that adding 0.5 wt% of NPs to the drilling fluid results in less porous structure.	95
Fig. IV- 6— EDS spectrum analysis of the top surface of the dried filter cake having 0.5 wt% ferric oxide NPs formed under static filtration at 250°F and 300 psi differential pressure.	96

Fig. IV- 7— SEM images of the bottom surface of the dried filter cakes having different ferric oxide NP concentrations formed under static condition at 300 psi differential pressure and 250°F: (a) with 0.0 wt% (X100-300), and (b) with 0.5 wt% of NPs (X150-500 μm). The images show that adding 0.5 wt% of NPs to the drilling fluid results in less porous surface.....	97
Fig. IV- 8—EDS spectrum analysis of the bottom surface of the dried filter cake having 0.5 wt% ferric oxide NP concentration formed under static condition at 300 psi differential pressure and 250°F. Traces of iron appears in this surface.....	97
Fig. IV- 9—Cumulative filtrate volume as a function of time for drilling fluids containing different concentrations of ferric oxide NPs at 250°F and 300 psi differential pressure.....	98
Fig. IV- 10—Cumulative filtrate volume as a function of time for drilling fluids containing 0.5 wt% of ferric oxide NPs at: (a) 300 psi and different temperatures, and (b) 250°F and different pressures.	101
Fig. IV- 11— Cumulative filtrate volume as a function of time for drilling fluids containing different concentrations of ferric oxide NPs under both static and dynamic conditions at 250°F and 500 psi differential pressure: (a) with 0.0 wt%, and (b) with 0.5 wt% of NPs.	103
Fig. IV- 12—SEM images (X100-300 μm) of the bottom surface of the dried filter cakes having different concentrations of ferric oxide NPs formed under dynamic filtration (100 rpm) at 250°F and 500 psi differential pressure: (a) with 0.0 wt%, and (b) with 0.5 wt% of NPs. The cake has 0.5 wt% of NPs shows less porous structure.	104
Fig. IV- 13—EDS spectrum analysis of the bottom surface of the dried filter cake having 0.5 wt% ferric oxide NP concentration formed under dynamic filtration (100 rpm) at 250°F and 300 psi differential pressure.	105
Fig. IV- 14— Cumulative filtrate volume as a function of time for the drilling fluids containing 0.5 wt% ferric oxide NP concentration under static filtration at 250°F and 300 psi differential pressure prepared using different times of ultrasonication (0, 0.5 and 1 hour).	106
Fig. IV- 15— Cumulative filtrate volume as a function of time for the drilling fluid containing 0.0 and 0.5 wt% ferric oxide NP concentrations under static filtration at 500 psi differential pressure and 250°F prepared using bentonite hydration for 16 hours.....	108

Fig. IV- 16— SEM images of the top surface of the dried filter cakes having 0.5 wt% of ferric oxide NPs formed under static conditions at 250°F and 500 psi differential pressure: (a) with no hydration (X100-300), and (b) with 16 hours of hydration (X150-500 μm).....	109
Fig. A- 1—Base Fluid in a water bath at 212°F (100°C) at time zero.....	133
Fig. A- 2—Base Fluid in a water bath at 212°F (100°C) after 30 minutes.....	133
Fig. A- 3—Base Fluid in a water bath at 212°F (100°C) after 60 minutes.....	134
Fig. A- 4—Base Fluid in a water bath at 212°F (100°C) after 90 minutes.....	134
Fig. A- 5—Base Fluid in a water bath at 212°F (100°C) after 120 minutes.....	135
Fig. A- 6—Base Fluid in a water bath at 212°F (100°C) after 150 minutes.....	135
Fig. A- 7—Base Fluid left for 16 hours after thermal aging in a water bath at 212°F (100°C) for 150 minutes.	136
Fig. A- 8—Base Fluid left for 24 hours at ambient pressure and temperature (no water bath).....	136

LIST OF TABLES

	Page
Table I- 1—Functions of the drilling fluid and the corresponding properties.	3
Table II- 1—XRF analysis of bentonite.	33
Table II- 2—Weights of bentonite and NPs used to prepare the suspensions.	41
Table II- 3—Laboratory formula to prepare 1 barrel equivalent of the bentonite based drilling fluid.	44
Table II- 4—Laboratory formula to prepare 1 barrel equivalent of the drilling fluid having 0.5 wt% of NPs.	45
Table III- 1—Zeta potential of 7 wt% Ca- bentonite suspension at 78°F.	50
Table III- 2—Zeta potential of ferric oxide NPs measured at different concentrations and two different temperatures (78°F and 100°F).	51
Table III- 3—Zeta potential of Silica NPs measured at different concentrations and two different temperatures (78°F and 100°F).	52
Table III- 4— Zeta potential of magnetic iron oxide (Fe ₃ O ₄) NPs at different concentrations.	53
Table III- 5— Zeta potential of zinc oxide (ZnO) NPs at different concentrations.	53
Table III- 6— Bingham Plastic and Herschel-Bulkley model constants of the base fluid (7 wt% Ca-bentonite) at different temperatures (pH = 8.36 at 78°F).	55
Table III- 7— Bingham Plastic and Herschel-Bulkley model constants fitted for the fluid containing 0.5 wt% of ferric oxide NPs at different temperatures (pH = 8.15 at 78°F).	58
Table III- 8 — Bingham Plastic and Herschel-Bulkley model constants fitted for the fluid containing 0.5 wt% of silica NPs at different temperatures (pH = 7.7 at 78°F).	60
Table III- 9— Bingham Plastic and Herschel-Bulkley model constants for the fluids containing 0.5 wt% of ferric oxide NPs at different temperatures measured after aging for 16 hours at 350°F (pH = 8.15 at 78°F).	64

Table III- 10— Bingham Plastic and Herschel-Bulkley model constants for fluid containing 0.5 wt% of silica NPs at different temperatures measured after aging for 16 hours at 350°F (pH = 7.7 at 78°F).	64
Table III- 11—Cumulative filtrate volume (for 30 min.) and filter cake properties of the fluids that having different NP types and concentrations at 250°F and 300 psi.....	65
Table III- 12— Cumulative filtrate volume (for 30 min.) and filter cake properties of the fluids having 0.5 wt% of ferric oxide NPs at different filtration conditions of pressure and temperature.	78
Table IV- 1— Properties of the Ca-bentonite-based drilling fluid and the drilling fluid containing 0.5 wt% of ferric oxide NPs.	89
Table IV- 2— The performed filter press experiments and the investigated parameter.	91
Table IV- 3—Filter cake permeability calculations for different NP concentrations at 250°F and 300 psi.....	99
Table IV- 4— Filter cake characteristics of the drilling fluid containing 0.5 wt% of ferric oxide NPs at different conditions of pressure and temperature.....	100
Table IV- 5— Filter cake characteristics of the drilling fluids that have 0.0 and 0.5 wt% of ferric oxide NPs at 500 psi and 250°F (effect of dynamic filtration).	102
Table IV- 6— Filter cake characteristics of the drilling fluid having 0.5 wt% of ferric oxide NPs at 300 psi and 250°F and different ultrasonication times.....	106
Table IV- 7— Filter cake characteristics of the drilling fluids that have 0.0 and 0.5 wt% of ferric oxide NPs at 500 psi and 250°F (effect of bentonite hydration).....	108
Table B- 1— Bingham Plastic and Herschel-Bulkley model constants of the base fluid at different temperatures.	138
Table B- 2—Apparent viscosity of the base fluid at different temperatures and shear rates.	138
Table B- 3—Rheograms of the base fluid at different temperatures.	138

Table B- 4— Bingham Plastic and Herschel-Bulkley model constants fitted for the fluid containing 0.5 wt% of ferric oxide NPs at different temperatures.....	139
Table B- 5—Apparent viscosity of the fluid containing 0.5 wt% of ferric oxide NPs at different temperatures and shear rates.....	139
Table B- 6—Rheograms of the fluid containing 0.5 wt% of ferric oxide NPs at different temperatures and shear rates.	139
Table B- 7— Bingham Plastic and Herschel-Bulkley model constants fitted for the fluid containing 0.5 wt% of ferric oxide NPs at 120°F and different NP concentrations.	140
Table B- 8— Bingham Plastic and Herschel-Bulkley model constants fitted for the fluid containing 0.5 wt% of ferric oxide NPs at 140°F and different NP concentrations.	140
Table B- 9— Bingham Plastic and Herschel-Bulkley model constants fitted for the fluid containing 0.5 wt% of silica NPs at different temperatures.	141
Table B- 10—Apparent viscosity of the fluid containing 0.5 wt% of silica NPs at different temperatures and shear rates.	141
Table B- 11—Rheograms of the fluid containing 0.5 wt% of silica NPs at different temperatures and shear rates.	141
Table B- 12— Bingham Plastic and Herschel-Bulkley model constants fitted for the fluid containing 1.5 wt% of silica NPs at different temperatures.	142
Table B- 13—Apparent viscosity of the fluid containing 1.5 wt% of silica NPs at different temperatures and shear rates.	142
Table B- 14—Rheograms of the fluid containing 1.5 wt% of silica NPs at different temperatures and shear rates.	142
Table B- 15— Bingham Plastic and Herschel-Bulkley model constants fitted for the fluid containing 2.5 wt% of silica NPs at different temperatures.	143
Table B- 16—Apparent viscosity of the fluid containing 2.5 wt% of silica NPs at different temperatures and shear rates.	143
Table B- 17—Rheograms of the fluid containing 2.5 wt% of silica NPs at different temperatures and shear rates.	143

Table B- 18— Bingham Plastic and Herschel-Bulkley model constants fitted for the fluid containing 0.5 wt% of ferric oxide NPs + 0.5 wt% of silica NPs at different temperatures.	144
Table B- 19—Apparent viscosity of the fluid containing 0.5 wt% of ferric oxide NPs + 0.5 wt% of silica NPs at different temperatures and shear rates.....	144
Table B- 20—Rheograms of the fluid containing 0.5 wt% of ferric oxide NPs + 0.5 wt% of silica NPs at different temperatures and shear rates.	144
Table B- 21— Bingham Plastic and Herschel-Bulkley model constants fitted for the fluid containing 0.5 wt% of ferric oxide NPs (using 15 min. ultrasonication) at different temperatures.	145
Table B- 22—Apparent viscosity of the fluid containing 0.5 wt% of ferric oxide NPs (using 15 min. ultrasonication) at different temperatures and shear rates.....	145
Table B- 23—Rheograms of the fluid containing 0.5 wt% of ferric oxide NPs (using 15 min. ultrasonication) at different temperatures and shear rates.	145
Table B- 24— Bingham Plastic and Herschel-Bulkley model constants for the base fluid at different temperatures measured after aging for 16 hours at 350°F.....	146
Table B- 25—Apparent viscosity of the base fluid at different temperatures and shear rates measured after aging for 16 hours at 350°F.....	146
Table B- 26—Rheograms of the base fluid at different temperatures and shear rates measured after aging for 16 hours at 350°F.	146
Table B- 27— Bingham Plastic and Herschel-Bulkley model constants for the fluid containing 0.5 wt% of ferric oxide NPs at different temperatures measured after aging for 16 hours at 350°F.....	147
Table B- 28—Apparent viscosity of the fluid containing 0.5 wt% of ferric oxide NPs at different temperatures and shear rates measured after aging for 16 hours at 350°F.....	147
Table B- 29—Rheograms of the fluid containing 0.5 wt% of ferric oxide NPs at different temperatures and shear rates measured after aging for 16 hours at 350°F.....	147

Table B- 30— Bingham Plastic and Herschel-Bulkley model constants for fluid containing 0.5 wt% of Silica NPs at different temperatures measured after aging for 16 hours at 350°F.....	148
Table B- 31—Apparent viscosity of the fluid containing 0.5 wt% of ferric oxide NPs at different temperatures and shear rates measured after aging for 16 hours at 350°F.....	148
Table B- 32—Rheograms (shear stress versus shear rate) of the fluid containing 0.5 wt% of ferric oxide NPs at different temperatures and shear rates measured after aging for 16 hours at 350°F.....	148
Table C- 1—Detailed fluid loss volumes for the base fluid and samples containing different concentrations of ferric oxide NPs at 250°F and 300 psi.....	150
Table C- 2— Detailed fluid loss volumes for the samples containing 0.5 wt% of ferric oxide NPs at a different pressures and temperatures.....	151
Table C- 3— Detailed fluid loss volumes for the samples containing silica, magnetic iron oxide, and zinc oxide NPs at 250°F and 300 psi.....	152
Table C- 4— Detailed fluid loss volumes for the base fluid and samples containing 0.5 wt% of ferric oxide and silica NPs at 250°F and 300 psi when using dynamic filtration (100 rpm) or ultrasonication for 15 minutes while preparation.....	153
Table D- 1—Detailed fluid loss volumes for the Ca-bentonite-based drilling fluid and fluids containing different concentrations of ferric oxide NPs at 250°F and 300 psi (No hydration, 1 hour of ultrasonication, and static filtration).....	155
Table D- 2— Detailed fluid loss volumes for the Ca-bentonite-based drilling fluid containing 0.5 wt% of ferric oxide NPs at different pressures and temperatures (No hydration, 1 hour of ultrasonication, and static filtration).....	156
Table D- 3— Detailed fluid loss volumes for the Ca-bentonite-based drilling fluid containing no NPs and 0.5 wt % of ferric oxide NPs at 250°F and 300 psi using different ultrasonication times while preparation (No hydration and static filtration).	157
Table D- 4— Detailed fluid loss volumes for the Ca-bentonite-based drilling fluid and fluids containing 0.5 wt% of ferric oxide at 250°F and 500 psi	

when using 16 hours of hydration while preparation or dynamic
filtration (100 rpm).158

CHAPTER I

INTRODUCTION AND LITERATURE REVIEW^{1,2}

Introduction

Drilling deeper, longer, and more complex oil and gas wells becomes possible by improvements in field technologies, especially by formulating and using more efficient drilling fluids. However, these fluids must be engineered so that they can minimize formation damage. The invasion of drilling fluid filtrate into formation is considered as one of the common sources of damage (Amaefule et al. 1988). The formation of a low permeability and thin filter cake (a high efficiency filter cake) on the face of the porous medium and proper filtrate fluid loss volumes can reduce the excessive formation damage problems. Additionally, optimizing the rheological properties is important for formulating stable and effective drilling fluids.

Generally, one can classify drilling fluids into three main types: water-based, synthetic-based, and oil-based drilling fluids. Synthetic-based and Oil-based drilling fluids have many disadvantages such as the higher cost, the environmental and disposal problems, and the safety and health issues (Growcock et al. 1998; Foxenberg et al. 2008). Because of the drawbacks of oil-based and synthetic-based types, a trend of selecting

¹ Reprinted with a permission from “Nanoparticle-Based Drilling Fluids for Minimizing Formation Damage in HTHP Applications” by Mahmoud, O., Nasr-El-Din, H. A., Vryzas, Z., and Kelessidis, V. C. SPE-171849-MS, Copyright 2016 by Society of Petroleum Engineers.

² Reprinted with a permission from “Characterization of Filter Cake Generated by Nanoparticle-Based Drilling Fluid for HP/HT Applications” by Mahmoud, O., Nasr-El-Din, H. A., Vryzas, Z., and Kelessidis, V. C. SPE-184572-MS, Copyright 2017 by Society of Petroleum Engineers.

water-based drilling fluids was followed. However, the need to address the drawbacks of water-based fluids, especially while drilling harsh conditions, is a top priority. Bentonite-based fluid is one of the most commonly used water-based drilling fluids. Bentonite is a montmorillonite clay that can provide good rheological properties, pumpability, and cutting carrying capacity while drilling (Bourgoyne et al. 1991). However, the temperature limit above which bentonite starts to chemically breakdown is 250°F (Kelessidis et al. 2006). The breakdown of bentonite increases the fluid loss into the formation and reduces the drilling fluid capability for carrying cuttings.

Nanoparticles (NPs), as additives, have been thoroughly investigated to address the challenges of bentonite-based drilling fluids. A NP is any particle having one or more dimensions in the range of 1 to 100 nanometer (nm). The small size of particles yields a high surface-area-to-volume ratio, which leads to many changes in the interparticle spacing and gives superior functions (Lu et al. 2007; Behari 2010). Different types of NPs have been tested for enhancing and controlling the rheological properties of drilling fluids (Agarwal et al. 2011; Amanullah et al. 2011; Abdo and Haneef 2013; Ismail et al. 2014) and for fluid loss mitigation (Javeri et al. 2011; Cai et al. 2012; Zakaria et al. 2012; Contreras et al. 2014).

In this chapter, a detailed literature survey and a brief introduction to the research problem have been presented. Additionally, the applications of NPs in the drilling fluid technology will be surveyed in order to examine the benefits behind using such particles. At the end of the chapter, the objectives of this research work have been defined and stated.

Drilling Fluid

The drilling fluid (mud) is a mixture of liquids, chemicals, and solids that are pumped into the wellbore to facilitate the drilling process. A variety of downhole conditions result in the choice of different types of drilling fluid. When choosing a particular mud, factors such as the depth, type of formation, and local structure should be considered. Drilling fluid must have different functions. **Table I-1** shows the functions of drilling muds and their corresponding properties (Bourgoyne et al. 1991).

Function of the Drilling Fluid	Corresponding Property
Controlling subsurface pressures and prevent caving.	Drilling fluid density
Carrying cuttings out of the hole.	Drilling fluid viscosity
Suspending cuttings while stopping circulation.	Drilling fluid gel strength
Cooling and lubricating the drill/string and bit.	Additive content
Forming a thin, impermeable filter cake on the face of the borehole.	Filtrate fluid loss control
Easily releasing the drilling cuttings when reaching the surface facilities.	Viscosity/gel strength
Helping in supporting the weight of the drill/string and casing.	Drilling fluid density
Ensuring getting maximum information out of the drilled formation.	
Not damaging the mud circulation system.	

Table I- 1—Functions of the drilling fluid and the corresponding properties.

Many additives have been introduced to help in the drilling process. The drilling fluid properties affect the drilled formation, wire line logs, and drill return logs. The drilling fluid must allow the obtaining of all information necessary for evaluating and estimating the productive capabilities of the penetrated formations.

Drilling mud is considered as the most important component in the drilling process and the success of a drilling operation is normally related to its efficiency. Various types

of drilling fluids are being classified and used based on their behavior during the drilling operation. Synthetic-based and oil-based drilling fluids have different disadvantages as aforementioned. However, water-based drilling fluids have drawbacks, especially when drilling high pressure/high temperature (HP/HT) wells. In this research work, we are focusing on water-based type, more specifically, the bentonite-based fluids.

Bentonite is a montmorillonite clay that has a film-like shape (**Fig. I-1**). Its basic structure consists of two silica sheets, where Si^{4+} is tetrahedrally coordinated with oxygen, combined with one layer via octahedral coordination. In the latter layer, the central ion might be either Mg^{2+} (a trioctahedral sheet) or Al^{3+} (a dioctahedral sheet). Charge shortages results in the clay particles because of the extensive isomorphous substitution (without fundamental change of the structure) for Si^{4+} and Al^{3+} by other cations (Grim 1968). Montmorillonite carries a negative charge mainly from the replacement of aluminum with magnesium, neutralized by soluble mono- or di-valent cations, which balance charge deficiencies (weak bonding).

Montmorillonite is a dispersible and hydrophilic clay mineral of the smectite group. It is a mineral that has a higher tendency to swell when becoming in contact with water. Furthermore, it has an extraordinary capability to exchange cations, typically sodium (Na^+) and calcium (Ca^{2+}). Based on the exchangeable cation, montmorillonite can be classified as Na- and Ca-montmorillonite. Na-montmorillonite is commonly known as a premium drilling fluid additive. The difference between Na- and Ca-montmorillonite is the relative proportions of the two cations in the interlayer region. In Ca-montmorillonite, the Ca^{2+} predominates; however, the Na^+ cations are dominants in Na-montmorillonite.

Although the cations occupy the same volume in space, the charge density of the Ca^{2+} is twice that of the Na^+ (Marcus 1991; Casillas-Ituarte et al. 2010). The negatively charged montmorillonite lattice sheets are more tightly held together by the Ca^{2+} (Bowyer and Moine-L 2008; Keren 1988). Thus, Ca-montmorillonite, having a better “glue” in between the lattice sheets, does not disperse in water as readily as Na-montmorillonite. This means that hydration (swelling) does not occur to the same extent. However, Ca-montmorillonite is a mineral with a high surface energy, and shows high affinity for water (Chassin et al. 1986). In **Appendix A**, the dehydration process of a suspension of 7 wt% bentonite consisting mainly of Ca-montmorillonite in deionized water at 212°F (100°C) is showed as a function of time.

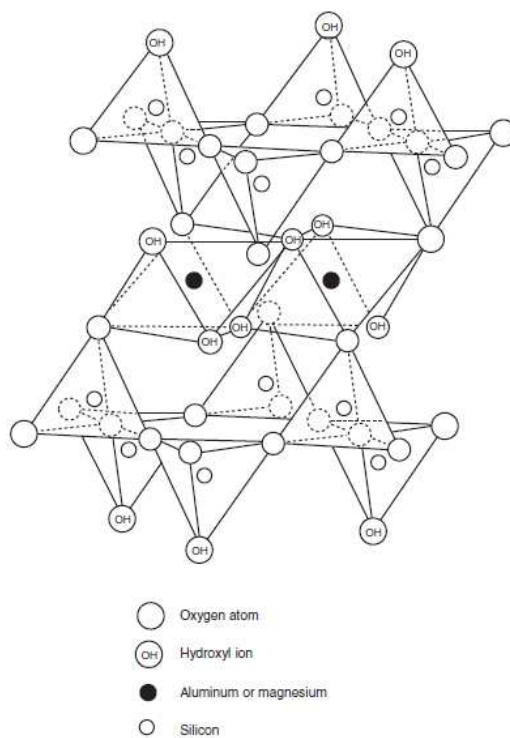


Fig. I- 1—Structure of montmorillonite (Grim 1968).

Ca-bentonite was selected to be used, as a lower-cost alternative of Na-bentonite. The objective is to formulate a promising water-based mud by improving the properties of Ca-bentonite using NPs. Reducing the filter loss properties of the formulated drilling fluid is the main goal of this research. Additionally, the rheological properties of the drilling fluid at downhole conditions will be investigated and optimized.

Invasion of mud filtrate while drilling is one of the most common sources of damaging the productive formations (Amaefule et al. 1988). This problem is a major contributor in the injectivity or productivity reduction in petroleum wells. Losses of the filtrate fluid into the porous formations during drilling happens because of the difference between the hydrostatic pressure of the mud column and the hydrostatic pressure of the fluids in the formation (Hoferock and Bratcher 1998). As a result of this filtrate fluid invasion a filter cake is forming on the face of the wellbore due to the accumulation and deposition of the solids and cuttings (Civan 1994, 1996). The filter cakes stabilize and protect the formation from extra drilling fluid invasion and allow better fluid circulation through the wellbore. **Figs. I-2** and **I-3** show schematic illustrations of the drilling fluid filtrate invasion through the deposited filter cake and porous formation and the generation of a filter cake on the wellbore (formation face) during drilling.

The most important factors and parameters that could control the drilling fluid filtrate invasion include: formation properties (permeability, porosity, pore size and structure), mud properties, and the properties of the deposited filter cake. Better designing of the drilling fluid and selecting the additives to be used can produce a good-quality filter cake. Such a cake can withstand high differential pressures (overbalance drilling) and

reduces the possibilities of many drilling problems. Filter cakes can be considered as a key to minimize formation damage and maximize reservoir return permeability.

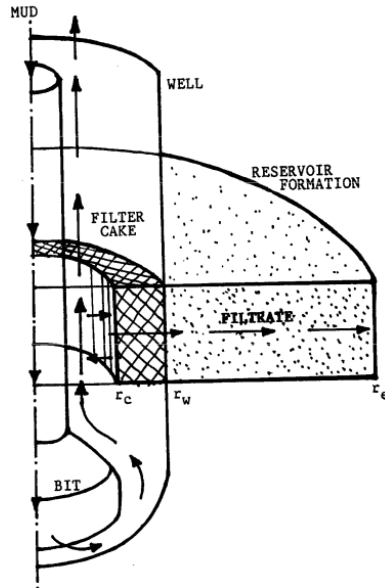


Fig. I- 2—Filtrate fluid invasion through the deposited filter cake and porous formation during drilling (Civan 1994).

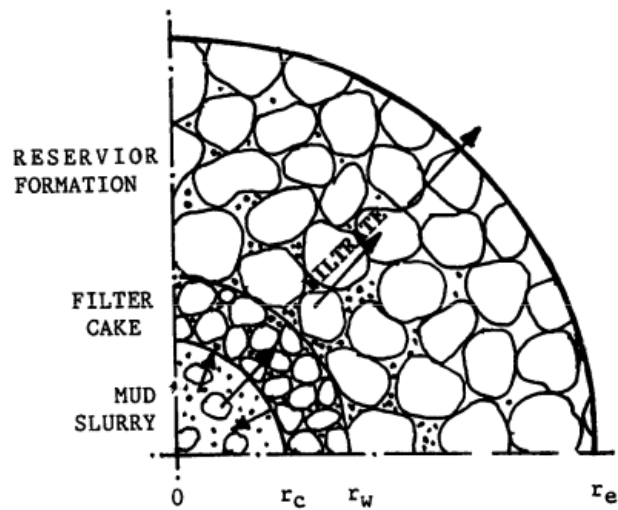


Fig. I- 3—Formation of the filter cake while filtrate fluid invasion (Civan 1994).

Characterizing the filter cake is very important because of their key rule in the drilling process. Filter cake properties, such as filtrate fluid loss, thickness, permeability,

porosity, structure, and texture are essential parameters that should be carefully identified and optimized. The structure and texture of the filter cake give better understanding of the interaction between different drilling additives. Scanning electron microscopy (SEM) was thoroughly used in the literature for such investigations (Hartman et al. 1988; Chenevert and Huycke 1991; Plank and Gossen 1991; Kelessidis et al. 2006; Barry et al. 2015). Additionally, thin-section photography was also introduced and used to investigate the filter cake structure and the interaction of solids and cuttings with the formation surface (Li and He 2015). The computed-tomography (CT) scan was also used in different studies to investigate the cake homogeneity, thickness, and porosity (Elkatatny et al. 2011, 2012, 2013). Bageri et al. (2013) summarized the most commonly techniques and models that used to evaluate and characterize the filter cake properties.

Applications of Nanoparticles in the Drilling Fluid Technology

The nanotechnology started as a promising technology at the end of the 1980's decade. By this beneficial technology new nano-materials can be developed and designed by rearranging molecules or atoms of particles with larger sizes (Ju et al. 2012). A nanometer (nm) is one thousand millionth of a meter. The range of the nano-scale is usually can be defined as the range starting from 1 nanometer up to 100 nanometer (**Fig. I-4**). So that, one can define nanotechnology as the technology of designing, fabricating and utilizing of functional structures and materials with at least one dimension measured in nanometers (Kelsall et al. 2005). The extraordinary change in properties when using nano-materials may be because of their relatively high surface-area-to-volume ratio when compared to the same materials in larger dimensions (**Fig. I-5**).

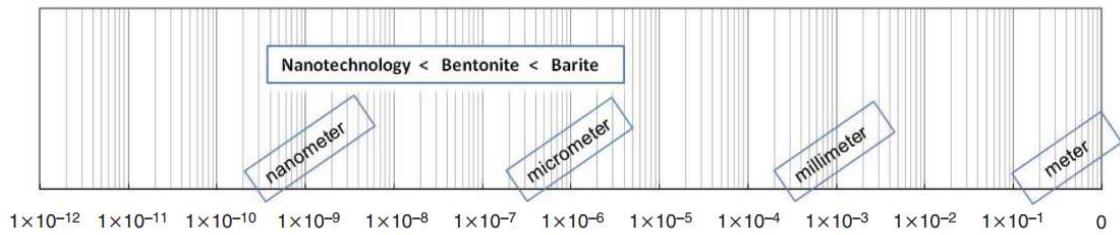


Fig. I- 4—Scale of particle-size (Cai et al. 2012).

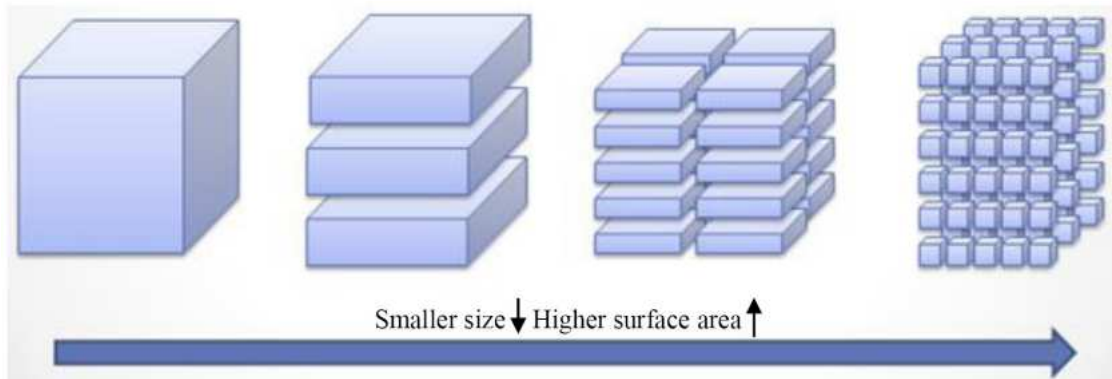


Fig. I- 5—Surface-area-to-volume ratio of nanoparticles (El-Diasty and Aly 2015)

Nanotechnology can contribute in different areas of the petroleum industry. Nanomaterials can be used to change reservoir properties such as wettability and improve mobility ratio. Its capability as a less expensive, more efficient, and environmentally friendly material might give it a more promising role in the coming developments. However, many of the applications are still only in laboratory and research development.

Several research studies have been conducted for developing novel drilling fluids using predominantly nanoparticles (NPs) among a variety of additives. NPs are now commercially available at affordable prices and are suitable as drilling fluid additives because of their attractive properties stemming from their high surface-area-to-volume ratio. Friedheim et al. (2012) and Hoelscher et al. (2013) provide a brief overview of the

nanotechnology applications in the drilling fluid industry. Different types of NPs have been used in the drilling fluid technology as rheological property controller, fluid loss reducer, and shale stabilizers. Two methods can be followed in the preparation of NPs-based drilling fluids, either by using ex-situ or in-situ procedures. The ex-situ preparation is the addition of NPs to the aqueous solution, which is later can be added to the drilling fluid. However, the addition of the precursors that generate the NPs directly to the drilling fluid is called in-situ preparation. Alsaba et al. (2014) recommend the in-situ procedures of NP preparation in order to mitigate the water content increasing in mud into the circulation system. In the following section, a detailed review of nanotechnology applications in drilling fluids has been presented; specifically, the applications of NPs as a rheological property modifiers, fluid loss controllers, and wellbore strengthening agents.

Rheological Property and Fluid Loss Controller

Different NPs-based drilling fluids had been formulated and tested by Amanullah et al. (2011). The authors noticed the difficulty of using either salt or fresh water as the fluid phase to prepare NPs-based drilling fluid without the use of chemical additives (i. e., surfactants or polymers). It was also found that the developed NPs-based drilling fluids had satisfactory rheological properties. Moreover, a significant reduction in the filtrate fluid and spurt loss were obtained when using NPs compared to the base. Additionally, the authors reported the deposition of a thin and compact filter cake, which might be resulted in preventing the problem of pipe sticking while drilling. The drilling fluid formulations of this NPs-based drilling fluids and also for a macroparticle-based drilling mud were reported in more details by Amanullah and Al-Arfaj (2013).

Agarwal et al. (2011) studied stabilizing invert emulsion fluids for HP/HT drilling applications by using nano-clay and nano-silica. The authors noticed that using nano-clay and nano-silica together was the way to get the best properties. It was also found that nano-clay is easily dispersed in the oil phase and it showed better gel structure. The test results showed also that the nature of nano-silica (either hydrophilic or hydrophobic) has significant effect on the behavior of the formed gel. When Agarwal et al. (2011) used barite as a weighing material, they found a loss of yield stress. However, they mentioned that the yield stress of the invert emulsion drilling fluid might be regained by increasing the nano-silica content. Moreover, they had reported that aging the NPs-based drilling fluid at 225°C for 96 hour results in relatively small decrease in the yield stress; however, the emulsion remained stable.

Jung et al. (2011) investigated the effectiveness of using iron oxide NPs (3 nm and 30 nm) to improve the HP/HT properties of Na-bentonite-based fluids. The rheological properties were studied at different temperatures (20-200°C) and pressures (1-100 atm). The filter cake characteristics and filtrate loss capacity were also investigated in this study. The authors reported that the increase in NP concentration resulted in an increase in viscosity and yield stress of the bentonite fluids. Furthermore, the smaller size NPs (3 nm) was found to be effective in improving the viscosity of this type of suspensions. Jung et al. (2011) explained the test results through two concepts. The first theory is that, oxide NPs embedded randomly on the surface of clay particle in the pore structure of the dispersion, which insure better connections between clay particles and enhance gelation of the fluids. The second theory was that this improvement in the rheological properties

upon adding oxide NPs may be due to the synergy generated by homocoagulation of the exceeds NPs and heterocoagulation of bentonite with NPs.

Javeri et al. (2011) studied the using of silicon NPs as additives to reduce the probability of pipe sticking by the generation of a thinner filter cake on the surface of formation. The size of silicon particles used in this study was 40-130 nm. The results showed the formation of a continuous, low permeability/low porosity filter cake. Furthermore, they mentioned that the filter cake thickness was less than in normal cases because there was less volume of filtrate entering the formation. Moreover, they found that the used NPs do not have high impact on the viscosity of the drilling fluid and have thermal stability at high temperatures up to 2500°F.

Manea (2011) designed a novel drilling fluid by applying nanotechnology. The author was focusing on water-based drilling fluids with low solid content by using nano-size polymers. In this study, a nano-polymer was synthesized and investigated as a filtrate loss reducer additive. Nano-size particles were synthesized by grinding in a planetary mill that have agate bowl and 20 agate ball of 20 mm diameter. The authors reported that the extraordinary properties of this polymer were obtained because of its ability to adsorb free water from the system and form gel. Furthermore, this nano-polymer was also found to be sensitive to the change of pH of suspensions with a swellability increases in alkaline medium. Moreover, the cumulative volume of filtrate fluid loss upon the addition of nano-polymer was found to have small values. The author explained the test results as an impact of the increase in total specific area with the decrease in particle size, which results in bigger interaction area with the continuous medium and significant swelling capability.

Ravi et al. (2011) presented a lost circulation formulation to reduce the filtrate fluid loss. The lost circulation composition comprised Portland cement in an amount of about 10 to 20 wt% (of the lost circulation composition), NPs (a particular nano-silica) in an amount of about 0.5 to 4 wt% and having a particle size of about 1 to 100 nm, amorphous silica in an amount of about 5 to 10 wt%, synthetic clay in an amount of about 0.5 to 2 wt%, sub-micron sized calcium carbonate in an amount of about 15 to 50 wt%, and water in an amount of about 60 to 75 wt%. Lost circulation additives were formed with a mix of cement and nano-materials to reduce the setting time for filter cake formation and gel strength development. However, the authors mentioned that high amounts of the NPs were required with the cement to produce the filter cake and develop the gel strength.

Abdo and Haneef (2012) investigated a new clay (ATR), which offers bigger surface area and higher reactivity, as a drilling fluid additive. The ATR was found to be consisting mainly of montmorillonite and has a chain like structure. Different sizes of ATR (micro and nano) were used in this study. ATR in NP sizes were found to be applicable for use as a drilling fluid additive and can generate better rheological properties (relatively low viscosity and high gel strength). Furthermore, regular bentonite (in smaller particle sizes) was also examined but was found to have inconsistent behavior because of high flocculation. Moreover, Abdo and Haneef (2012) reported that a combination of regular bentonite and ATR NPs displays the best and optimized set of properties because of the combining effect of the characteristics bentonite (high density) and ATR NPs (low viscosity and high gel strength).

Graphene oxide (GO) was used with water-based drilling fluids as a fluid loss reducer (Kosynkin et al. 2012). In this study, dispersions of GO in xanthan gum aqueous solutions were tested using standard API filtration tests. It was noticed that the best GO concentration that should be used is 0.2 wt% by carbon content. Additionally, better performance was obtained when using a combination of two shapes of GO (large flake and powdered GO in a ratio of 3:1). When using this combination, an average fluid loss volume of 6.1 ml and a filter cake thickness of 20 μm were obtained. A regular drilling fluid containing 12 g/L of clays and polymers was also tested in this study. In this case, an average fluid loss of 7.2 ml (+18 %) and a filter cake thickness of 280 μm were obtained. Moreover, the authors reported that the GO solutions exhibited higher thermal stability and shear thinning behavior when compared with clay-based fluid loss additives.

Friedheim et al. (2012) also investigated the effectiveness of using GO NPs as viscosity and fluid loss control additives with a slurry of bentonite and barite in water. It was found that GO NPs have a significant potential on the rheological parameters when used in a concentration of 2 lb/bbl. Furthermore, the system was also examined after aging for 16 hours at 150°F. The authors reported that the GO NPs effectively enhance both rheological and filtrate loss properties of the system. The authors concluded that the GO NPs are easily deformable to fit into the contours of the formation because of their sheet-like structure; however, the cost effectiveness and the long-term stability of GO NPs is a critical issue that must be addressed for field application.

Polyanionic cellulose (PAC) and Carboxymethyl cellulose (CMC) polymers in NP sizes were investigated as fluid loss reducer additives (Fereydouni et al. 2012). An in-

house made CMC NPs were used in this study, which made by using of ball milling at 500 rpm rotational velocity for 1 to 1.5 hour at 25 to 30°C. PAC NPs were also made in-house (ball milling at 400 rpm, 2 to 2.5 hour residence time, and room temperature). The authors reported a reduction of the API fluid loss volume and filter cake thickness when using CMC and PAC NPs compared with regular-size polymers of the same type. Moreover, a cost advantage when using CMC and PAC NPs was also reported in this study.

Abdo and Haneef (2013) investigated the using of a natural clay mineral in nano-sizes, palygorskite (Pal), to stabilize the rheological properties of drilling fluid at HP/HT environments. Pal were reported to be available in Oman and has a fibrous rod-like microstructure (**Fig. I-6**). In this study, Pal was synthesized and tested in nano-sizes of 10-20 nm. It was found that the elongate needle shape of Pal NPs gave them unique colloidal properties when compared to the flake-shape of montmorillonite particles. Moreover, it was reported that montmorillonite alone was found to not be stable at HP/HT environments. However, adding a small concentration of Pal increased the montmorillonite stability at such conditions.

Nasser et al. (2013) developed a nano-fluid by using nano-graphite and nano-silicon wires. The authors concluded that the developed nano-fluids showed better rheological properties at temperatures up to 90°C. More specifically, this nano-fluids had higher viscosity when compared with that of a regular drilling fluid at the range of tested temperatures.

Anoop et al. (2014) studied the rheological properties of nano-fluids composed of mineral oil and silica NPs at HP/HT environments. It was found that the viscosity of the

nano-fluids increases with the increase in NP concentration. Furthermore, a decrease in the viscosity of the nano-fluids at higher temperatures was also reported. The power law was found to be the best fit model for all cases. Moreover, there was non-essential reduction in the viscosity of the nano-fluids at a temperature of 100°C.

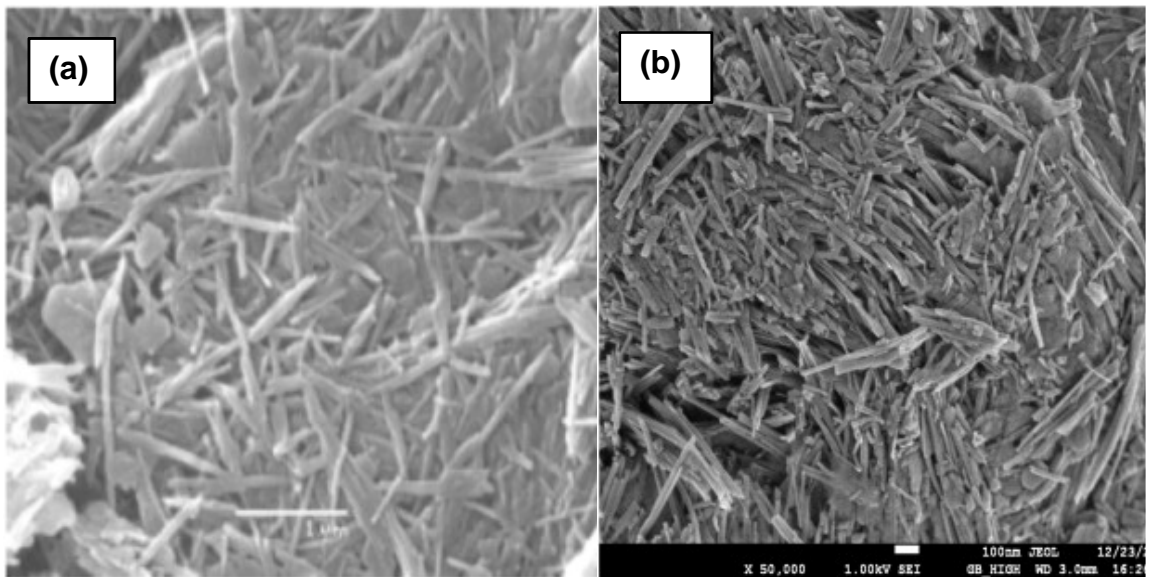


Fig. I- 6—SEM images of Pal: (a) regular Pal (needle like clusters), and (b) uniformly dispersed Pal NPs (Abdo and Haneef 2013).

Zakaria and Husein (2014) developed an in-house NP fluid loss circulation material (LCM). The aim of this study was to reduce the invasion of fluids in very tight formations such as shale. Both in-situ and ex-situ procedures of NP preparation and addition to oil-based drilling fluid were investigated in this study. Standard API filter press test results showed a reduction greater than 70% in the fluid invasion compared to 9% reduction when using a commercial LCM. Moreover, thinner mud cakes were deposited when using this materials, which indicating high potential for mitigating formation

damage and differential pipe sticking. Additionally, a good stability was found when sealing this NPs-based drilling fluid for a period of more than 6 weeks.

Contreras et al. (2014) examined the effectiveness of using in-house prepared iron-based NPs (NP1) and calcium-based NPs (NP2) as LCM with oil-based drilling fluids in the presence of glide graphite. Both API fluid loss (at 100 psi and 78°F) and HP/HT filtration tests (at 500 psi and 250°F) were conducted. Ceramic disks of 775 md permeability were used to simulate porous formation. It was found that under HP/HT conditions, NP1 gave higher reduction in the fluid loss when used at low concentrations; however, NP2 showed a perfect performance at high concentration. Under API filtration, these results were found to be reversed. It was also reported that the effect of graphite as a filtrate reduction agent becomes less significant under both HP/HT and LP/LT with increasing the NP concentration. However, using graphite in combination with NP1 yielded a better filtration loss reduction at both HP/HT and LP/LT (**Fig. I-7**).

Multi-walled carbon nano-tubes (MWCNTs) were also investigated as an additive to water-based and ester-based drilling fluids (Ismail et al. 2014). Determining the optimum concentration of MWCNTs to generate better rheological properties at various temperatures was the goal of this research. In the case of water-based drilling fluid, it was found that the major rheological properties (plastic viscosity, yield point and gel strength) are not much affected by using different concentration of MWCNTs. However, in the case of ester-based drilling fluid, emulsion stability and gel strength are slightly increased with the increase in MWCNTs concentration. Moreover, it was also found that increasing the temperature resulted in a decrease in the rheological properties of water-based drilling

fluid. However, ester-based drilling fluid showed an increase in all of the rheological properties when increasing temperature.











Sample Description and Thickness	Filter Cake after 30min	
Control Sample (CS) 1.5±0.1mm		
Graphite 0.5wt% 1.6±0.1mm		
Graphite 2.0wt% 1.6±0.3mm		
Only 0.5 wt% NP1 1.5±0.3mm		
Only 2.5 wt% NP2 1.5±0.5mm		

Fig. I- 7—Images of the generated filter cakes (Contreras et al. 2014).

William et al. (2014) studied the effect of using nano-fluids of CuO and ZnO NPs (< 50 nm) in a xanthan gum (XG) as an additive with water-based drilling fluids. Two-step method was used to prepare the nano-fluids (Ponmani et al. 2014). Different NP concentrations into a base fluid 0.4 wt% XG in water were investigated. An ultrasonication tank was used in the preparation with a sonication time of one hour. The rheological properties of the nano-fluid/water-based drilling muds (NWBM) were examined at different temperatures (up to 110°C) and pressures (0.1 and 10 MPa). It was found that the thermal and electrical properties of the NWBM improved by 35% compared to base fluid (without nano-fluids), further enhancements were observed with the increase in the NP concentration. The CuO NPs-based nano-fluids were found to have better thermal properties at HP/HT condition compared with ZnO NP-based nano-fluids. Moreover, the test results showed that at higher temperatures, the effect of pressure on the rheological properties of NWBM are more significant, which indicated better rheological stability. The authors reported that stabilizing the viscosity of NWBM at higher temperatures is the most important role that the nano-fluids played.

Barry et al. (2015) examined the effectiveness of using two types of NP intercalated clay hybrids, iron-oxide clay hybrid (ICH) and aluminosilicate clay hybrid (ASCH) on the properties of Na-bentonite suspensions. In this study, both API fluid loss, LP/LT (25°C, 6.9 bar), and HP/HT fluid loss (200°C and 70 bar) were investigated. The results showed a reduction in the fluid loss of up to 37% and 47% in both LP/LT and HP/HT fluid loss when using ICH and ASCH with bentonite fluids compared to the base (without NPs). Furthermore, it was found that adding 0.5 wt% of pure Fe₂O₃ NPs (3 and

30 nm) into bentonite suspensions increased the API fluid loss by 14% compared to the base; however, it decreased the filtration volume at HP/HT by 28% compared to the base fluid. Moreover, the authors concluded that the reduction in both LP/LT and HP/HT filtrate volume when using clay hybrids (ICH and ASCH) was because of the reconstruction of clay platelet in suspension due to the changes in surface charge. Both SEM images (**Fig. I-8**) and zeta potential measurements were used to demonstrate the aforementioned conclusions.

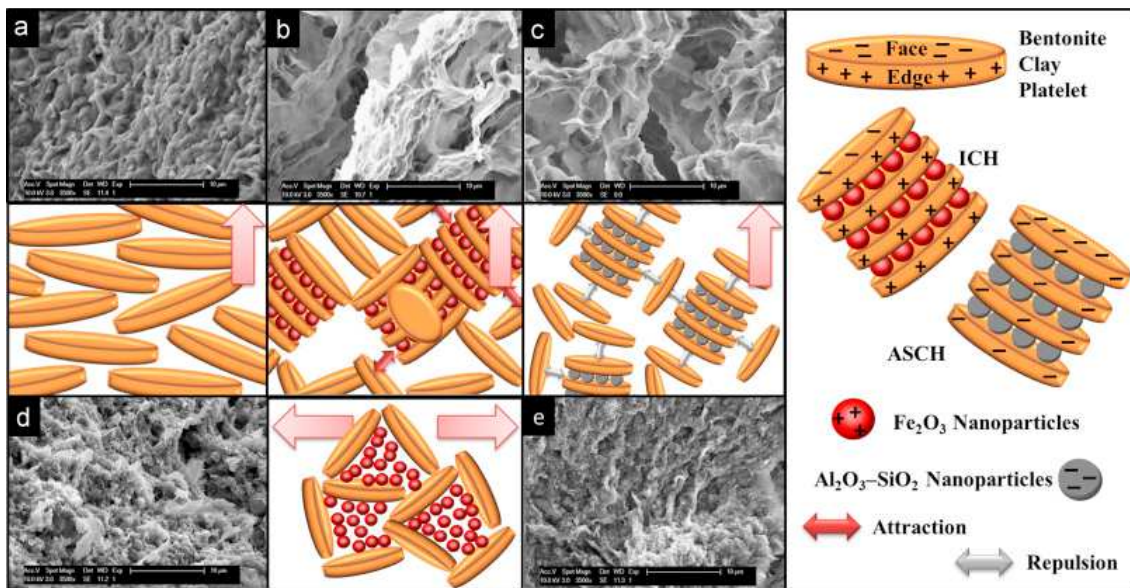


Fig. I- 8—SEM images of the filter cakes after LP/LT filter press experiments for different samples with the corresponding illustrations of bentonite clay platelet interaction (Barry et al. 2015).

TiO₂/polyacrylamide (TiO₂/PAM) nano-composite was also investigated to improve the rheological properties of water-based drilling fluid (Sadeghalvaad and Sabbaghi 2015). Enhancement in the plastic viscosity and yield point of the drilling fluid were reported when adding the nano-composite. Additionally, it was found that the increase in nano-composite concentration results in an increase in the shear thinning

behavior. Moreover, SEM images showed that the pure PAM sample has a smooth surface and the grains of TiO_2 appears on the surface and in between the PAM particles in the nano-composite (**Fig. I-9**).

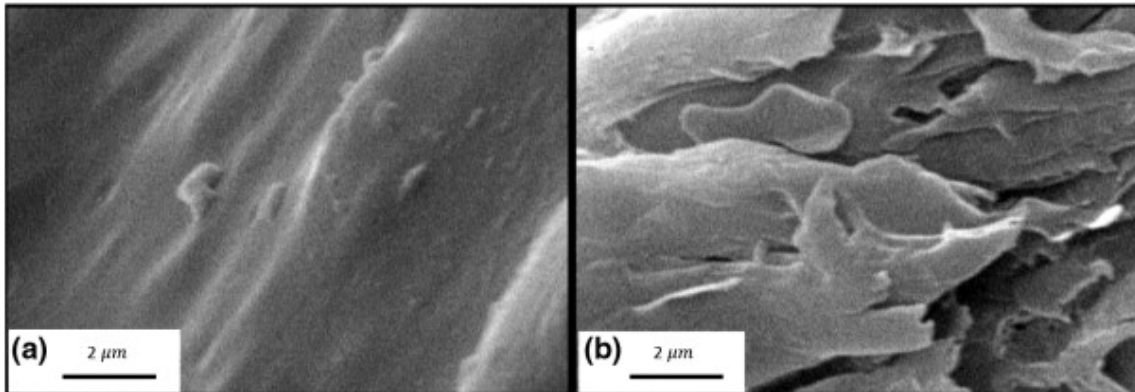


Fig. I- 9—SEM images of: (a) pure polyacrylamide (PAM), and (b) TiO_2 /polyacrylamide (TiO_2 /PAM) nano-composite (Sadeghalvaad and Sabbaghi 2015).

Li et al. (2015a) examined using polyanionic cellulose (PAC) and cellulose nano-crystals (CNC) with bentonite-based drilling fluids. The effect of CNC was found to be more significant than PAC on improving the rheological properties of PAC/CNC/bentonite-based drilling fluids. Furthermore, the Sisko model was found to well-performing the fluid rheological properties. Moreover, the test results showed a little effect of the CNC on the API fluid loss of PAC/CNC/bentonite based drilling fluids. However, a better reduction in the API fluid loss was reported when increasing the concentrations of bentonite and PAC.

The effect of using cellulose NPs (CNP) (microfibrillated cellulose, MFC, and cellulose nano-crystals, CNC) on the rheological and fluid loss behavior of bentonite-based drilling fluids was also studied by Li et al. (2015b). It was found that using MFC and CNC improved the shear stress, yield point, and viscosity of the drilling fluids, which

yielding better cutting carrying capability. Furthermore, a reduction in the filter cake thickness and filtrate loss were also noticed for CNC/bentonite fluids; however, MFC was found to have relatively small effect on the fluid loss in addition to generating thicker filter cakes. The authors explained that the CNC polymer forms films and creates core-shell structure. It was also concluded that the properties of CNC/bentonite fluids are suitable for mitigating differential pipe sticking.

Mao et al. (2015) introduced and developed a type of hydrophobic nano-silica composite associated with a polymer (SDFL) to be used for enhancing the properties of water-based drilling fluids. It was reported that the SDFL has a core-shell structure. Excellent thermal stability, filtrate loss reduction, and rheological properties were obtained when using SDFL compared to the base. For example, a reduction of 69% in the HP/HT fluid loss was obtained when using 0.5 wt% of the SDFL.

Using Fe_4O_3 NPs as a drilling fluid additive was also investigated (Amarfio et al. 2015). It was reported that at defined shear rates, using Fe_4O_3 NPs can keep stable shear stresses of the fluid with the increase in temperature. Additionally, a predictive model was developed to estimate the Fe_4O_3 NPs mass fractions and shear rates when drilling at higher temperature.

Taha and Lee (2015) investigated the applicability of a nano-graphene fluid to enhance the drilling fluid performance. The authors applied the tested nano-based drilling fluid in drilling an onshore well under HP/HT conditions. Enhancement in the thermal stability and a reduction of 30% in the fluid loss were observed when using nano-graphene compared to the control. Furthermore, improvements in the rate of penetration (ROP) by

125%, a reduction in the torque by 20%, and an increase of greater than 75% in the bit life were reported in this study when using nano-graphene.

A composite of zinc oxide NPs and an acrylamide (ZnO-Am) was also investigated as a water-based drilling fluid additive for drilling shale formations (Aftab et al. 2016). Over a temperature range up to 150°F, both apparent viscosity and plastic viscosity were increased when using the ZnO-Am. Furthermore, a reduction of 14% in the API fluid loss was observed when using the composite compared to the control fluid. However, at HP/HT a slightly less reduction in the fluid loss volume was obtained. Moreover, it was found that using the composite resulted in a decrease in the shale swelling capacity from 16% to 9%.

Amarfio and Abdulkadir (2016) examined the using of Al₂O₃ NPs to enhance the properties of water-based drilling fluids. It was found that using Al₂O₃ NPs resulted in an improved thermal stability under high temperatures. Furthermore, it was reported that at defined shear rates, using Al₂O₃ NPs can keep stable shear stresses of the fluid with the increase in temperature.

Li et al. (2016) studied the using of SiO₂ NPs as a drilling fluid additive while drilling unconventional wells. Enhancements in the rheological properties and a reduction in the filtrate fluid loss were observed when using NPs compared to the control (without using NPs). Furthermore, it was reported that NP-based drilling fluid was able to generate a thin filter cake with a better texture.

Salih et al. (2016) examined the using of nano-silica as a drilling fluid additive. The authors reported that using nano-silica in a concentration of 0.1 to 0.3 wt% has more

impact on the drilling fluid properties than at the other concentrations (greater than 0.5 wt%). Furthermore, the pH of the fluid was reported to have a great impact on the sensitivity of nano-silica in the fluids.

Belayneh et al. (2016) studied the using of SiO₂ NPs as a bentonite-based drilling fluid additive. The bentonite fluids used in this study were treated by different types of polymers (HV-CMC, LV-CMC, and XG) and salts (KCl, NaCl). The control fluid formulated for this study was containing 0.3 g of XG in 25 g bentonite per 500 g water, 0.2 g LV-CMC, and 2.5 g KCl. An upward shift on the rheogram (shear stress versus shear rate) of the control fluid was observed when adding the NPs. Additionally, a shear thinning behavior was noticed in this case. It was also found that adding 0.25g of SiO₂ NPs gave a maximum value of yield stress (10 Pa) when compared to that of the control (5.5 Pa). Moreover, the optimum NP concentration was found to be 0.25 g, which gave a reduction of 4.5% in the API fluid loss compared to that of the control. However, Adding less than (0.2 g) or greater than this concentration (0.3 g) resulted in increasing the fluid loss by 8.7% and 13%, respectively, compared to the control.

Tin oxide (SnO₂) NPs were also investigated as an additive to water-based drilling fluid (Parizad and Shahbazi 2016). The test results revealed improvements in the rheological, thixotropy, electrical thermal, and filtration and filter cake properties of the drilling fluid upon the addition of SnO₂ NPs. It was found that adding 2.5 g/L of SnO₂ NPs resulted in a reduction of 20% in the filtrate loss volume. However, less improvements on the filtration characteristics was noticed in case of using higher NP concentrations. Additionally, it was reported that the increase in the NP concentration

yielded an increase in the flow consistency index (K) and a reduction in the flow behavior index (n).

Wellbore Strengthening and Shale Stability agents

Sensoy et al. (2009) discussed the effectiveness of silica NPs to reduce shale permeability around the wellbore. The theory explained was that the NPs are playing a key role of plugging the pore throats and building an internal filter cake, which reducing the invasion of the fluids into shale formations. It was found that a concentration of at least 10 wt% of silica NPs having an average size of 20 nm should be used for successful shale plugging. The SEM were used in this research to investigate the type of plugging (**Fig. I-10**). It was noticed that the NPs plugged the pores that have the same NP size. Additionally, a group of NPs can aggregate together and plug one big pore throat. Moreover, four types of real drilling fluids were studied with and without the addition of NPs. The authors reported a reduction of 16 to 72% in the fluid loss into Atoka shale when using NPs. However, in the case of Gulf of Mexico shale the reduction in the fluid penetration was noticed to be from 17 to 27%.

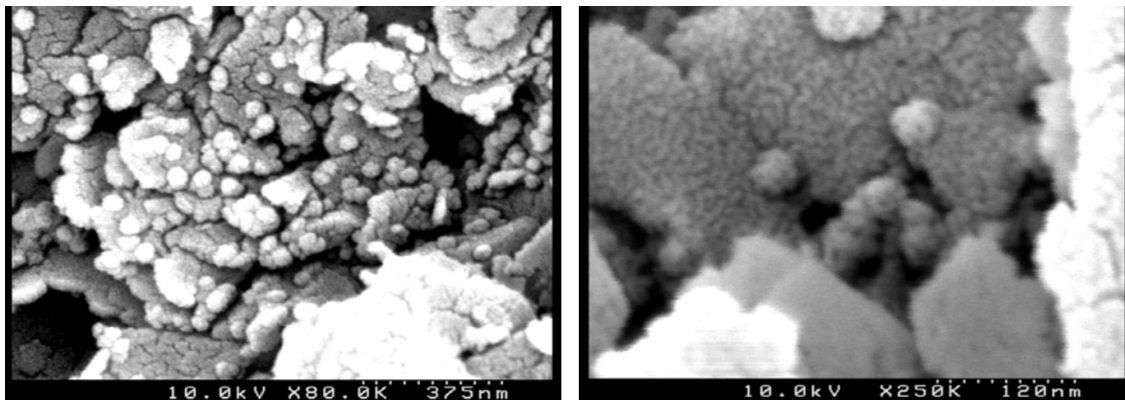


Fig. I- 10—SEM images of: (a) NPs plugging different pore throats, (b) aggregated particles plugging a pore throat (Sensoy et al. 2009).

Srivatsa et al. (2011) studied a bio polymer-surfactant fluid containing NPs as a drilling fluid additive for fluid loss reduction. Silica NPs were found to give better results when compared sized calcium carbonates. Furthermore, it was also noticed that the surfactant had low thermal stability at high temperatures. However, the bio-polymer was reported to be stable up to 350°F. The authors concluded that a combination of silica NPs and bio-polymer is recommended for high temperature drilling. Additionally, the increase in NP concentration was found to reduce the fluid loss; however, the aggregation of NPs in the polymer fluid might be a restriction of increasing the NP concentration.

Cai et al. (2012) also investigated the capability of nonmodified silica NPs as shale plugging additives in the drilling fluid. In this study, six different types of commercial and nonmodified silica NPs were examined and screened. Two types of regularly used water-base drilling fluid were studied in the presence and absence of 10 wt% of NPs. Atoka shale outcrops and the three-step pressure penetration experiment were used throughout this study. A higher reduction in the shale permeability was observed upon the addition of nonmodified NPs. Furthermore, an increase in plastic viscosity, a decrease in yield point, and a reduction in the filtrate fluid loss were also noticed when adding NPs compared with the base. Moreover, the most effective sizes and concentrations of NPs to get a highly reducing in the shale permeability was reported to be from 7 to 15 nm and 10 wt%, respectively.

Hoelscher et al. (2012) investigated the application of silica NPs (5 to 100 nm) as a water-based drilling fluids additive with shale formations. The NPs were screened by running stability tests in various salt solutions and temperatures. The successful NP sizes

were then used to run a modified API filter loss test, in which the smallest available hydrophilic filter membrane (100 nm pores) was used. Furthermore, for better understanding of the mechanism of shale pore plugging, a shale membrane tester was used. It was reported that, silica NPs at low concentrations in a water-based drilling fluid can physically plug shale pores, which was considered as a more environmentally friendly and cost-effective method.

Silica NPs with 20 nm diameter was also examined as a water-based drilling fluid additives for shale drilling (Sharma et al. 2012). The authors reported that the developed drilling fluids are stable with a proper range of change in the rheological properties at elevated pressures and temperatures. The NP-based fluids were also reported to have good lubricant capabilities. Additionally, a reduction of 10 to 100 times was observed in the filtrate penetration into the shale when using NPs. Some tests were also conducted to reveal the effect of NPs on naturally-fractured shale. For shales without fractures, it was reported that using the NPs alone can effectively plug the pores. However, using NPs alone could not be effectively plug the pores of fractured shales. In the latter case, a suitable NP size and concentration should be used to formulate an effective NP-based drilling fluid.

Two types of aqueous silica NPs were also investigated for shale wellbore stability maintenance through physical plugging the pore throats (Akhtarmanesh et al. 2013). It was reported that the NP-based fluids had convenient stability for long time at room temperatures. Different tests were conducted using real shale outcrops from a field in Iran. Three different drilling fluids were investigated with and without adding aqueous silica

NPs. It was found that the fluid invasion into this shale were reduced up to 68% upon the addition of NPs. Moreover, a concentration of 10 wt% of NPs was found to be the minimum concentration needed to obtain a satisfactory reduction in the permeability and fluid invasion. Additionally, using NPs of 35 nm size showed better pore plugging performance when compared to the 50 nm NPs.

Nwaoji et al. (2013) developed and tested a NPs-based lost circulation material (LCM) as a blend for drilling application to achieve wellbore strengthening. Different types of core outcrops were used to conduct hydraulic fracture experiments. It was found that a blend of iron-III hydroxide NPs (1 ml) and graphite (5 gm) in water-base fluid increased the fracture pressure by 70% with a moderate impact on the rheological properties. Moreover, a blend of calcium carbonate NPs (10 ml) and graphite (5 gm) in invert emulsion drilling fluid increased the fracture pressure by 36% with a moderate impact on the rheological properties. Additionally, an increase of 25% in the fracture pressure was achieved when using impermeable concrete core, which revealed the well-performance of these NPs-based blends in wellbore strengthening.

Husein and Hareland (2014) presented a type of drilling fluid that containing NPs and granular particles, which can act as a LCM to provide wellbore strengthening. The examined drilling fluid was an invert emulsion-based fluid. Different types of NPs were investigated (i.e., hydroxide, oxide, sulphate, sulphide, and carbonate) in addition to a granular particles (graphite or calcium carbonate). Low NP and granular particle concentrations were used (less than 5 wt% and less than 10 wt%, respectively). It was reported that, because of the low concentrations of the NPs and granular particles there

was insignificantly change in the other properties of the fluid. However, the developed fluids showed better applicability to strengthening the wellbore. Moreover, this study had investigated both the in-situ and ex-situ preparation of NPs in the drilling fluids.

Based on the aforementioned survey, metal oxide NPs, more specifically iron oxides and silica NPs, were found to be capable of reducing the filtration loss, forming a good-quality filter cake (i.e., thin and very low permeability cake with less filtrate invasion), and maintaining optimal rheological properties when used in low concentrations. All of the previous work was focusing mainly on investigating the properties of water-based drilling fluids in the presence of NPs. For bentonite-based drilling fluids, the Na-montmorillonite was the mostly used clay. However, to the best of our knowledge, the Ca-bentonite were not investigated as a drilling fluid additive in the previous work. In the following research, the effectiveness of NPs to improve the rheological and fluid loss properties of bentonite-based drilling fluid consisting mainly of Ca-montmorillonite will be investigated under downhole conditions.

Research Objectives

This research work aims at experimentally investigate the effectiveness of using different types of NPs on the filter cake properties of Ca-bentonite fluids at downhole conditions up to 500 psi and 350°F using real Indiana limestone outcrops. A combination of CT scan, SEM-EDS, and ICP-OES will be used to provide detailed insights on the rule that the NPs play for building the filter cake structure. Furthermore, a sensitivity analysis of the rheological properties of this NPs/Ca-bentonite-based drilling fluids will be conducted at temperatures up to 200°F to assess their stability. Moreover, this work

intends to determine the optimum NP concentration, which provides a base for more efficient and environmentally friendly drilling operations and less formation damage.

A complete NPs/Ca-bentonite-based drilling fluid will be formulated and tested in order to reveal the effectiveness of using NPs to enhance the properties of Ca-bentonite-based fluids in the presence of polymers and different drilling fluid additives. Moreover, the effect of NP concentration, temperature, differential pressure, drilling conditions (static or dynamic), and the drilling fluid preparation method on the filter cake properties will be investigated.

CHAPTER II

EXPERIMENTAL SETUP AND MATERIALS^{3,4}

Introduction

In this chapter, the materials that used in this research work are introduced. The characterization of the bentonite showed that it was consisting mainly of Ca-montmorillonite. Furthermore, the specification of the nanoparticles (NPs) and the drilling fluid additives (i.e., viscosifiers, filtrate control additives, thinners, alkalinity agents, and weighting materials) are presented. Additionally, the Indiana limestone outcrops, which used to simulate the formation, are characterized on the basis of their porosity and permeability. Moreover, the experimental setups, fluid preparation methods, and the procedures that were followed for each measurement are discussed in details.

Materials

Bentonite

The bentonite was supplied by a local service company in powder form (specific gravity = 2.6, and tan color). It was an untreated bentonite that meets *API specifications* 13A, section 10 requirements (2010). The X-ray diffraction (XRD) mineralogical analysis of the bentonite (**Fig. II-1**) showed that it mainly contained Ca-montmorillonite

³ Reprinted with a permission from “Nanoparticle-Based Drilling Fluids for Minimizing Formation Damage in HTHP Applications” by Mahmoud, O., Nasr-El-Din, H. A., Vryzas, Z., and Kelessidis, V. C. SPE-171849-MS, Copyright 2016 by Society of Petroleum Engineers.

⁴ Reprinted with a permission from “Characterization of Filter Cake Generated by Nanoparticle-Based Drilling Fluid for HP/HT Applications” by Mahmoud, O., Nasr-El-Din, H. A., Vryzas, Z., and Kelessidis, V. C. SPE-184572-MS, Copyright 2017 by Society of Petroleum Engineers.

($\text{Al}_2\text{Ca}_{0.5}\text{O}_{12}\text{Si}_4$) and Mg-montmorillonite minerals ($\text{Al}_{0.86}\text{Fe}_{0.1}\text{H.Li}_{0.08}\text{Mg}_{0.14}\text{O}_{10}\text{Si}_{3.9}$) with the calcium type being the predominant mineral, and it had low percentages of quartz (SiO_2) and illite ($\text{Al}_2\text{H}_2\text{K.O}_{12}\text{Si}_4$). **Table II-1** shows the X-ray fluorescence (XRF) analysis of bentonite as oxides. The XRF values revealed that the $\text{SiO}_2:\text{Al}_2\text{O}_3$ ratio is 3:1, as expected for montmorillonite. The ratio $[(\text{CaO}+\text{MgO})/(\text{Na}_2\text{O}+\text{K}_2\text{O})]$ confirmed that it is mainly Ca-montmorillonite (Veblen et al. 1990; Garcia-Romero and Suarez 2010). The d_{50} of the bentonite was 68 μm , as determined by sieve analysis (**Fig. II-2**). The used bentonite is consisting mainly of Ca-montmorillonite, which is a natural clay of the smectite group. These type of clay minerals have particles with a plate-like, crystalline structure as shown by SEM (**Fig. II-3**). Clays of the smectite group are belong to the phyllosilicate 2:1 family. Their crystalline structure is formed by an Al^{3+} octahedral layer sandwiched between two Si^{4+} tetrahedral layers. A high negative charge is included in the layers because of the interfoliaceous cations (Grandjean 1997; Luckham and Rossi 1999).

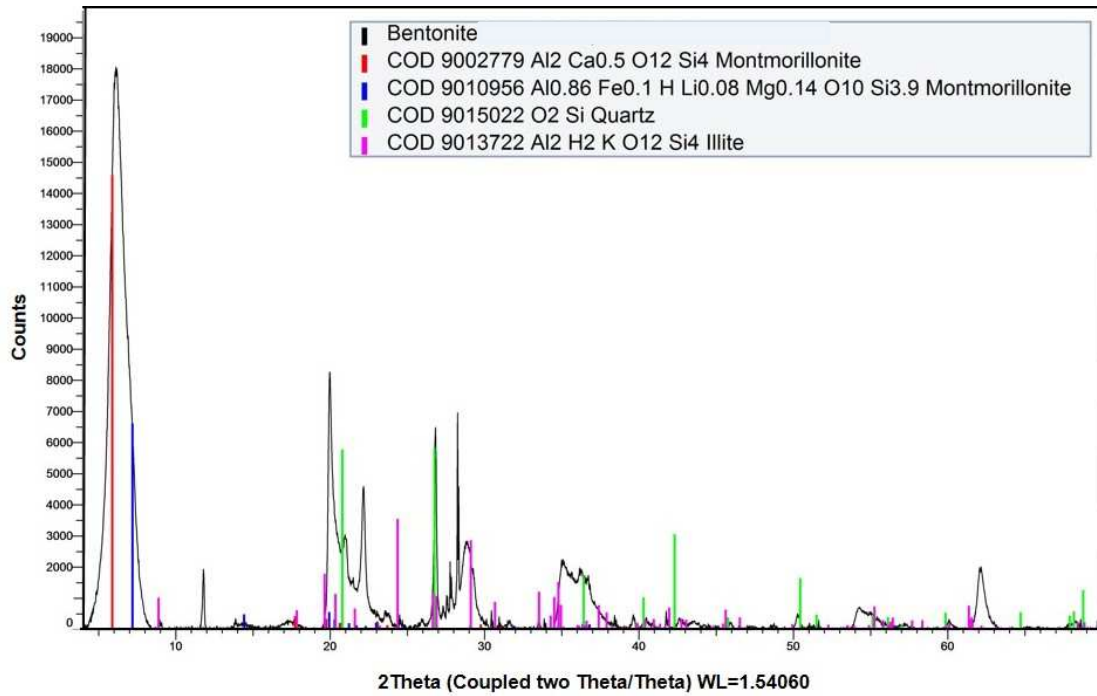


Fig. II- 1— Spectrum XRD of bentonite.

Oxides	SiO ₂	Al ₂ O ₃	Fe ₂ O ₃	MgO	SO ₃	CaO	K ₂ O	P ₂ O ₅	TiO ₂
Concentration (wt%)	64.93	17.28	7.49	3.3	2.01	1.97	0.94	0.94	0.35

Table II- 1—XRF analysis of bentonite.

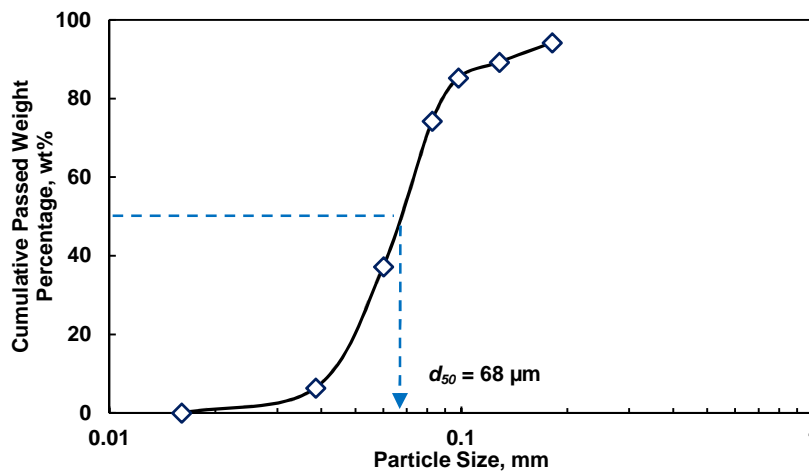


Fig. II- 2—Particle-size distribution of bentonite.

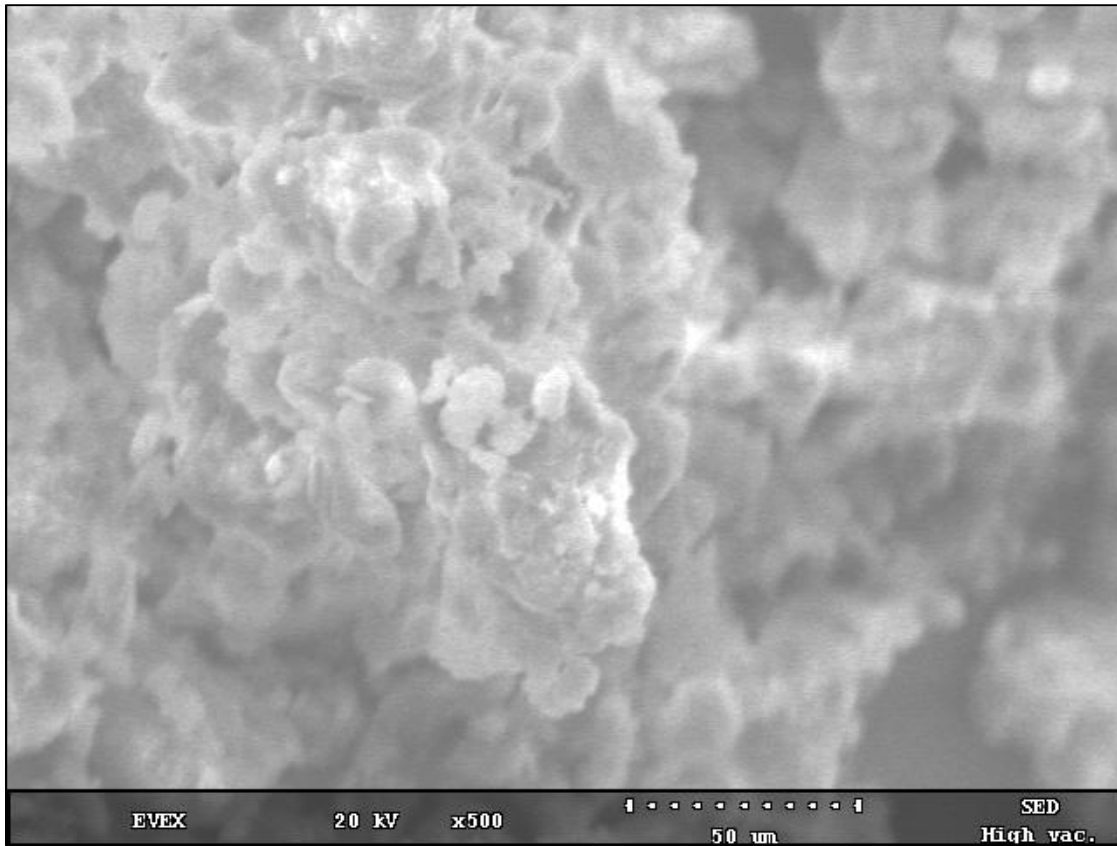


Fig. II- 3—Scanning electron microscopy image of bentonite (X500-50 μm).

Nanoparticles

The NPs used throughout this research work were supplied by Sigma Aldrich and used as received, which are:

- The ferric oxide (Fe_2O_3) NPs (molecular weight = 159.69 g/mol) were supplied in powder form. These NPs had a dark brown color with a spherical shape and an average diameter of less than 50 nm. The surface area of these NPs was 50-245 m^2/g with a purity of greater than 97% as per manufacturer specifications. **Fig. II-4** shows the SEM image of the Fe_2O_3 NPs as received.

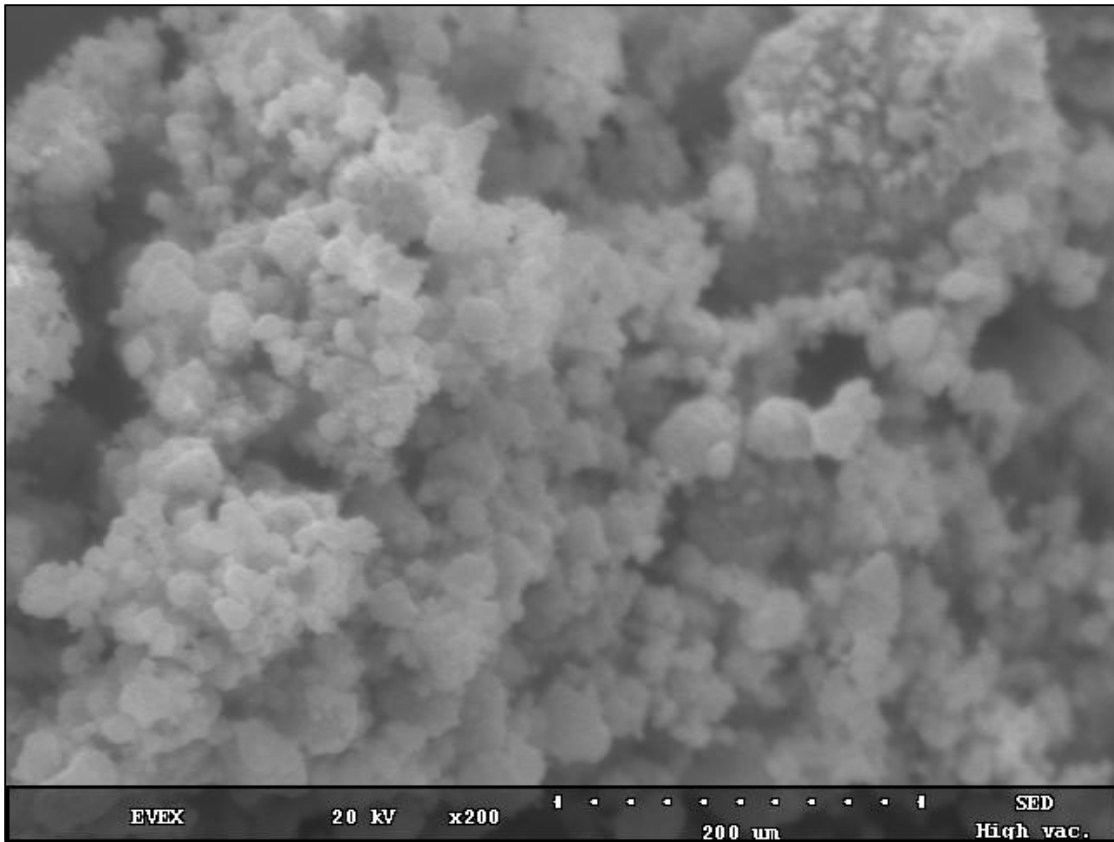


Fig. II- 4— Scanning electron microscopy image of ferric oxide NPs (X200-200 μm).

- The silica (SiO_2) NPs had a white color. These particles had a molecular weight of 60.08 g/mol, a specific surface area of 175-225 m^2/g , an average diameter of 12 nm, and a purity of greater than 97% as per manufacturer specifications.
- The magnetic iron oxide (Fe_3O_4) NPs: With dark color and a spherical shape, these particles had a diameter of 50-100 nm, a molecular weight of 231.53 g/mol, a surface area of greater than 60 m^2/g , a density of 4.8-5.1 g/ml, and a purity of greater than 97% as per manufacturer specifications.

- The zinc oxide (ZnO) NPs: These particles had a white color, a molecular weight of 81.39 g/mol, a specific surface area of 15-25 m²/g, an average diameter of less than 100 nm, and a purity of greater than 97% as per manufacturer specifications.

Drilling Fluid Additives

The polymer (Hyperbranched bis-MPA polyester-64-hydroxyl, generation a4) was used to control the rheological properties. It was supplied by Sigma Aldrich in powder form and white color. It has a molecular weight of 7323.32 g/mol and its chemical formula is C₃₁₅H₅₁₂O₁₈₉.

Polyanionic cellulose (PAC-R) polymer was used to control the rheological and filtration properties. Ferro-chrome lignosulfonate-based thinner and sodium hydroxide (NaOH) pellets were used as thinning and alkalinity control agents. Calcium carbonate (CaCO₃) of d_{50} equals 25 μm and manganese tetraoxide ($d_{50} = 5$ μm) were used as weighting materials. All of the above mentioned materials were provided by a local service company.

Core Outcrops and Deionized Water

Throughout the sample preparation, deionized water was used, which obtained from a purification water system that has a resistivity of 18.2 MΩ.cm at 78°F. Indiana limestone cores of 2.5-in. diameter and 1-in. thickness were used to simulate the formation in the filtration experiments at the tested conditions. The initial porosity of the Indiana limestone core disks were determined by dividing the pore volume by the disk bulk volume. The pore volume for each core was determined as the difference in weight of the core in saturated and dried conditions. The initial porosity of the cores was found to have

an average value of 10-15 vol%. The permeability of these cores was determined using Darcy's equation and was found to be within an average value of 200 md.

Zeta Potential Measurements

Zeta potential can be defined as the potential difference between the stationary layer of fluid attached to a dispersed particle and the medium in which the particle is dispersed (Hunter 1988). Potential stability of a colloidal system might be revealed from the magnitude of zeta potential measurement. If the measured zeta potentials of particles dispersed in a medium within a value of ± 30 mV, this means higher tendency of the particles to aggregate and flocculate over time. However, the particles with zeta potentials out of the range of ± 30 mV are normally considered to be stable.

The zeta potential of the prepared suspensions was determined using the Phase Analysis Light Scattering (PALS) technique (Alotaibi et al. 2011) (**Fig. II-5**). The electrode of the instrument is coated with Pd. A He-Ne laser is used as a light source. The zeta potential range of the instrument is from -200 to $+200$ mV with an accuracy of $\pm 2\%$ and it normally measures the electrophoretic mobility of charged, colloidal suspensions.

NP suspensions for zeta potential measurements were prepared by mixing the NP with deionized water for 5 minutes under mechanical stirring using a five-spindle, single speed multi mixer (load speed of 11,000 rpm) (**Fig. II-6**). Each solution was then mixed using an Ultrasonic Homogenizer model 150VT (**Fig. II-7**) for 15 minutes at ambient conditions. Different suspensions with different NP concentration (0.1 to 0.5 wt%) were prepared for the measurement at different temperatures. Bentonite suspensions were prepared by adding 7 wt% of bentonite to deionized water and mixing for 20 minutes

under mechanical stirring. The suspensions were then sonicated for 15 minutes at ambient conditions. HCl or NaOH puffer solution were used to adjust the pH of the suspensions. Then, the solutions were shaken and the pH was measured directly before running the measurement using a pH/Ion 510 microprocessor-based meter. A polystyrene cuvette was used to hold 1.5 ml of the sample. At least five runs were automatically averaged for each measurement within a standard error of $\pm 3\%$.

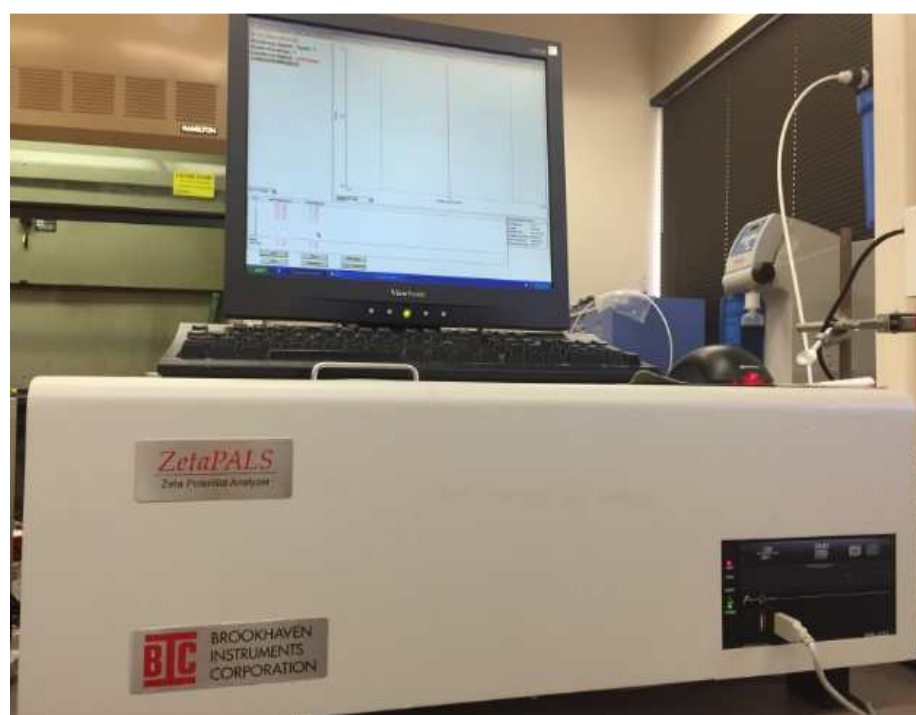


Fig. II- 5—Brookhaven Zeta Potential Analyzer (ZetaPALS).



Fig. II- 6—OFITE Multi Mixer (11,000 RPM).



Fig. II- 7—Model 150 VT Ultrasonic Homogenizer.

Rheological Measurements

NPs/Ca-Bentonite Suspensions

The effectiveness of adding NPs on the rheological behavior of bentonite suspension was examined using a rotational viscometer (Grace M3600) (**Fig. II-8**). The measurements were conducted at fixed speeds of 600, 300, 200, 100, 60, 30, 6, and 3 rpm. At the inner fixed cylinder of the viscometer, these speeds give Newtonian shear rates of 1021.38, 510.67, 340.46, 170.23, 102.14, 51.069, 10.21, and 5.11 s^{-1} , respectively (Kelessidis and Maglione 2008). The rheological studies were conducted at various temperatures from 120 to 200°F and ambient pressure.



Fig. II- 8—Grace M3600 Viscometer.

The examined samples were prepared by following the American Petroleum Institute Standards (*API Specifications 13A* 1993; *API 13B-1* 2003). The base fluid was formed using a bentonite concentration of 7 wt% mixed in 600 ml of deionized water. Different NP concentrations were used (0.3, 0.5, 1.5 and 2.5% by weight). First, bentonite was added to deionized water and mixed for 20 minutes under mechanical stirring using the multi mixer. After that, the desired concentration of NP was added slowly to minimize the agglomeration, and mixing continued for 20 more minutes. The samples were then sealed in plastic containers and left for 16 hours at room temperature for bentonite to hydrate. The samples were remixed for 5 minutes before conducting the rheological measurements. **Table II-2** shows the weights of NP and bentonite used to prepare different NPs/Ca-bentonite suspensions.

Nanoparticle Concentration, wt%	Weight, g	
	Bentonite	Nanoparticle
0.0	45.161	0.000
0.3	45.307	1.942
0.5	45.405	3.243
1.0	45.652	6.522
1.5	45.902	9.836
2.0	46.154	13.187
2.5	46.409	16.575

Table II- 2—Weights of bentonite and NPs used to prepare the suspensions.

Rheological measurements were also conducted on some samples after thermal aging. Dynamic aging of the samples was carried out using an aging cell to determine if the NPs could maintain effectiveness in preserving the rheological properties of these types of drilling fluids. A volume of 200 ml of the fluids that have 0.5 wt% NPs was put

inside a Teflon liner and loaded in the aging cell (**Fig. II-9**). The aging cell was pressurized to 300 psi by nitrogen gas at 78°F. Then, the cell was placed in the rolling oven at 350°F for 16 hours. After that, the cell was cooled, and the aged fluid was agitated for five minutes at 11,000 rpm before running the rheological measurements.



Fig. II- 9—Aging Cell and Teflon Liner.

Fully Formulated Drilling Fluid

A complete Ca-bentonite-based drilling fluid formulation was used to investigate the effectiveness of using ferric oxide NPs as an additive to enhance the drilling fluid properties at HP/HT conditions. The drilling fluid was prepared by mixing 319 ml of deionized water with 7 wt% of bentonite for 20 minutes using the multi-mixer (11,000 rpm). After that the desired amount of NPs were added slowly and mixing continued for

10 more minutes. The wt% of NPs was calculated based on the total weight of bentonite suspension. For instance, the weight of 0.5 wt% NPs was 1.724 g, while the weight of 7 wt% bentonite was 24.14 g in the drilling fluid formula that contains a concentration of 0.5 wt% NPs. The suspension was then ultrasonicated for one hour at ambient conditions using the Ultrasonic Homogenizer.

After that, the drilling fluid additives were added slowly to the NPs/Ca-bentonite suspension under mechanical stirring using the multi mixer (**Table II-3**). Firstly, 0.25 g of the hyper-branched polymer and 0.25 g of PAC-R were added slowly and mixed for 10 minutes for each of them. Then, 1 g of the thinner and 0.5 g of NaOH were added simultaneously and mixed for a total time of 10 minutes. Finally, 30 g and 20 g of the weighting materials CaCO_3 and Mn_3O_4 , respectively, were added separately and mixed for 10 minutes. **Table II-4** summarizes the laboratory formula and mixing times to prepare a 1 barrel equivalent of the drilling fluid that contains 0.5 wt% of NPs.

Filtration Loss Measurements

NPs/Ca-Bentonite Suspension

The filtration characteristics and filter cake generation of the NPs/Ca-bentonite suspensions were investigated using an OFITE HP/HT filter press (**Fig. II-10**). The setup includes a 500 ml cell which was modified to use 2.5-in. in diameter and 1-in. in thickness cores instead of filter papers, cell caps, valve stems, heating element, and a nitrogen-gas line. The suspensions were put in the cell, and the cell was then put in the heating jacket. A differential pressure from 300 to 500 psi and a temperature range of 175 to 250°F were used. Furthermore, the fluid loss volume was measured as a function of time for 30

minutes, as per API standards. The filtrate fluids were collected and analyzed for the concentrations of key ions using ICP-OES. Moreover, a Toshiba Aquilion RXL CT scanner was used to investigate the produced filter cakes. CT images were taken through the full cake diameter and analyzed using Imagej® software. A Miniature Scanning Electron Microscope with X-ray NanoAnalysis (Evex Mini-SEM) was used for the SEM-EDS analysis of the filter cakes.

Additive	Description/Function	Amount Added				Mixing Time, min
		Lab Units (per 350 ml)		Field Unit (per bbl)		
		Quantity	Unit	Quantity	Unit	
Deionized Water	Base liquid	319	ml	0.911	bbl	—
Ca-Bentonite	Clay for viscosity/API filtrate control	24	g	24	lbm	20
Hyper-branched Polymer	Viscosifier	0.25	g	0.25	lbm	10
Pac-R	API HP/HT filtrate control	0.25	g	0.25	lbm	10
Lignosulfonate-based Thinner	Thinner	1	g	1	lbm	10
Caustic soda	Alkalinity agent	0.5	g	0.5	lbm	
Calcium carbonate (25 µm)	Weighting and bridging material	30	g	30	lbm	10
Manganese tetraoxide (5 µm)	Weighting material	20	g	20	lbm	10

Table II- 3—Laboratory formula to prepare 1 barrel equivalent of the bentonite based drilling fluid.

Additive	Description/Function	Amount Added				Mixing Time, min
		Lab Units (per 350 ml)		Field Unit (per bbl)		
		Quantity	Unit	Quantity	Unit	
Deionized Water	Base liquid	319	ml	0.911	bbl	—
Ca-Bentonite	Clay for viscosity/API filtrate control	24.14	g	24.14	lbm	20
Ferric oxide NPs	Nanoparticles	1.724	g	1.724	lbm	10
Ultrasonication for 1 hour						
Hyper-branched Polymer	Viscosifier	0.25	g	0.25	lbm	10
Pac-R	API HP/HT filtrate control	0.25	g	0.25	lbm	10
Lignosulfonate-based Thinner	Thinner	1	g	1	lbm	10
Caustic soda	Alkalinity agent	0.5	g	0.5	lbm	
Calcium carbonate (25 µm)	Weighting and bridging material	30	g	30	lbm	10
Manganese tetraoxide (5 µm)	Weighting material	20	g	20	lbm	10

Table II- 4—Laboratory formula to prepare 1 barrel equivalent of the drilling fluid having 0.5 wt% of NPs.



Fig. II- 10—OFITE Dynamic HP/HT Filter Press.

Fully Formulated Drilling Fluid

The filtration properties and the filter cake characteristics of the NPs/Ca-bentonite-base drilling fluids were investigated at different conditions of pressure and temperature using the HP/HT filter press. In this study, the effectiveness of ferric oxide NPs on the filter cake properties of Ca-bentonite-based drilling fluids had been investigated. A complete drilling fluid formula containing polymer and different drilling fluid additives was formulated and examined. The filtration volume was determined with time for 30 minutes, and the filtrate fluids were collected. The CT scanner was used to investigate the formed filter cakes. CT images were taken through the full cake diameter and analyzed

using the software. The CT data was analyzed to determine the filter cake thickness and CT number (CTN). SEM-EDS was used to analyze the dried filter cakes for surface morphology and elemental content. Moreover, a parametric study was conducted on the performance of the formulated NPs/Ca-bentonite-based drilling fluid to reveal their effectiveness. The investigated parameters were: the NP concentration, drilling fluid preparation method (using ultrasonication and bentonite hydration), filtration temperature and differential pressure, and the drilling conditions (static or dynamic filtration).

CHAPTER III

USING NANOPARTICLES TO DEVELOP MODIFIED CA- BENTONITE FLUIDS ^{5,6}

Introduction

In this chapter, the analysis of the measurements carried out on the NPs/Ca-bentonite suspensions are presented and discussed. The objective is to investigate experimentally the influence of using NPs on the properties of Ca-bentonite-based fluids under downhole conditions (up to 350°F and 500 psi). Different types of oxide NPs were used in this study. Zeta potential measurements were conducted at different temperatures and NP concentrations, which gave insights onto their stability in suspensions and the role of charge potential. Furthermore, the sensitivity of the rheological properties of these NPs/Ca-bentonite fluids are studied at temperatures up to 200°F, with and without using thermal aging (at 350°F for 16 hours), to assess their stability. A combination of computed-tomography (CT) scan, scanning electron microscopy-energy dispersive spectroscopy (SEM-EDS), X-ray diffraction (XRD), and inductively coupled plasma-optical emission spectrometry (ICP-OES) provided detailed insights on the effect of NPs on the filter cake characteristics and the role of NPs in building the cake structure. The

⁵ Reprinted with a permission from “Nanoparticle-Based Drilling Fluids for Minimizing Formation Damage in HTHP Applications” by Mahmoud, O., Nasr-El-Din, H. A., Vryzas, Z., and Kelessidis, V. C. SPE-171849-MS, Copyright 2016 by Society of Petroleum Engineers.

⁶ Reprinted with a permission from “Development and Testing of Novel Drilling Fluids Using Fe₂O₃ and SiO₂ Nanoparticles for Enhanced Drilling Operations” by Vryzas, Z., Mahmoud, O., Nasr-El-Din, H. A., and Kelessidis, V. C. IPTC-18381-MS, Copyright 2015 by Society of Petroleum Engineers.

obtained rheological measurements were fitted to the classical drilling fluid models to determine the best fit-model, which can then be applied for more efficient drilling fluid design.

A reduction of 43% in the filtrate fluid volume was achieved when using 0.5 wt% of ferric oxide or magnetic iron oxide NPs compared to that of the base fluid. However, using silica or zinc oxide NPs led to an increase in the filtrate loss volume and filter cake thickness. Using 0.5 wt% of ferric oxide NPs provided less agglomeration and reduced the filter cake permeability. Additionally, the EDS and ICP-OES analysis showed a replacement of the cations dissociated from the bentonite by NPs, which promoted the formation of a rigid clay-platelet structure. Moreover, the produced filter cakes consisted of two layers, as indicated by the CT scan analysis. Increasing the concentration of NPs resulted in an increase in the fluid loss and filter cake thickness. At a higher ferric oxide or magnetic iron oxide NP concentration (2.5 wt%), a new layer of NPs formed, which adversely affected the filter cake characteristics, as demonstrated by CT scan analysis and SEM-EDS elemental mapping. The NPs/Ca-bentonite fluids have stable rheological properties at different temperatures (up to 200°F) and different NP concentrations. Additionally, aging these fluids at 350°F for 16 hours showed minor changes in rheological properties. The Herschel-Bulkley was found to be the best fit model for the experimental data of the tested NPs/Ca-bentonite fluids with R^2 values higher than 0.99 and minimum $\sum Q^2$ values, especially at higher temperatures.

Zeta Potential Analysis

The zeta potential (ζ) measurements gives a good indication about the potential stability of a colloidal system. If the suspended particles in the system have a large negative or positive ζ , then they will repulse each other and there will be no tendency for them to come together. This repulsion results in a greater separation between particles in the suspension and reduces the particle aggregation/flocculation caused by Van der Waals interactions. However, if the particles have lower magnitudes of ζ then there will be no force to prevent the particles coming together and flocculating (Hunter 1988). A general dividing line can be drawn between the stable and unstable suspension cases. Particles with ζ values of more positive than +30 mV or more negative than -30 mV are generally considered stable.

Bentonite

A sample of 7 wt% of bentonite suspension had been prepared for such measurement. The pH of the suspension was 8.65. The measurements showed that, the used Ca-bentonite had a mean ζ of -44.8 mV, which indicated stable suspension with a negative surface charge (**Table III-1**). Generally, the ζ of bentonite suspensions is negative over a pH range of 2 to 12 (Missana and Adellm 2000; Yalcin et al. 2002), which reveals high affinity to attach with particles that have positive surface charge.

pH	Zeta potential (ξ) (mV)				Standard Deviation	Standard Error
	Run 1	Run 2	Run 3	Mean		
8.65	- 43.01	- 46.39	- 45.00	- 44.80	1.6988	0.9808

Table III- 1—Zeta potential of 7 wt% Ca- bentonite suspension at 78°F.

Nanoparticles

Often, the NPs are applied in wet conditions, which resulting in potential changes in charged conditions because of aggregation and surface reactions. **Table II-2** shows the ζ of the Fe₂O₃ NPs suspensions that had different NP concentration at two different temperatures 78°F and 100°F. The measured ζ values ranged from +39.53 to +44.96 mV at 78°F and from +39.12 to +48.43 mV at 100°F, which indicating a stable NP suspension and a positively charged NP surface. The measurements at two different temperature showed that the change in temperature had a relatively small effect on the surface charge of these particles. Wang et al. (2013) measured the effect of pH on the zeta potential of different types of iron-based NPs at various particle concentrations. The authors reported that the ζ of those NPs is positive at low pH and decreases with increasing the pH until becomes negative at high pH.

Nanoparticle Concentration, wt%	pH*	Temperature = 78°F		Temperature = 100°F	
		Zeta Potential, mV	Standard Error	Zeta Potential, mV	Standard Error
0.1	5.90	+40.25	1.13	+39.12	0.42
0.2	4.66	+44.96	0.56	+40.47	0.72
0.3	4.28	+43.89	0.93	+48.43	0.94
0.4	4.15	+42.29	1.03	+42.10	1.31
0.5	4.05	+39.53	0.84	+41.48	1.60

* pH was measured at 78°F

Table III- 2—Zeta potential of ferric oxide NPs measured at different concentrations and two different temperatures (78°F and 100°F).

On the other hand, the zeta potential of silica NPs ranged from -26.72 to -20.87 mV at 78°F and from -24.05 to -13.44 mV at 100°F, which indicated an incipient

instability of the colloidal suspension (**Table II-3**). The increase in temperature adversely affected the stability of silica NPs in suspensions by changing the ζ values toward the range of instability. Shin et al. (2008) measured the ζ of silica NPs with an average size of 150 (± 17.9) nm. The ζ value of this pure silica NPs was reported to be -43.1(± 1.9) mV. Xu et al. (2003) used silica powder of a mean volumetric diameter of 0.83 μm to evaluate the influence of complexation on the ζ of this powder. The authors found that the ζ of the pure silica powder suspensions were negatively charged over a wide range of pH.

Nanoparticle Concentration, wt%	pH*	Temperature = 78°F		Temperature = 100°F	
		Zeta Potential, mV	Standard Error	Zeta Potential, mV	Standard Error
0.1	7.01	-25.81	0.50	-22.99	0.98
0.2	6.58	-25.20	0.78	-19.86	1.23
0.3	6.33	-24.70	0.86	-18.56	1.38
0.4	6.23	-20.87	0.37	-13.44	0.94
0.5	6.25	-26.72	0.55	-24.05	1.19

* pH was measured at 78°F

Table III- 3—Zeta potential of Silica NPs measured at different concentrations and two different temperatures (78°F and 100°F).

Zeta potential measurements of magnetic iron oxide (Fe_3O_4) NPs (average diameter 50-100 nm) are shown in **Table III-4**. The zeta potential shifted from negative values at low concentration to positive values at concentration greater than 0.25 wt%. At a NP concentration of 0.5 wt%, the zeta potential was +18.7 mV. In addition, the values are in the range of low stability suspensions. These results matched what was mentioned in the literature (Wang et al. 2013).

Zeta potential measurements of zinc oxide (ZnO) NPs (average diameter <100 nm) are shown in **Table III-5**. The zeta potential values for the suspensions of ZnO NPs showed that the surface charge of this type of particles is almost neutral with a maximum value of nearly +1 mV at a NP concentration of 0.3 wt%.

Nanoparticle Concentration, wt%	pH	Temperature = 78°F	
		Zeta Potential, mV	Standard Error
0.1	6.02	-18.71	2.17
0.2	5.61	-22.38	1.20
0.3	5.69	17.41	1.51
0.4	5.51	18.71	1.04
0.5	5.33	18.78	1.14

* pH was measured at 78°F

Table III- 4— Zeta potential of magnetic iron oxide (Fe₃O₄) NPs at different concentrations.

Nanoparticle Concentration, wt%	pH	Temperature = 78°F	
		Zeta Potential, mV	Standard Error
0.1	7.12	0.17	0.21
0.2	7.19	0.81	0.28
0.3	7.34	0.97	0.71
0.4	7.50	0.51	0.57
0.5	7.57	0.11	0.41

* pH was measured at 78°F

Table III- 5— Zeta potential of zinc oxide (ZnO) NPs at different concentrations.

Rheological Analysis

The rheological studies were conducted on the Ca-bentonite-based suspensions having different concentrations of NPs at various temperatures (120, 140, 160, 180, and 200°F) and ambient pressure. The fluctuations in the data may be due to a possible

evaporation of water from the base fluid at atmospheric pressure (see **Appendix A** for more information about Ca-bentonite dehydration). The resulted shear stress versus shear rate data was fitted to the most common non-Newtonian rheological models (Bingham Plastic and Herschel-Bulkley). These models can be described as follows (**Eqs. III-1**, and **III-2**):

Bingham Plastic model:

$$\tau = \tau_o + \mu_p \dot{\gamma} \quad , \dots\dots\dots \text{(III-1)}$$

where τ is the shear stress (lbf/100 ft²), τ_o is the yield stress (lbf/100 ft²), μ_p is the plastic viscosity (cp), and $\dot{\gamma}$ is the shear rate (s⁻¹).

Herschel-Bulkley model:

$$\tau = \tau_o + K \dot{\gamma}^n \quad , \dots\dots\dots \text{(III-2)}$$

where K is the consistency index (lbf. sⁿ/100 ft²), and n is the flow behavior index (dimensionless).

Ca-Bentonite Base Fluid

Fig. III-1 shows the shear stress versus shear rate (rheograms) of the base fluid (7 wt% bentonite in deionized water) at different temperatures. The yield stress increased and the viscosity decreased with the increase in temperature. The yield stress was estimated from the rheograms by extrapolating the shear stress-shear rate curve to zero shear rate and fitting the experimental data with the rheological model. The rheological parameters were determined by the least-square fit method (**Table III-6**). The regression coefficient (R^2) and sum of square errors ($\sum Q^2$) were used to indicate the best fit between

measured and predicted values. The results indicated that the Herschel-Bulkley model best fitted the experimental data with R^2 and $\sum Q^2$ values better than the other model especially at high temperatures.

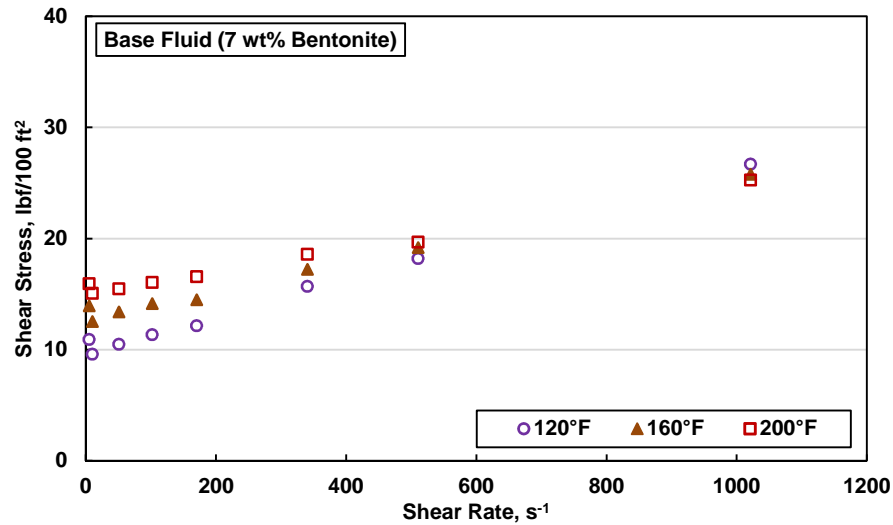


Fig. III- 1— Rheograms of the base fluid (7 wt% bentonite) at different temperatures.

Temperature	Bingham Plastic Model				Herschel-Bulkley Model				
	τ_o	μ_p	R^2	$\sum Q^2$	τ_o	k	n	R^2	$\sum Q^2$
(°F)	(lbf/100 ft ²)	(cp)		(lbf/100 ft ²) ²	(lbf/100 ft ²)	(lbf. s ⁿ /100 ft ²)			(lbf/100 ft ²) ²
120	9.64	8.00	0.9966	1.7547	9.25	0.0331	0.9046	0.9947	2.8112
140	10.41	7.08	0.9961	1.6646	10.26	0.0228	0.9389	0.9949	2.0196
160	12.75	6.11	0.9942	1.6235	12.31	0.0278	0.8923	0.9984	0.5174
180	14.32	6.21	0.9953	1.4850	14.36	0.0120	1.0105	0.9997	0.0826
200	14.96	4.84	0.9944	1.0835	14.88	0.0145	0.9486	0.9979	0.4083

Table III- 6— Bingham Plastic and Herschel-Bulkley model constants of the base fluid (7 wt% Ca-bentonite) at different temperatures (pH = 8.36 at 78°F).

Annis (1967) reported that at high temperatures the flow curves of bentonite suspensions becomes more shear-thinning and non-Newtonian with increasing temperature, which results in higher yield stresses and lower plastic viscosities.

Additionally, this change indicated a flocculation of bentonite in suspension, which was found to increase with time at high temperatures. Bentonite becomes more dispersed when exposed to high temperatures for long times. This cause the increase in the number of individual clay platelets in suspension, and the increase in viscosities at low shear rates. Moreover, the flocculation of clay suspension at high temperatures was reported to be a result of modifications in the electrical double layer surrounding the clay platelets due to release of the ions (Alderman et al. 1988).

NPs/Ca-Bentonite Fluids

Better rheological properties at high temperatures were obtained when adding ferric oxide NPs to the base fluid. **Fig. III-2** shows the rheograms of the fluids that have 0.5 wt% ferric oxide NPs at different temperatures. Higher yield stress values were obtained at different temperatures comparing to that of the base fluid (Fig. III-1). Higher yield stress results in more efficient hole-cleaning while drilling by ensuring better dynamic suspension of the drilling cuttings.

For bentonite suspensions, the zeta potential (ζ) is negative over a pH range from 2 to 12 (Missana and Adell 2000; Yalcin et al. 2002). Table III-1 shows that the ζ of the bentonite used at this study had a mean value of -44.8 mV at 78°F. Table III-2 shows the zeta potential (ζ) of the Fe₂O₃ NP suspensions. The ζ of this type of NPs were relatively constant, positive, and ranged from +39.53 to +44.96 mV at 78°F and from +39.12 to +48.43 mV at 100°F. These measurements indicated the randomly embedding of ferric oxide NPs on the surface of clay particle in the formed pore structure, which supported gelation and increased the yield stress and viscosity of suspension (Baird and Walz 2006;

Szabo et al. 2007; Jung et al. 2011; Barry et al. 2015). The same behavior was followed when using different concentrations of magnetic iron oxide Fe_3O_4 NPs.

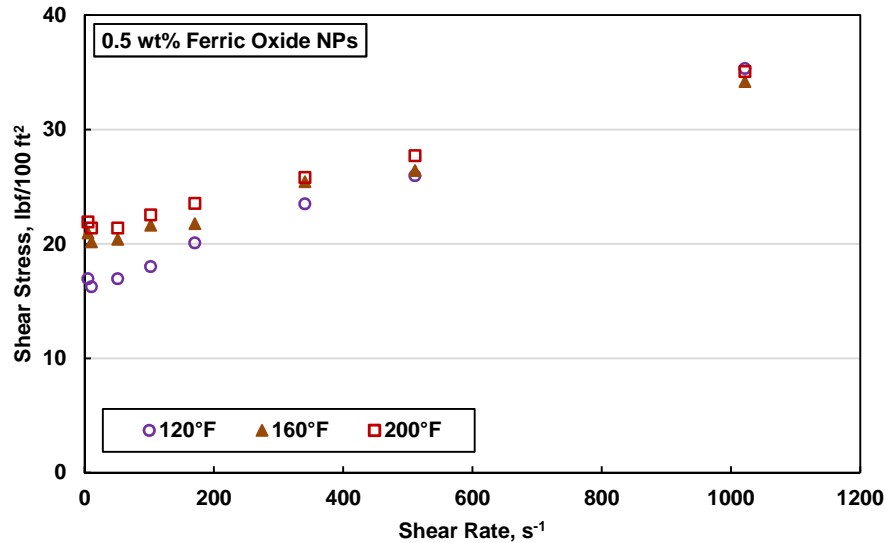


Fig. III- 2— Rheograms of the fluid containing 0.5 wt% of ferric oxide NPs at different temperatures.

This enhancement in the rheological properties increased with increasing the NP concentration. **Fig. III-3** shows the rheograms of different ferric oxide NP concentrations at 140°F. This might be explained as a synergy effect of homocoagulation between the exceeded ferric oxide NPs and heterocoagulation of ferric oxide NPs with bentonite particles in suspension (Tombácz et al. 2001). **Table III-7** shows the fitted rheological parameters of the fluids containing 0.5 wt% of ferric oxide NPs at different temperatures. The Herschel-Bulkley model best fitted the experimental data with R^2 values higher than 0.99 and minimum $\sum Q^2$ values, especially at higher temperatures. In addition, the increase in the consistency index (K) implies a relatively increased viscosity compared to that of the base fluid. For more details, see **Appendix B**.

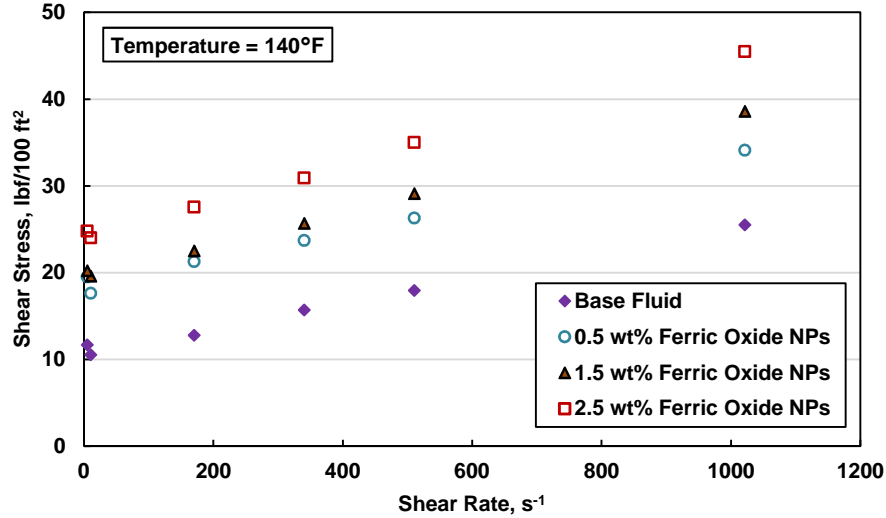


Fig. III- 3— Rheograms of the fluid containing different concentrations of ferric oxide NPs at 140°F.

Temperature (°F)	Bingham Plastic Model				Herschel-Bulkley Model				
	τ_o (lbf/100 ft ²)	μ_p (cp)	R^2	$\sum Q^2$ (lbf/100 ft ²) ²	τ_o (lbf/100 ft ²)	k (lbf. s ⁿ /100 ft ²)	n	R^2	$\sum Q^2$ (lbf/100 ft ²) ²
120	16.36	8.90	0.9977	1.5315	15.55	0.0628	0.8303	0.9968	2.2210
140	18.55	7.29	0.9950	2.0324	17.21	0.0706	0.7907	0.9945	3.0057
160	20.09	6.61	0.9931	2.2420	19.70	0.0334	0.8764	0.9936	2.5098
180	20.66	6.24	0.9961	1.1418	20.18	0.0277	0.8964	0.9985	0.5145
200	21.16	6.51	0.9974	0.8486	21.04	0.0165	0.9736	0.9987	0.4398

Table III- 7— Bingham Plastic and Herschel-Bulkley model constants fitted for the fluid containing 0.5 wt% of ferric oxide NPs at different temperatures (pH = 8.15 at 78°F).

Using silica NPs resulted in a decrease in yield stress. Fig. III-4 and Table III-8 show the rheograms and the fitted rheological parameters of the fluids that have 0.5 wt% of silica NPs at different temperatures. Fig. III-5 shows the rheograms at 140°F and

different silica NPs concentrations. The Herschel-Bulkley was the best fit model of the experimental data. A better viscosity profile (an increase in K and a decrease in n values) was obtained when adding silica NPs. Despite the fact that the decrease in the NP size can enhance the rheological properties of Ca-bentonite suspensions, the addition of negatively charged NPs could have an adversely effect on the properties of such suspension. The zeta potential (ζ) for the suspensions of silica NPs are negative and range from -26.72 to -20.87 mV at 78°F and from -24.05 to -13.44 mV at 100°F (Table III-3). The clay surface has a strong negative charge; however, the edge surfaces of the layers has a much weaker positively charged double layer. The addition of negatively charged NPs resulted in a weak edge-to-edge platelet structure, and thus, a weak yield structure (Luckham and Rossi 1999). The same behavior was followed when using different concentrations of magnetic iron oxide zinc oxide NPs.

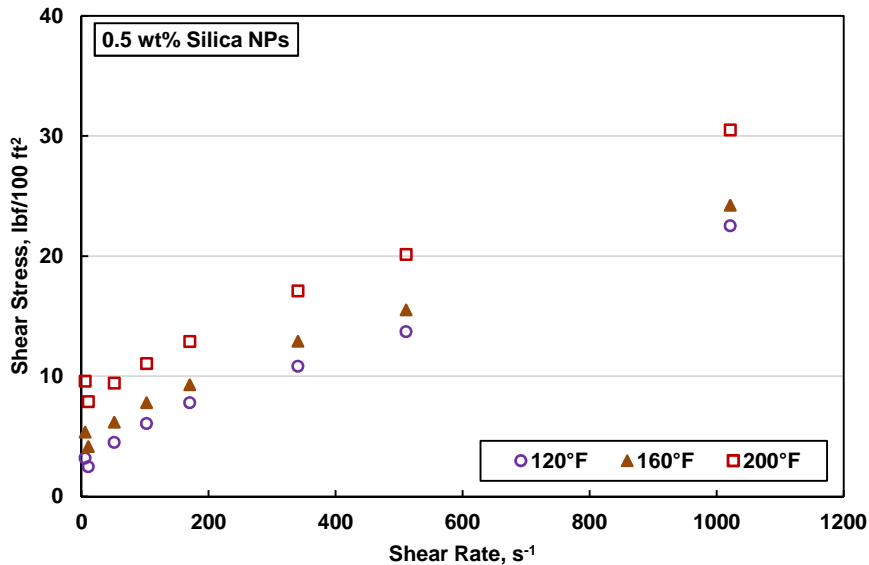


Fig. III- 4— Rheograms of the fluid containing 0.5 wt% of silica NPs at different temperatures.

The apparent viscosity of all the fluids tested in this work decreased with increasing shear rate (i.e., shear-thinning behavior) (**Fig. III-6**). An increase in the concentration of NPs stabilized the viscosity at higher temperatures, which is an indication of the capability of NPs to restrain and suppress the reduction in viscosity (for more details, see **Appendix B**).

Temperature	Bingham Plastic Model				Herschel-Bulkley Model				
	τ_o	μ_p	R^2	$\sum Q^2$	τ_o	k	n	R^2	$\sum Q^2$
	(°F)	(lbf/100 ft ²)	(cp)	(lbf/100 ft ²) ²	(lbf/100 ft ²)	(lbf. s ⁿ /100 ft ²)			(lbf/100 ft ²) ²
120	3.49	9.59	0.9934	5.0166	2.95	0.0627	0.8289	0.9984	1.1188
140	4.18	9.63	0.9933	4.6674	3.71	0.0718	0.8130	0.9975	2.0959
160	5.26	9.63	0.9929	5.4799	5.16	0.0489	0.8608	0.9974	2.2486
180	6.86	9.86	0.9924	6.0933	6.60	0.0343	0.9199	0.9951	3.8995
200	9.35	9.91	0.9959	4.5486	9.48	0.0177	1.0221	0.9956	5.1903

Table III- 8 — Bingham Plastic and Herschel-Bulkley model constants fitted for the fluid containing 0.5 wt% of silica NPs at different temperatures (pH = 7.7 at 78°F).

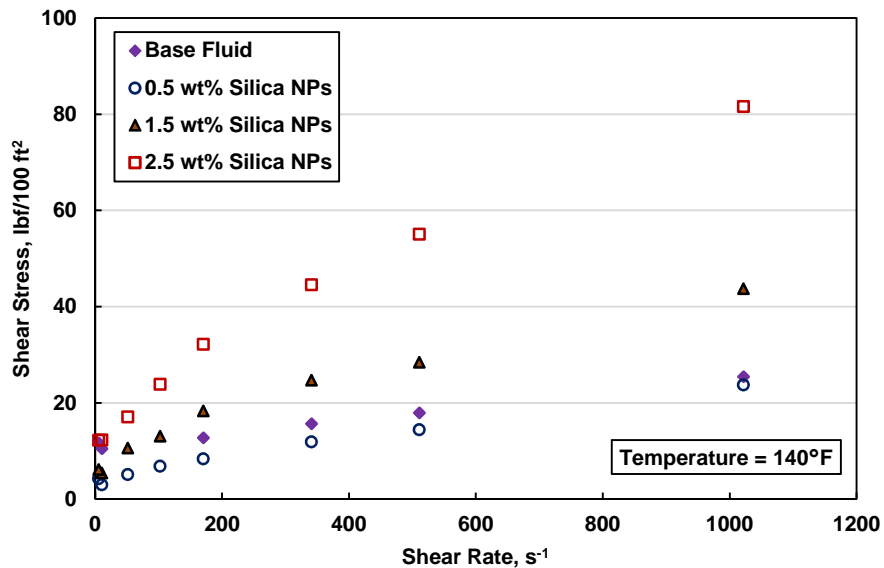


Fig. III- 5— Rheograms of fluid containing different concentrations of silica NPs at 140°F.

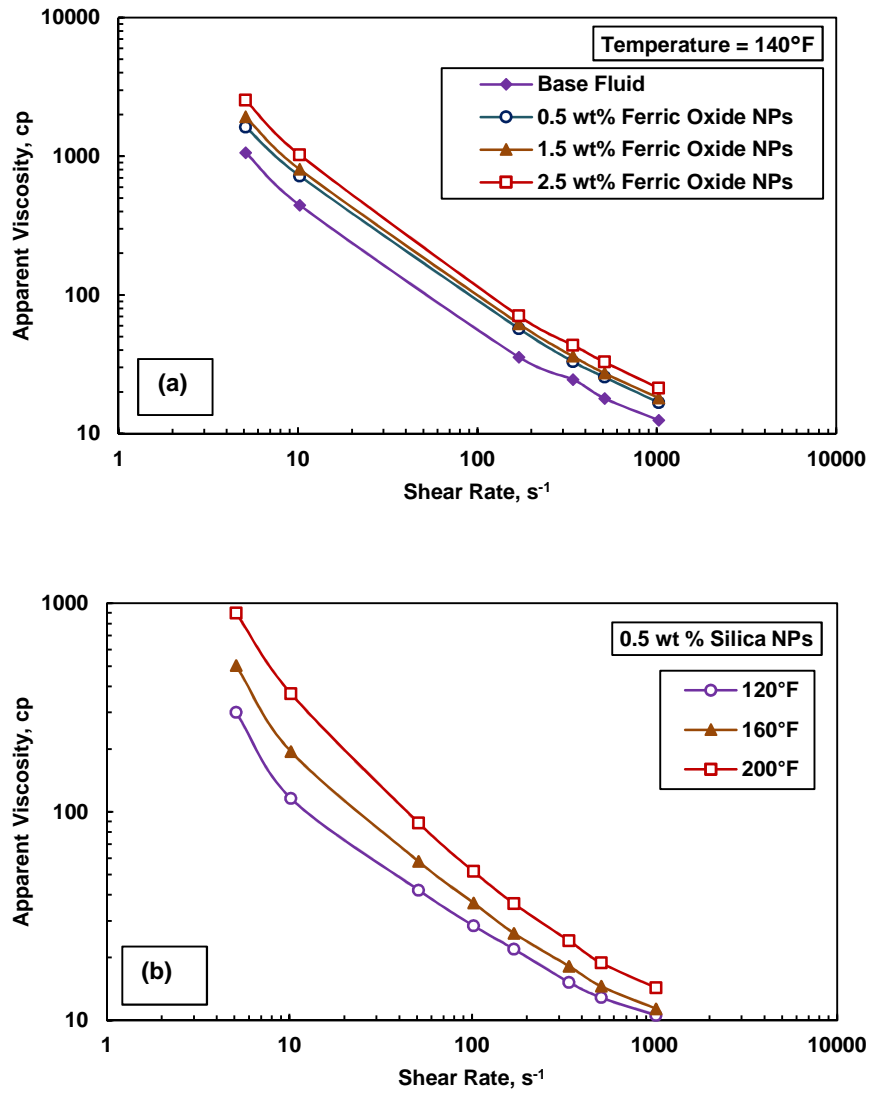


Fig. III- 6—The change of apparent viscosity with shear rate for the fluids having: (a) different ferric oxide NP concentrations at 140°F, (b) a silica NP concentration of 0.5 wt% at different temperatures.

Effect of Aging

After dynamically aged at 350°F for 16 hours, rheological property measurements were conducted on samples containing 0.5 wt% of NPs to determine if the NPs could maintain effectiveness in preserving the rheological properties of these fluids.

Tables III-9 and **III-10** show the rheological parameters at different temperatures for the aged drilling fluids having 0.5 wt% of NPs. The experimental data after aging for NPs/Ca-bentonite-based fluids fitted the Herschel-Bulkley model with a regression coefficient (R^2) higher than 0.9, but relatively higher sum of square errors, $\sum Q^2$. Aging samples having ferric oxide NPs resulted in minor changes in the rheological properties at different temperatures compared to the unaged suspensions. This indicated a stable rheological behavior of this fluids at high temperature conditions. For the samples having silica NPs, aging resulted in a change in the yield stress by two or three times at all temperatures compared to the unaged suspensions. This change indicated unstable rheological properties behavior of this silica NPs/Ca-bentonite-based fluid. For more details, see **Appendix B**.

Filtration Loss Analysis

Filter Press Results

Table III-11 shows the filtration and filter cake characteristics for the experiments conducted at a differential pressure of 300 psi and 250°F. Three identical filtration tests had been conducted using three samples of the base fluid. The results revealed that the cumulative filtrate volume and filter cake thickness were within 5% of each other, which indicating the repeatability of the filtration test results (**Table III-11**). Adding ferric oxide or magnetic iron oxide NPs at 0.5 wt% concentration improved the fluid loss and filter cake characteristics. A reduction of 42.5 vol% in the filtrate loss volume was achieved compared to that of the base fluid (**Table III-11** and **Fig. III-7**). The high temperatures induced the dissociation of Ca^{2+} cations from the surface of bentonite (Ramos-Tejada et

al. 2001; Laribi et al. 2006). Strong electrical attraction produced between the ferric oxide NPs (with large surface-area-to-volume ratio and positive surface charge) and the negatively charged face of the clay platelet. Additionally, this also kept the clay platelet dispersed and flocculated in suspension, which generated a low porosity/low permeability filter cake. Using 0.3 wt% of ferric oxide NPs was not enough for building a rigid clay platelet structure, which resulted in higher filtrate fluid volume compared to the sample that had 0.5 wt% NPs. However, at higher NP concentration (1.5 and 2.5 wt%), the filtrate volume and filter cake thickness increased because of the agglomeration of the excess NPs, which reduced the filter cake efficiency. The fluid loss results when using magnetic iron oxide Fe_3O_4 NPs were almost the same compared to the samples containing ferric oxide NP; however, the filter cake thickness values were lower. Moreover, the samples containing silica or zinc oxide NPs showed lower filter cake efficiency at different NP concentrations (Table III-11 and Fig. III-7). Adding silica NPs at any concentration increased the filtrate volume and filter cake thickness. The silica NPs, with negative surface charge, acted as a diflocculant in the bentonite suspension, which promoted clay platelet dispersion at elevated temperatures (Bourgoyne et al. 1991). This led to the formation of a weak edge-to-edge bentonite platelet structure (Luckham and Rossi 1999). In addition, the silica NPs were also found to be unstable in suspensions (Table III- 3).

The effect of dynamic filtration was examined at 100 rpm for the sample that have 0.5 wt% of ferric oxide NPs. A decrease in the filter cake thickness by 18.24% and an increase in the filtrate volume by 79.71 vol% was obtained compared to the sample that has the same NP concentration under static condition (Table III-11). The cake is

simultaneously eroded and deposited because of the circulation that affect the solid particles under dynamic condition (Al-Abduwani et al. 2005), which led to these changes in filtrate volume and cake thickness. For more details of the filtrate loss volumes, see **Appendix C**.

Temperature	Bingham Plastic Model				Herschel-Bulkley Model				
	τ_o	μ_p	R^2	$\sum Q^2$	τ_o	k	n	R^2	$\sum Q^2$
(°F)	(lbf/100 ft ²)	(cp)		(lbf/100 ft ²) ²	(lbf/100 ft ²)	(lbf. s ⁿ /100 ft ²)			(lbf/100 ft ²) ²
120	11.93	27.15	0.9810	120.3	16.56	0.0127	1.1792	0.9653	186.4
140	15.24	26.21	0.9839	90.95	13.89	0.1470	0.8491	0.9933	30.49
160	17.37	26.83	0.9884	70.99	17.06	0.0828	0.9281	0.9924	39.73
180	23.52	25.53	0.9809	95.62	26.92	0.0333	1.0417	0.9795	88.76
200	27.71	25.55	0.9878	66.72	27.46	0.1287	0.8603	0.9938	23.56

Table III- 9— Bingham Plastic and Herschel-Bulkley model constants for the fluids containing 0.5 wt% of ferric oxide NPs at different temperatures measured after aging for 16 hours at 350°F (pH = 8.15 at 78°F).

Temperature	Bingham Plastic Model				Herschel-Bulkley Model				
	τ_o	μ_p	R^2	$\sum Q^2$	τ_o	k	n	R^2	$\sum Q^2$
(°F)	(lbf/100 ft ²)	(cp)		(lbf/100 ft ²) ²	(lbf/100 ft ²)	(lbf. s ⁿ /100 ft ²)			(lbf/100 ft ²) ²
120	10.12	34.08	0.9827	177.8	14.51	0.0961	0.9243	0.9881	185.7
140	14.75	32.58	0.9938	75.97	10.91	0.3033	0.7771	0.9995	3.55
160	18.54	27.25	0.9975	16.22	18.30	0.0889	0.9383	0.9985	9.63
180	20.64	27.25	0.9968	24.91	20.46	0.0602	0.9924	0.9967	23.86
200	21.97	27.04	0.9943	41.49	19.57	0.1767	0.8412	1.5628	7.71

Table III- 10— Bingham Plastic and Herschel-Bulkley model constants for fluid containing 0.5 wt% of silica NPs at different temperatures measured after aging for 16 hours at 350°F (pH = 7.7 at 78°F).

Ferric Oxide NPs (wt%)	Mode of Filtration	Filter Cake Thickness (in.)	Percentage Change In Thickness (%)	Cumulative Filtrate Volume (ml)	Percentage Change in Filtrate Volume (%)	Filter Cake Permeability (μ d)	Percentage Change in Permeability (%)	Spurt Loss Volume (ml)
0.0*	Static	0.3084	—	12	—	1.459	—	6.0
0.0	Static	0.3102	—	12	—	1.492	—	6.4
0.0	Static	0.3005	—	11.9	—	1.428	—	6.7
0.3	Static	0.3123	1.25	10	-16.67	0.857	-41.278	1.5
0.5	Static	0.3618	17.32	6.9	-42.5	0.345	-76.384	0.5
1.5	Static	0.433	40.4	9	-25	0.664	-54.464	2.5
2.5	Static	0.476	54.35	11.9	-0.83	1.298	-11.023	3.5
0.5	Dynamic	0.2958	-18.24**	12.4	79.71**	1.113	222.607**	0.5
Silica NPs								
(wt%)								
0.5	Static	0.3462	12.26	13.6	13.33	1.338	-8.247	3.5
1.5	Static	0.428	38.78	18.9	57.5	2.93	100.822	1.0
Magnetic Fe₃O₄ NPs								
(wt%)								
0.5	Static	0.2176	-29.44	9.25	-22.92	0.936	-35.846	0.5
1.5	Static	0.2921	-5.29	9	-25	0.885	-39.342	0.5
2.5	Static	0.2667	-13.52	9	-25	0.785	-46.196	0.5
Zinc Oxide NPs								
(wt%)								
0.5	Static	0.3412	10.64	13.2	10	2.71	85.744	3

* The base fluid that used in calculating the percent changes in the different properties

** The percentage compared to that of the same concentration under static filtration.

Table III- 11—Cumulative filtrate volume (for 30 min.) and filter cake properties of the fluids that having different NP types and concentrations at 250°F and 300 psi.

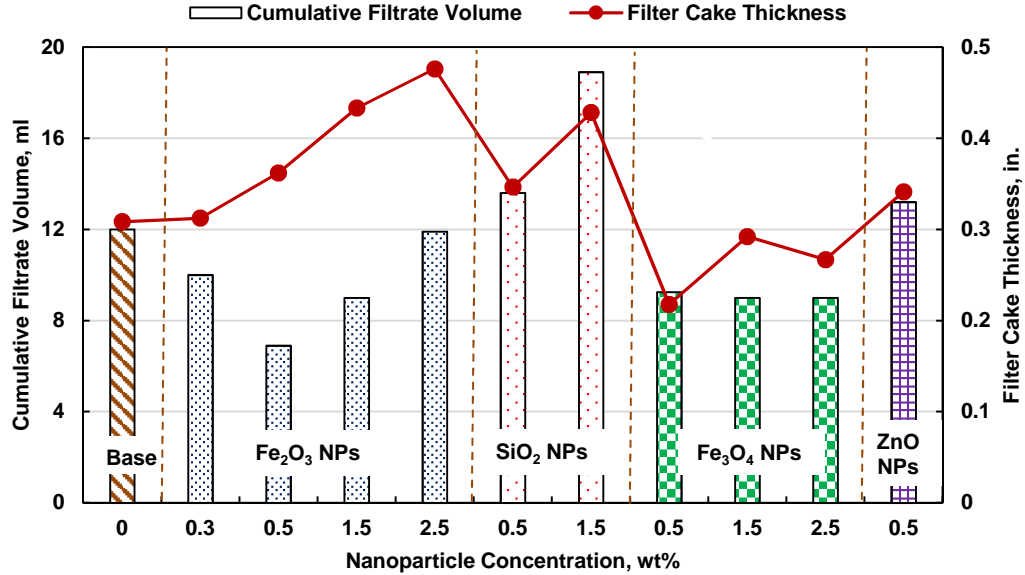


Fig. III- 7—Cumulative filtrate volume (30 minutes) and filter cake thickness for the cakes having different NP concentrations formed under static filtrations at 250°F and 300 psi differential pressure.

CT Scan Analysis of the Filter Cake

The filter cakes were CT scanned after the filtration test using a computed-tomography (CT) scanner. The images were taken through the full cake diameter. The filter cake generally consisted of two layers under wet conditions (**Fig. III-8**). The top layer (close to the drilling fluid) had a low CT-number (CTN) compared to the bottom layer (close to the formation surface). CT attenuation data is normally presented in a standardized scale with Hounsfield units (HU) that is normalized to air at -1000 HU and water at 0.0 HU. Thus, each HU represents a 0.1% change in density with respect to the calibration density scale (Wellington and Vinegar 1987; Akin and Kovsky 2003).

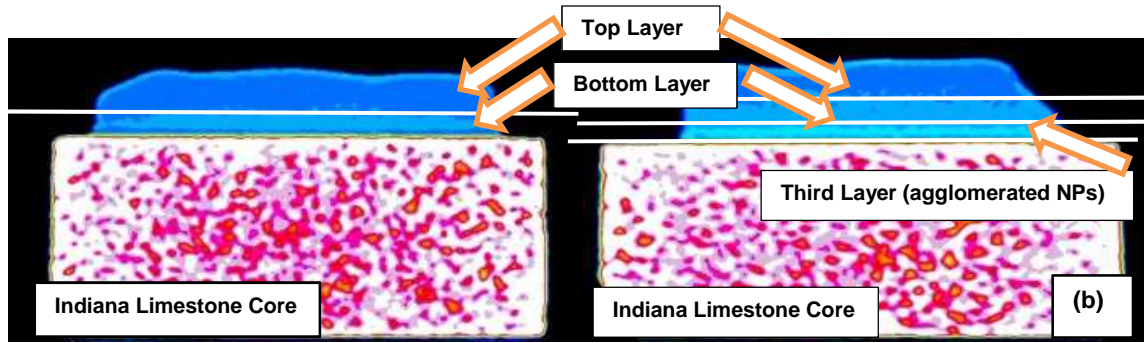


Fig. III- 8—CT scan images of the filter cakes having ferric oxide NPs under static conditions at 250°F and 300 psi differential pressure, (a) with 0.5 wt%, and (b) with 2.5 wt% of NPs.

Fig. III-9 shows the CTN profile through the filter cake diameter for each layer. The CTNs were averaged to be 299.46, 285.25, 292.89, and 305.27 HU for the top layer of the filter cakes that have 0.0, 0.3, 0.5, and 1.5 wt% of ferric oxide NPs, respectively. The CTNs of the bottom layer increased with the increase in the ferric oxide NP concentration. The average CTN of the bottom layer were 362.07, 377.08, 384.78, and 450.99 HU for the cakes that have 0.0, 0.3, 0.5, and 1.5 wt% of ferric oxide NPs, respectively. The specific gravities of bentonite and ferric oxide and magnetic iron oxide are 2.6, 5.24, and 5.17, respectively. The CTN profiles indicated that the NPs playing a key role in building the bentonite clay platelet structure in the bottom layer. Moreover, increasing the NP concentration reduced the cake efficiency. The NPs agglomerated and a new layer (third layer) of NPs (average CTN = 545.37 HU) settled down below the main filter cake layer (bottom layer) when using high NP concentration of 2.5 wt%. Jung et al. (2011) noticed the same behavior with Na-bentonite suspension that had 5.0 wt% of 3 nm ferric oxide NPs. They reported that a filter cake was produced with a nondeformable and relatively dense lower layer and a very large airy upper layer. The authors attributed that to the compaction of NPs. Fig. III-10 shows the 3D cross-section of the filter cake when

using 2.5 wt% of ferric oxide NPs, in which the agglomerated NPs (the third layer) appeared as a layer has a reddish brown color.

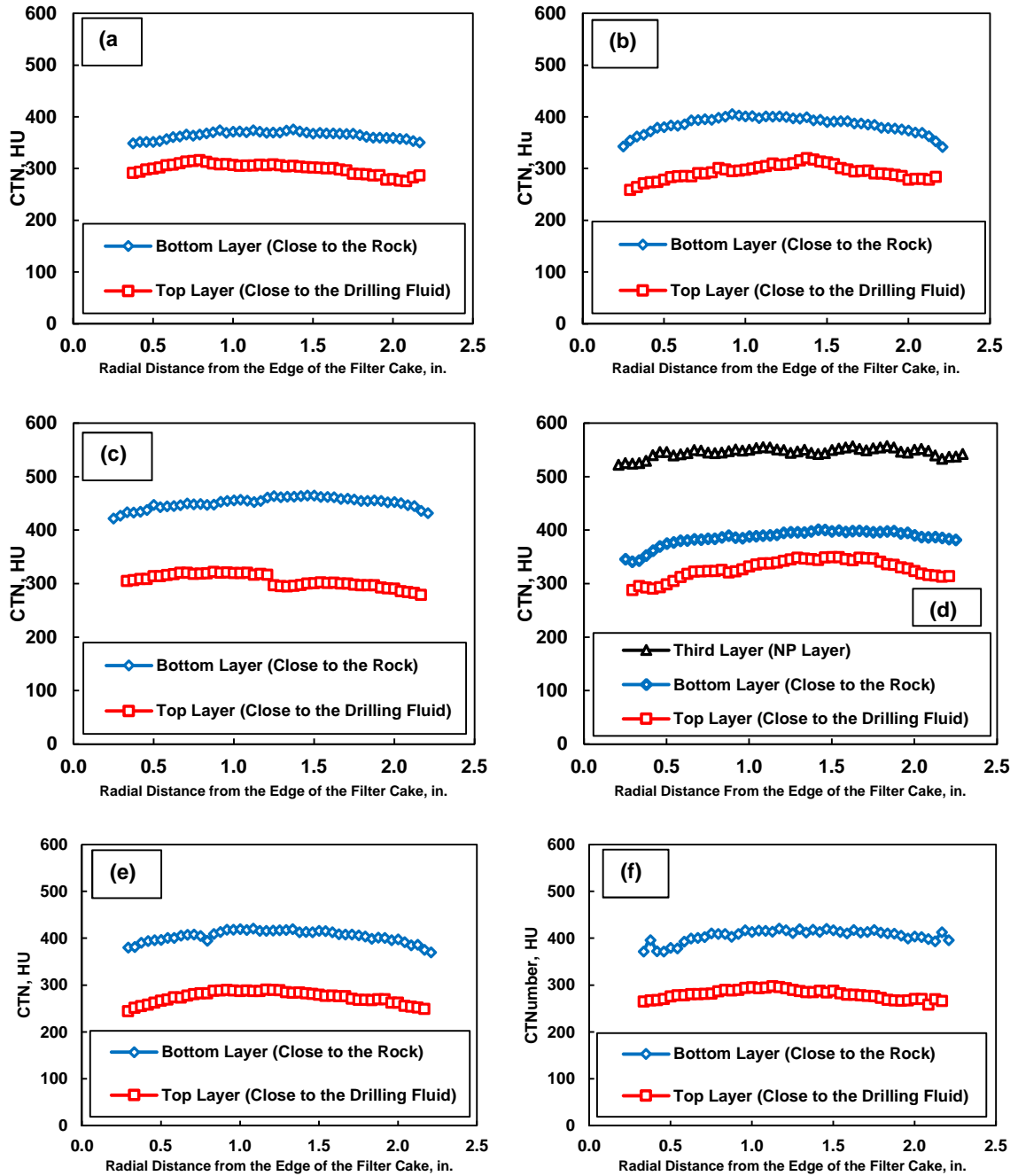


Fig. III- 9—CTNs through the filter cake of the samples that have different nanoparticle concentrations under static conditions at a differential pressure of 300 psi and a temperature of 250°F: (a) 0.0 wt%, (b) 0.5 wt% ferric oxide, (c) 1.5 wt% ferric oxide, (d) 2.5 wt% ferric oxide, (e) 0.5 wt% silica, and (f) 1.5 wt% silica nanoparticles.

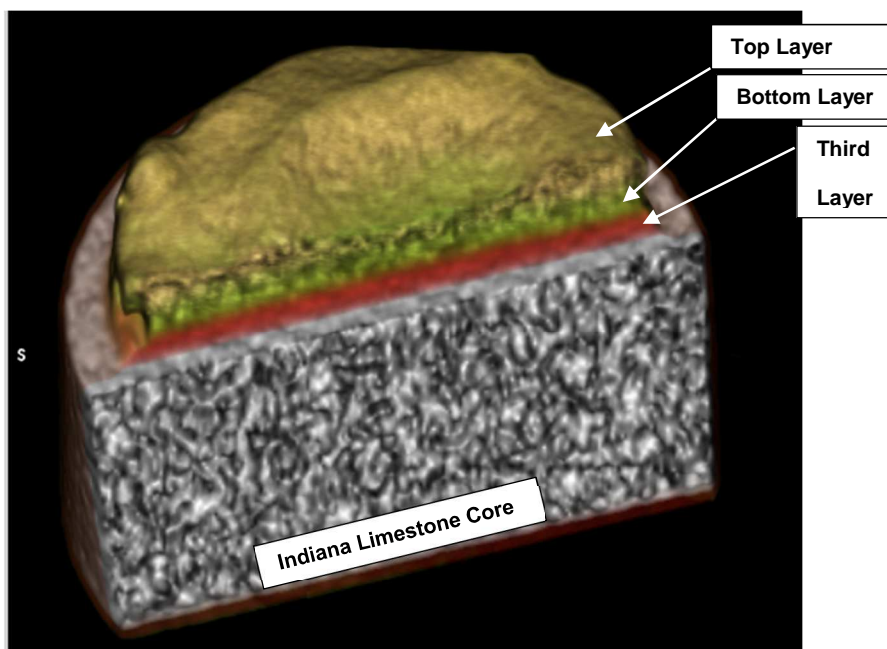


Fig. III- 10—3D CT scan cross-section of the filter cake having 2.5 wt% of ferric oxide NPs.

The CTNs were averaged to be 274.51 and 280.46 HU for the top layer of the filter cakes that have 0.5 and 1.5 wt% silica NPs, respectively (Fig. III-9e and III-9f). However, the average CTNs of the bottom layer were 404.40 and 405.84 HU for the same cakes, respectively (Fig. III-9e and III-9f). The CTN results for the filter cakes containing silica NPs revealed that this type of NPs settled down in the bottom layer without building a good structure with the bentonite particles, which reduced the cake efficiency.

Figs. III-11 and **III-12** shows the CT scan analysis of the filter cake containing 2.5 wt% of magnetic iron oxide Fe_3O_4 NPs through the filter cake in the direction of fluid flow. The CTNs were averaged to be 158.75, 226.12, 241.77, 265.90, 311.46 and 407.85 HU for the CT-slice numbers 1, 2, 3, 4, 5 and 6, respectively. The CTNs of the filter cake slices increased with the increase of the slice number in the direction of flow. Additionally,

the CT-slice numbers 2, 3, and 4 presented the top layer of the filter cake in this case; however the CT-slice number 5 presented the bottom layer of the filter cake. Again, the NPs agglomerated at this concentration (2.5 wt% of NPs) and a new layer (third layer) of NPs (average CTN = 407.85 HU) settled down below the main filter cake layer (bottom layer), which presented in the CT-slice number 6.

SEM-EDS Analysis of the Filter Cake

The filter cakes were dried in an oven at 250°F for three hours before running the SEM-EDS analysis. **Fig. III-13** shows the SEM images of filter cakes for the samples that have different ferric oxide NP concentrations. The bottom layer of the filter cake with 0.5 wt% ferric oxide NPs had a smoother surface morphology (**Fig. III-13b**) with minor agglomeration and low porosity/low permeability structure compared to the cakes with higher NP concentration.

Moreover, the EDS elemental analysis of the filter cakes containing ferric oxide NPs shows that the increase in NP concentration resulted in an increase in iron concentration and a decrease in calcium and magnesium concentrations in the filter cakes (**Fig. III-14**). This results confirmed the dissociation of cations from the Ca-bentonite clay surface and the embedding of ferric oxide NPs on the surface of clay particle, which support linking between bentonite particles. The EDS analysis of the third layer in the cake formed when using 2.5 wt% ferric oxide NPs showed that it is mainly contained ferric oxide NPs. The morphology of this layer showed high porosity/high permeability structure (**Fig. III-15a**). The SEM-EDS analysis for the filter cake that has 0.5 wt% of silica NPs showed the formation of a high porous/high permeable clay platelet structure

(Fig. III-15b). Additionally, Fig. III-14 shows also the EDS elemental analysis of the filter cake containing 0.5 wt% of silica NPs, which indicating that this layer is mainly contained silica NPs as revealed from the CT scan analysis.

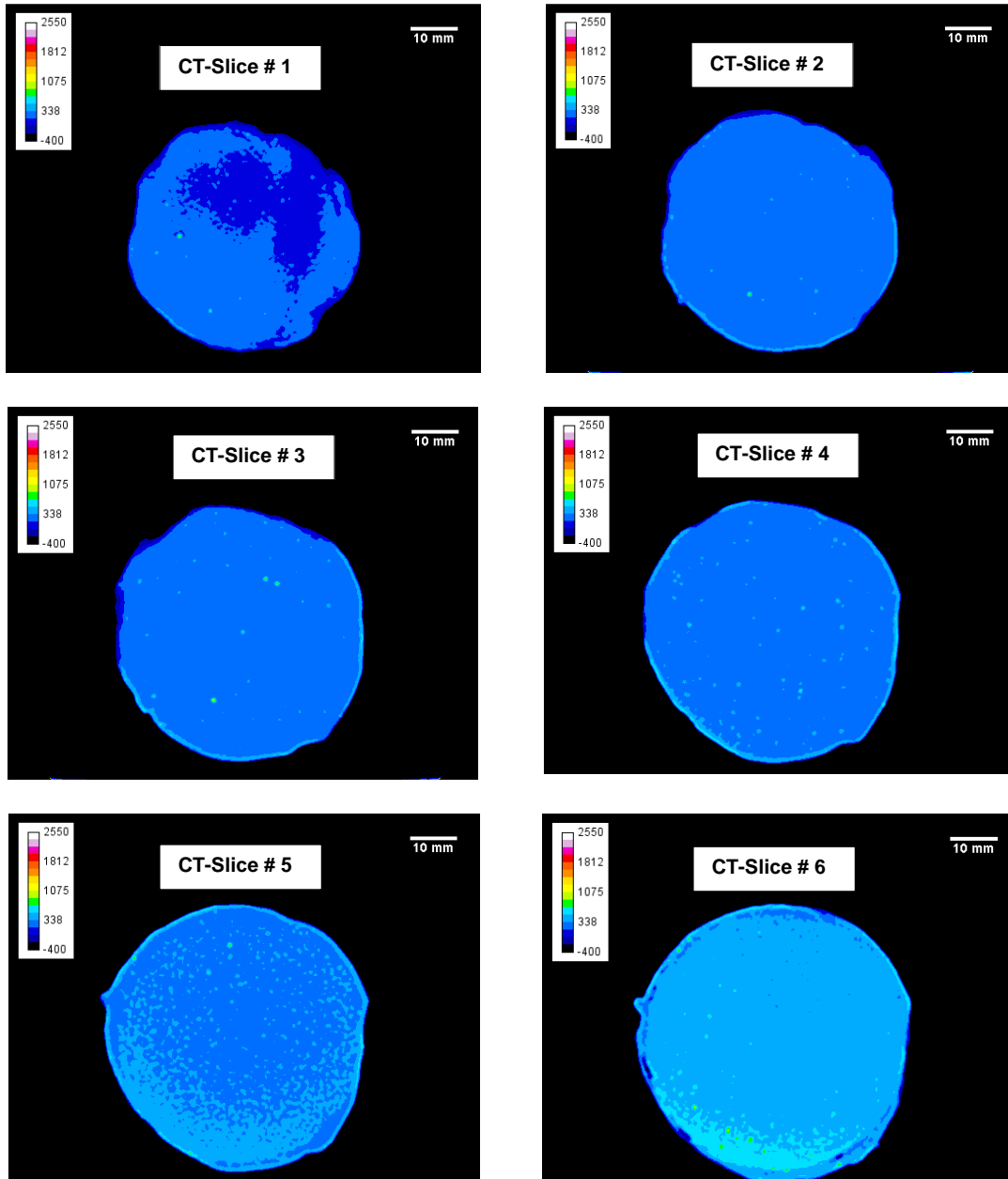


Fig. III- 11— CT scan images through the filter cake in the direction of fluid flow for the sample that has 2.5 wt% magnetic iron oxide Fe_3O_4 nanoparticles under static conditions at 250°F and a differential pressure of 300 psi.

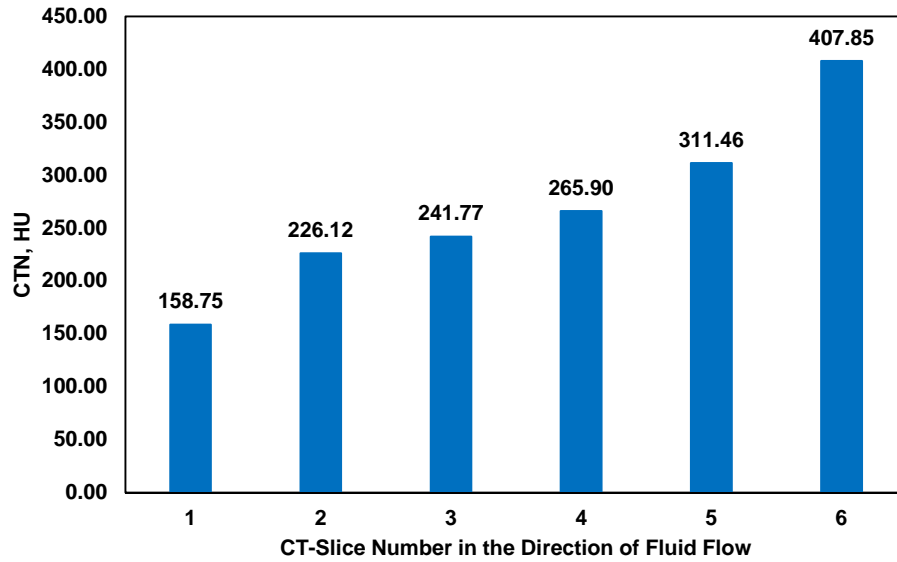


Fig. III- 12— CTN profile through the filter cake in the direction of fluid flow for the sample that has 2.5 wt% magnetic iron oxide Fe₃O₄ nanoparticles under static conditions at 250°F and a differential pressure of 300 psi.

Filter Cake Permeability

As a supportive way to quantify the changes in the filter cake properties upon the addition of NPs, the filter cake permeability was calculated using the Bourgoyne et al. (1991) model. In this model, the permeability was calculated using **Eq. III-3** and the relationship between the cumulative filtrate volume and the square root of time (**Fig. III-16**):

$$V_f = 8.4 \times 10^{-5} \sqrt{k_c \Delta p_c \left(\frac{f_{sc}}{f_{sm}} - 1 \right)} A \frac{\sqrt{t}}{\sqrt{\mu}}, \quad \dots\dots\dots \text{(III-3)}$$

where A = cross-sectional area of the core (in.²), k_c = permeability of the filter cake (d), t = time of filtration (s), V_f = cumulative filtrate volume (ft³), Δp_c = pressure drop across the filter cake (psi), μ = viscosity of the filtrate (cp), f_{sc} = volume fraction of the solids in the cake, and f_{sm} = initial volume fraction of solids in the drilling fluid. The pressure drop

across the filter cake was determined as the difference between the total applied differential pressure and the pressure drop across the core (using Darcy's equation for linear flow). The viscosity of the filtrate was assumed to be constant and equals the viscosity of the filtrate of the base fluid = 0.32 cp at 250°F, which was determined by extrapolating the data of **Fig. III-17** to 250°F. It was measured using a capillary tube viscometer.

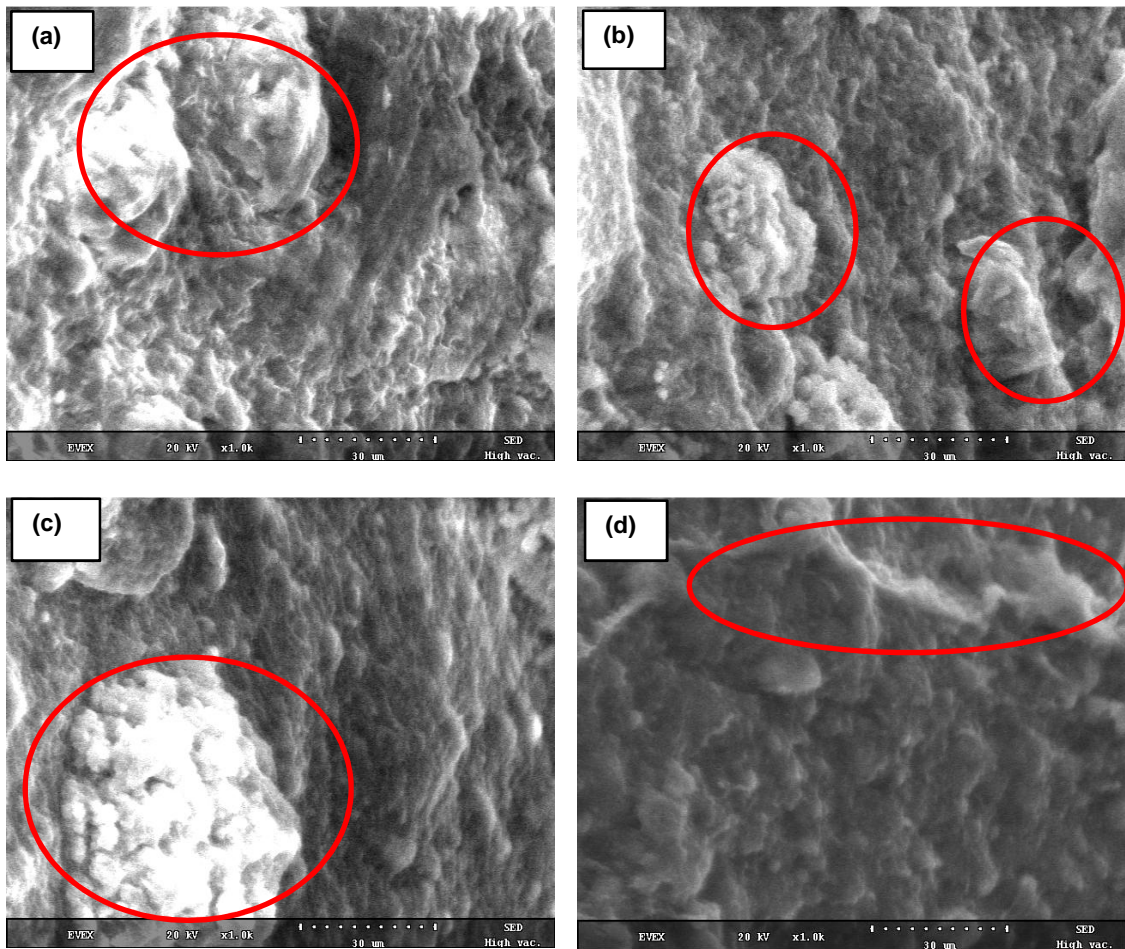


Fig. III- 13—SEM images (X1000-30 μm) of the dried filter cake surface for samples having different concentrations ferric oxide NPs: (a) 0.0 wt%, (b) 0.5 wt%, (c) 1.5 wt%, and (d) 2.5 wt% of NPs. The images show that adding 0.5 wt% to the base fluid results in less agglomeration (shown as red circles) and less porous surface compared to the filter cakes containing higher NP concentration or that for the base fluid.

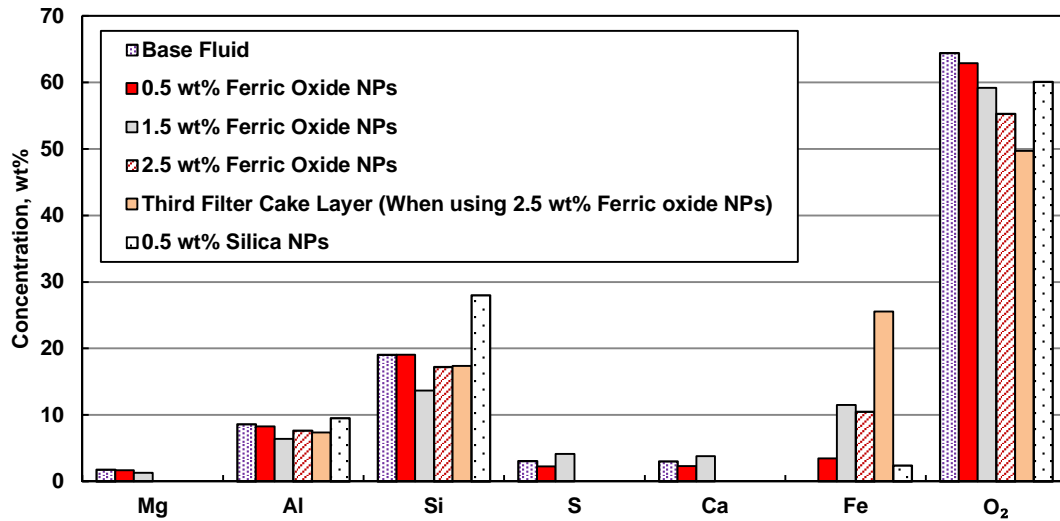


Fig. III- 14—EDS elemental analysis of the surface of the bottom layer of the filter cakes as a function of nanoparticle concentration.

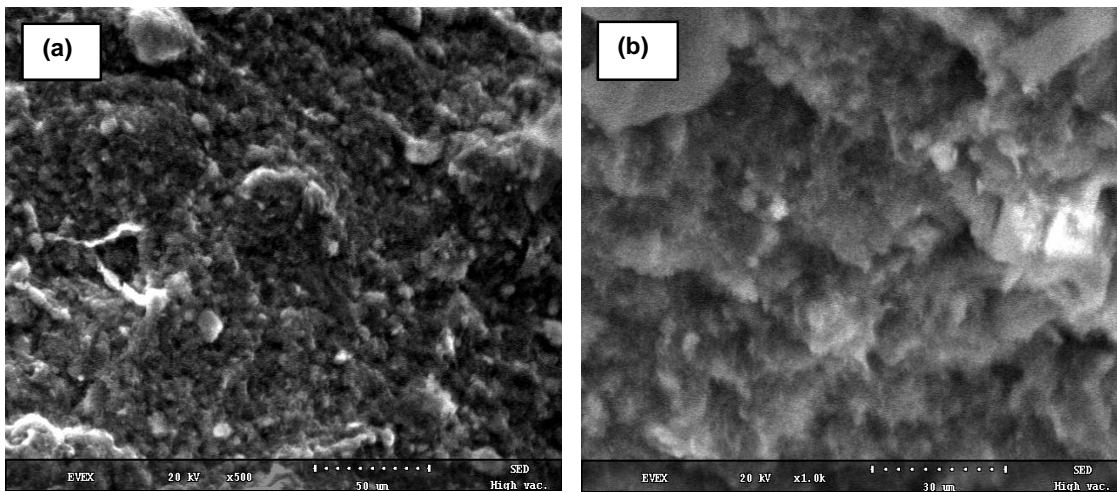


Fig. III- 15—SEM images: (a) for the surface of the third layer (agglomerated ferric oxide NP layer) formed in the filter cake containing 2.5 wt% of ferric oxide NPs (X500-50 μm), and (b) for the surface of the filter cake containing 0.5 wt% of silica NPs (X1000-30 μm). Both images show highly porous/permeable microstructure. Image (b) shows different clay-platelet structure compared to the filter cakes containing ferric oxide NPs (SEM images in Fig. III-13).

Adding 0.5 wt% of ferric oxide NPs resulted in the formation of a less permeable filter cake. Its permeability was 0.345 μd with a reduction of 76.38% compared to that of the filter cake formed when using the base fluid (Table III-11). However, using ferric

oxide NPs in any other concentration (either less or greater than 0.5 wt%) or silica NPs generated a higher permeability filter cake (Table III-11). It was also noted that using magnetic iron oxide Fe_3O_4 resulted in a reduction the filter cake permeability at different NP concentrations. However, using ferric oxide NPs in any other concentration (either less or greater than 0.5 wt%), silica, or zinc oxide NPs generated a higher permeability filter cake (Table III-11).

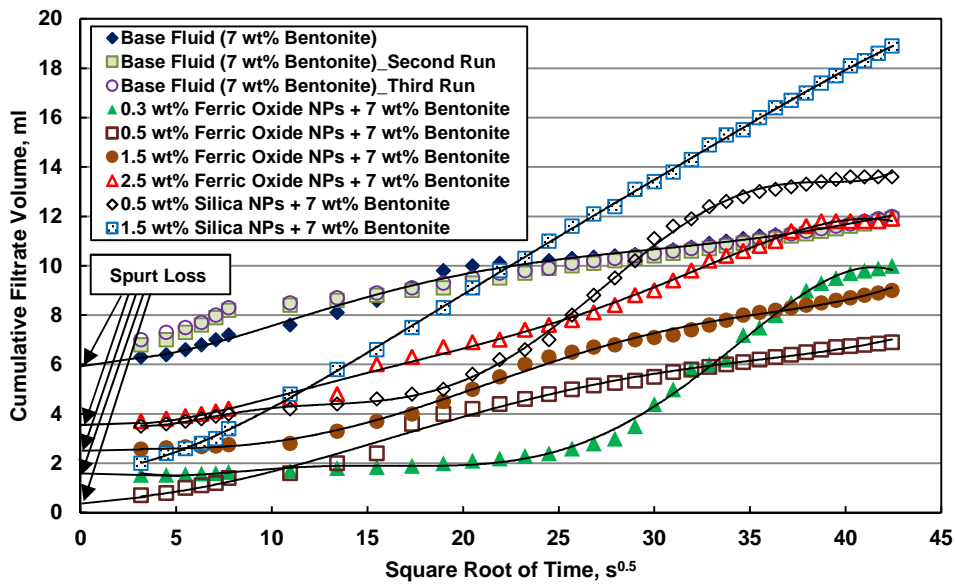


Fig. III- 16—Cumulative filtrate volume (for 30 min.) as a function of square root of time for the fluids containing different concentrations of ferric oxide NPs at 250°F and 300 psi differential pressure.

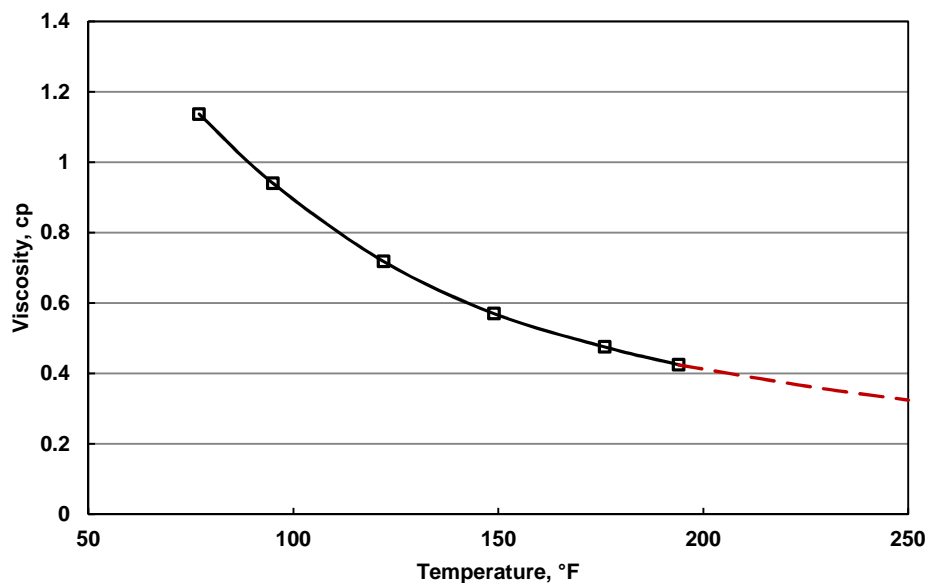


Fig. III- 17—Viscosity of the filtrate fluid against temperature for the base fluid.

Elemental Analysis of Filtrate Fluid

The filtrate fluid samples were collected to measure the concentration of cations using ICP-OES. **Fig. III-18** shows the concentration of different cations in the filtrate fluid of the samples that have different concentrations of ferric oxide NPs. The concentration of Ca^{2+} increased with the increase of NP concentration, which confirmed the dissociation of Ca^{2+} cations. A decrease in the concentration of Al^{3+} and Si^{4+} cations in the filtrate with the addition of NPs was also observed, which indicated better NPs/Ca-bentonite platelet structure. However, the increase in NP concentration resulted in the agglomeration of NPs and the formation of high porosity/high permeability filter cakes as indicated by SEM-EDS and CT scan.

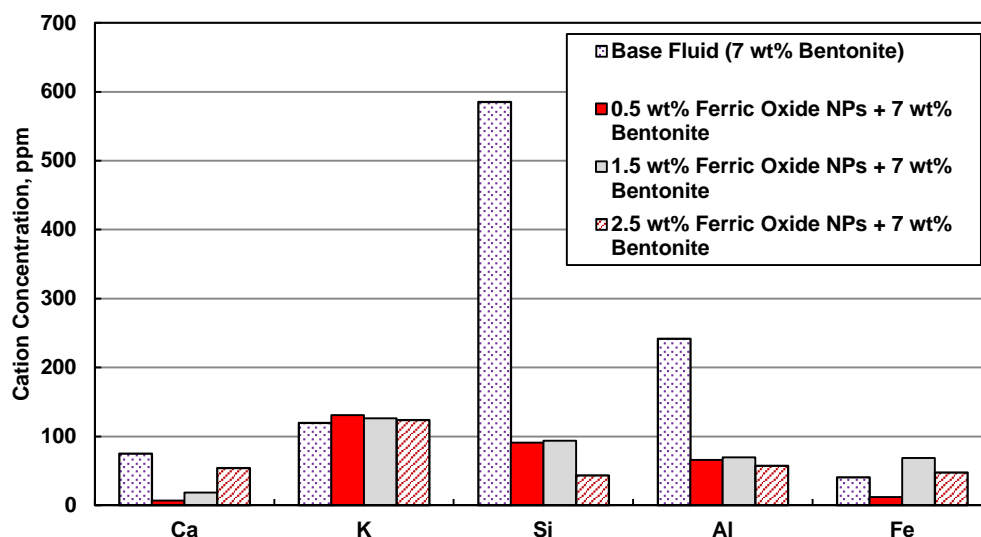


Fig. III- 18— ICP-OES analysis of the filtrate fluids for the samples having different ferric oxide NP concentrations at 300 psi and 250°F.

Effect of Filtration Temperature and Pressure

The fluid containing 0.5 wt% of ferric oxide NPs was selected for testing the effect of pressure and temperature on the filter cake characteristics. The selection was based on the higher performance of the samples containing 0.5 wt% of ferric oxide NPs. The fluids containing silica NPs showed a lower performance at 300 psi and 250°F as discussed in the aforementioned results. A series of filter press measurements was conducted using a fluid that has 0.5 wt% ferric oxide NPs at a differential pressure range from 200 to 500 psi and temperatures of 175, 200, 250, 300 and 350°F (**Table III-12**). With the increase in temperature from 175 to 300°F at a constant pressure of 300 psi, the efficiency of the formed filter cakes increased (less filtrate volume, less permeability, and relatively small increase in the thickness), which indicates that the ferric oxide NPs increased the filter cake ability to withstand higher temperatures. Furthermore, the efficiency of the filter

cakes increased then decreased when changing pressure from 200 up to 400 psi at constant temperature of 250°F, with the best performance achieved at a pressure of 300 psi. Moreover, at 500 psi and 350°F, a good-quality filter cake with a permeability of 0.060 μd is formed. This revealed the applicability of this type of NPs/Ca-bentonite fluids to drill harsh environments. Additionally, it indicated that the effect of temperature on the filter cake properties of this NPs/Ca-bentonite suspensions was predominant when compared with pressure effect. For more details of the filtrate loss volumes, see **Appendix C**.

Temperature (°F)	Pressure (psi)	Filter Cake Thickness (in.)	Cumulative Filtrate Volume (ml)	Filter Cake Permeability (μd)
175	300	0.2314	12.4	1.113
200	300	0.2673	11.8	1.008
250	300	0.2618	6.9	0.345
300	300	0.2923	6.4	0.296
250	200	0.3184	13.0	1.830
250	400	0.2796	9.6	0.500
350	500	0.2876	3.3	0.060

Table III- 12— Cumulative filtrate volume (for 30 min.) and filter cake properties of the fluids having 0.5 wt% of ferric oxide NPs at different filtration conditions of pressure and temperature.

Formation Damage Analysis

CT scan analysis was conducted for investigating the effect of the NPs/Ca-bentonite based fluids on damaging the cores. The core disks were CT scanned in dry, wet, and directly after the filtration experiment to study the change in the CTNs in the direction of flow (**Fig. III-19**). CT attenuation data is normally presented in a standardized scale

with Hounsfield units (HU) that is normalized to air at –1000 HU and water at 0.0 HU. Thus, each HU represents a 0.1% change in density with respect to the calibration density scale (Wellington and Vinegar 1987; Akin and Kavscek 2003). So that, the increase in the CTNs of the core after experiments might represent the percentage of the solid particles which accompanied the filtrate invasion into the formation. On other words, the CTNs can be used to check the change in the core porosity after the experiments.

The porosity of the core disks can be determined using the CTNs a using the following equation (**Eq. III-4**)

$$Porosity = \frac{CTN\ of\ the\ core\ in\ wet\ conditions - CTN\ of\ the\ core\ in\ dry\ conditions}{CTN\ of\ water - CTN\ of\ air} \dots\dots (III-4)$$

The CTNs of water and air are 0.0 and –1000 HU, respectively. For calculating the initial porosity of the core disks, the CTNs of the wet cores saturated with deionized water were used. However, the final core porosity of the core was calculated using the CTNs of the cores measured directly after the filtration experiments.

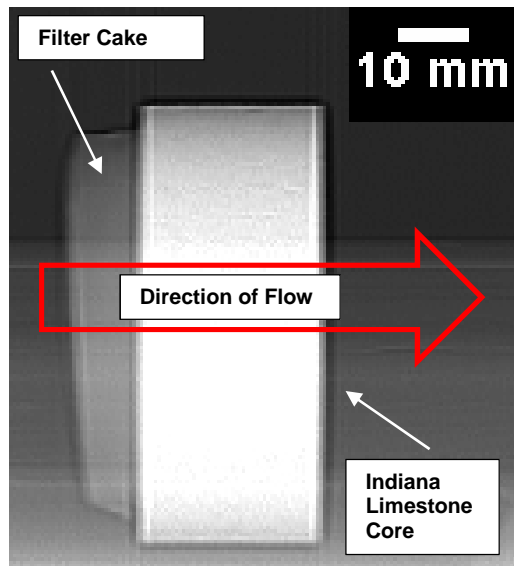


Fig. III- 19—CT scan image of the filter cake and core disk in the direction of fluid flow.

Three different core disks were analyzed as examples of the formation damage analysis when using this type of NPs/Ca-bentonite based fluids. **Figs. III-20** and **III-21** show the CTN and porosity profiles of the core disk used for running the experiment of the sample having 0.5 wt% of zinc oxide NPs, which shows lower filtration performance. The CTNs were averaged to be 1921.68, 2025.58, and 1980.33 HU for the dry, saturated core before experiment, and saturated core after experiment, respectively. The change in the CTN after the experiments revealed a change in the core porosity. More specifically, a decrease in the core porosity was occurred after the experiment. The porosity was calculated using Eq. III-4 and was averaged to be 10.38% and 7.31% for the core disk before and after the experiment, respectively (Fig. III-21). This revealed a little damage of the formation due to the invasion of solids with the filtrate fluid. The first 0.2 inches of the core thickness (close to the filter cake) showed an increase in the porosity after the experiment, which might be due to the increase in the fracture porosity at this region because of the high spurt pressure.

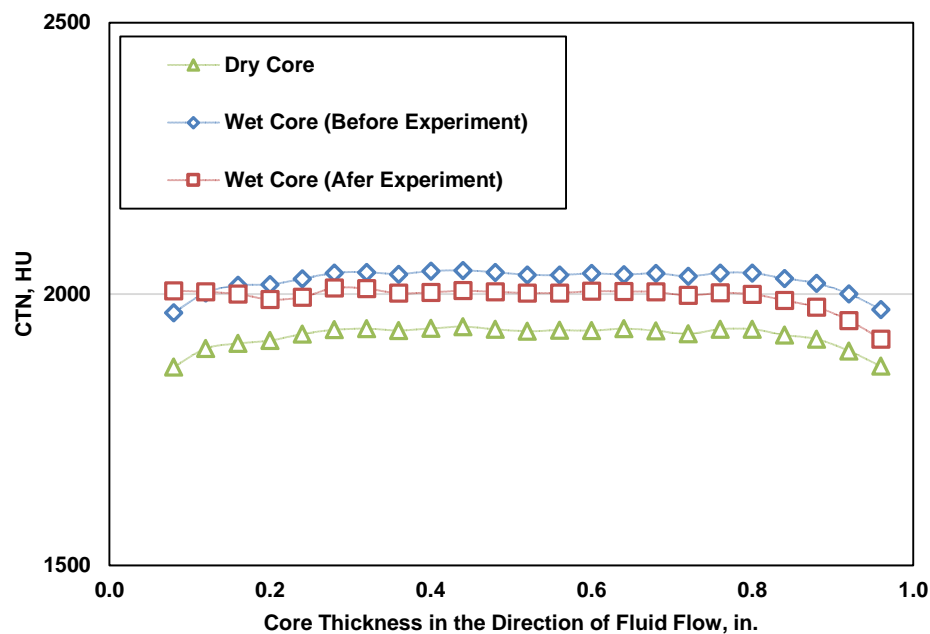


Fig. III- 20—CTN profile through the core disk (in the direction of fluid flow) used for running the experiment of the sample having 0.5 wt% of zinc oxide NPs.

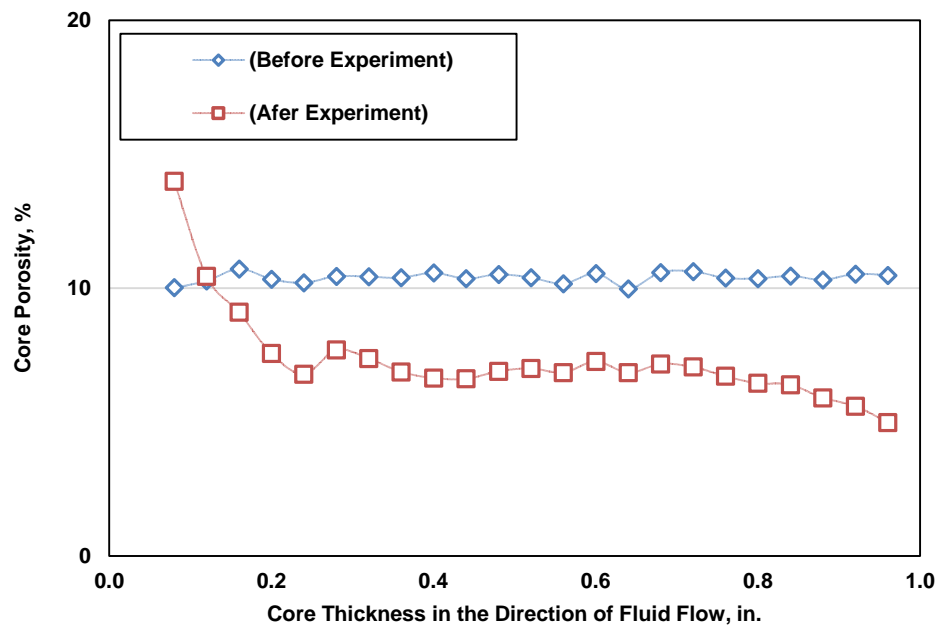


Fig. III- 21—Porosity profile through the core disk (in the direction of fluid flow) used for running the experiment of the sample having 0.5 wt% of zinc oxide NPs.

Figs. III-22 and III-23 show the CTN and porosity profiles of the core disk used for running the experiment of the sample having 1.5 wt% of magnetic iron oxide Fe_3O_4 NPs, which shows higher filtration performance. The CTNs were averaged to be 1928.89, 2031.51, and 2012.835 HU for the dry, saturated core before experiment, and saturated core after experiment, respectively. Again, a decrease in the core porosity was occurred after the experiment. The porosity was averaged to be 10.26% and 8.39% for the core disk before and after the experiment, respectively. A little damage of the formation where occurred. The first 0.2 inches of the core thickness showed an increase in the porosity after the experiment, which confirming the hypothesis of the fracture porosity increase at this region because of the high spurt pressure.

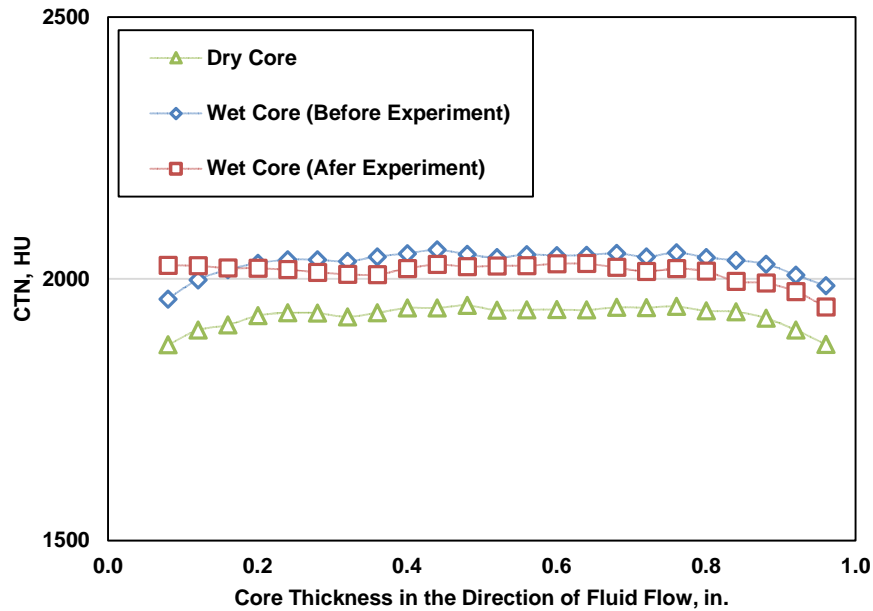


Fig. III- 22—CTN profile through the core disk (in the direction of fluid flow) used for running the experiment of the sample having 1.5 wt% of magnetic iron oxide Fe_3O_4 NPs.

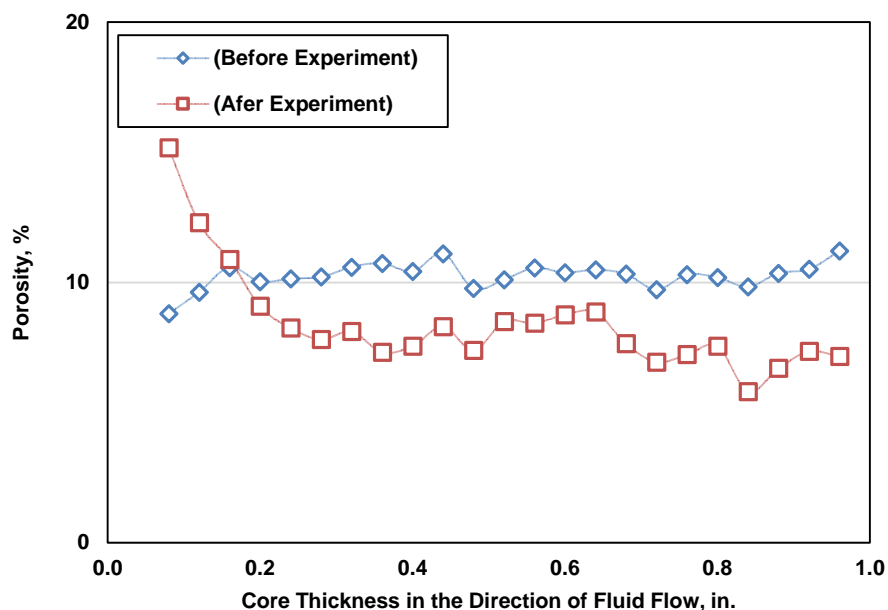


Fig. III- 23—Porosity profile through the core disk (in the direction of fluid flow) used for running the experiment of the sample having 1.5 wt% of magnetic iron oxide Fe₃O₄ NPs.

The more interesting part was that the decrease in the core porosity when using magnetic iron oxide Fe₃O₄ NPs was small compared to that when using zinc oxide NPs, which confirming the formation of a good-quality filter cake. That was also confirmed when analyzing the CTN profiles of the core disk used for running the experiment of the sample having 2.5 wt% of magnetic iron oxide Fe₃O₄ NPs. The CTNs were averaged to be 1940.29, 2038.44, and 2019.99 HU for the dry, saturated core before experiment, and saturated core after experiment, respectively (Figs. III-24). The porosity was averaged to be 9.83% and 8.49% for the core disk before and after the experiment, respectively, which reveals a little damage of the formation (Figs. III-25).

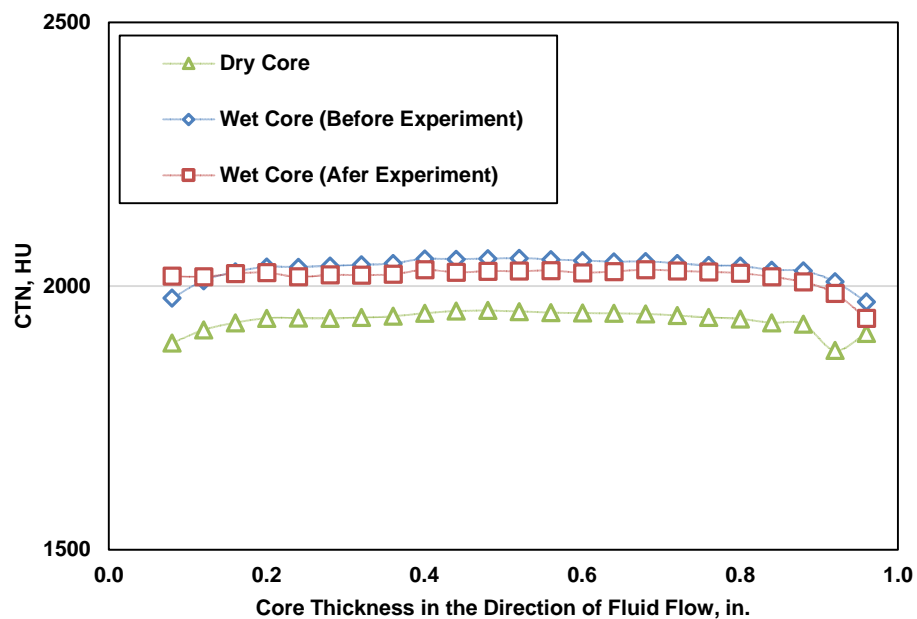


Fig. III- 24—CTN profile through the core disk (in the direction of fluid flow) used for running the experiment of the sample having 2.5 wt% of magnetic iron oxide Fe₃O₄ NPs.

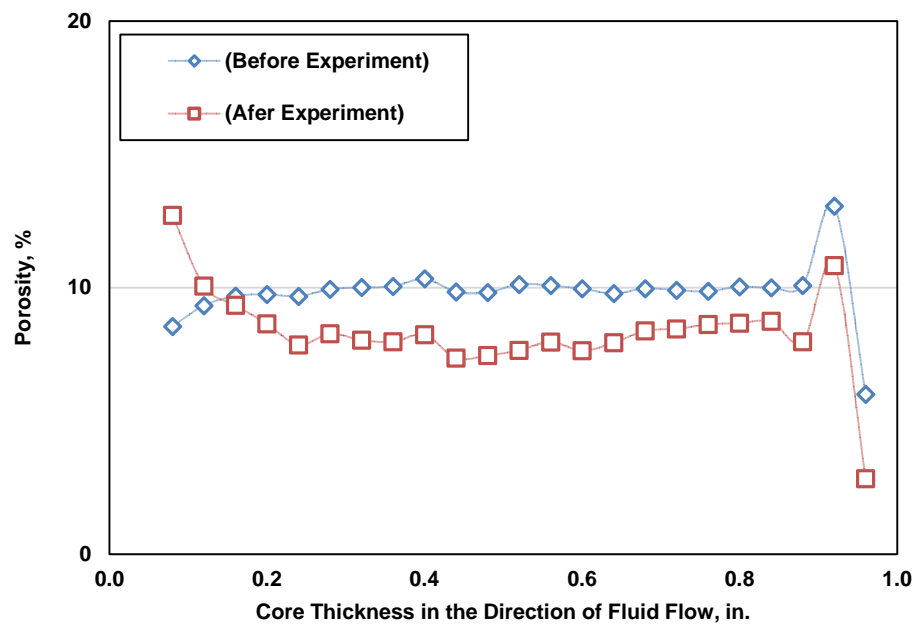


Fig. III- 25—CTN profile through the core disk (in the direction of fluid flow) used for running the experiment of the sample having 2.5 wt% of magnetic iron oxide Fe₃O₄ NPs.

Conclusions

The effectiveness of using different types of oxide NPs for improving the rheological properties and filter cake characteristics of Ca-bentonite-based fluids had been investigated. Results yielded the following conclusions:

1. Adding ferric oxide and magnetic iron oxide NPs at an optimum concentration of 0.5 wt% improved the filter cake characteristics at the investigated conditions (up to 350°F and 500 psi); however, using silica or zinc oxide NPs reduced the filter cake efficiency of such fluids.
2. The filter cake of these fluids consisted of two layers as revealed by CT scan analysis. The layer close to the rock surface was the main layer, in which the NPs played a key role in building the filter cake microstructure.
3. Using the optimum NP concentration generated a rigid/smooth surface filter cake morphology with less particle agglomeration and low porosity/low permeability structure as indicated by SEM-EDS analysis.
4. A third layer consisting mainly of the agglomerated NPs formed when using higher concentrations of ferric oxide or magnetic iron oxide NPs (2.5 wt%), which reduced the total filter cake efficiency.
5. The ferric oxide and magnetic iron oxide NPs promoted better clay-platelet microstructure after the dissociation of Ca^{2+} cations from the bentonite at such conditions because of their positively surface charge, which produced a good-quality filter cake.

6. The filter cakes that have optimum concentration of ferric oxide NPs could withstand downhole conditions up to 350°F and 500 psi. Moreover, the effect of temperature on the filter cake characteristics was predominant compared to pressure.
7. Ferric oxide and magnetic iron oxide NPs with positive surface charges were stable in suspensions and building a strong yield structure with Ca-bentonite, which produced fluids with better rheological properties. On the other hand, using silica NPs that had negative surface charge generated suspensions with higher viscosities and weaker yield structure.
8. Aging at 350°F for 16 hours shows that the rheological properties of Ca-bentonite-based fluids that has ferric oxide NPs remains stable over time with minor loss in the gel structure. On the other hand, aging silica NP-based fluids under the same conditions showed unstable rheological properties.
9. The Herschel-Bulkley was found to be the best fit model for the experimental data of the tested NPs/Ca-bentonite fluids with R^2 values higher than 0.99 and minimum $\sum Q^2$ values, especially at higher temperatures.
10. The CT scan analysis of the core disks showed a little decrease of the core porosity after the filtration process using the NPs/Ca-bentonite suspensions, which confirming its capability to minimize formation damage.

CHAPTER IV

CHARACTERIZATION OF THE FILTER CAKE GENERATED BY NANOPARTICLE/CA-BENTONITE-BASED DRILLING FLUID ⁷

Introduction

Having an efficient filter cake is an important property of the drilling fluid and can affect success of the drilling operations. This chapter focuses on characterizing the filter cake produced by Ca-bentonite-based drilling fluid that contains ferric oxide (Fe_2O_3) nanoparticles (NPs) at downhole conditions. A complete drilling fluid formula was formulated and used for this part of study to check the effect of using this type of NPs in the presence of different drilling fluid additives. Furthermore, the effect of different parameters on the filter cake characteristics, such as NP concentration, fluid preparation method, and filtration conditions were investigated.

The results showed that the ferric oxide NPs improved the filter cake and filtration properties of Ca-bentonite-based drilling fluid in the presence of polymer and other additives. It was found that lower NP concentration is preferred for obtaining a good-quality filter cake. The best filter cake characteristics were obtained when using 0.3-0.5 wt% of NPs. Furthermore, this drilling fluid can withstand downhole conditions up to 500 psi and 350°F. At such conditions, filter cake properties of 0.151-in. thickness, 6.9 ml

⁷ Reprinted with a permission from “Characterization of Filter Cake Generated by Nanoparticle-Based Drilling Fluid for HP/HT Applications” by Mahmoud, O., Nasr-El-Din, H. A., Vryzas, Z., and Kelessidis, V. C. SPE-184572-MS, Copyright 2017 by Society of Petroleum Engineers.

filtrate volume, and 0.428 μd permeability were obtained. The addition of NPs to the drilling fluid improved the filter cake properties under both static and dynamic filtration. Additionally, SEM-EDS analysis confirmed the efficiency of using this type of NPs to generate a smoother, less porous filter cake morphology. Moreover, ultrasonication for one hour and bentonite hydration for 16 hours are recommended for better preparation of this types of NPs/Ca-bentonite-based drilling fluids.

Properties of the Drilling Fluid

Table IV-1 summarizes the properties of the Ca-bentonite-based drilling fluid (without the addition of NPs) and the drilling fluid that contains 0.5 wt% of NPs. The density of the drilling fluid was measured at ambient conditions using mud balance and was determined to be 9.6 ppg. The drilling fluid was measured to have a pH of 11. The rheological properties of the drilling fluid were determined at 140°F and atmospheric pressure using the rotational viscometer. The Ca-bentonite-based drilling fluid has a plastic viscosity of 17.6 cp, and yield point of 11.7 lbf/100 ft². The 10-s and 10-min gel strength were measured to be 8 and 13 lbf/100 ft², respectively. However, the properties of the drilling fluid that contains 0.5 wt% of NPs were 15 cp for the plastic viscosity and 12, 10, and 17 lbf/100 ft² for the yield point, 10-s and 10-min gel strength, respectively. The results showed a relatively small change in the rheological properties of the drilling fluid when adding NPs. The addition of NPs increased the yield stress and gel strength of this type of Ca-bentonite-based drilling fluids, which improves their cutting carrying capacity (Bourgoyne et al. 1991).

Fig. IV-1 shows the particle size distribution of the solids presented in the drilling fluid using sieve analysis. The mean diameter of the solids used, d_{50} , was 123 μm , which confirmed the applicability of this drilling fluid formulation to prevent pore blockage of the formation (Abrams 1977).

Property	Condition	Unit	Value	
			Bentonite Based Drilling Fluid	Drilling Fluid Contains 0.5 wt% of Nanoparticles
Density	78°F and 14.7 psi	ppg	9.5	9.6
Plastic viscosity	140°F and 14.7 psi	cp	17.6	15
Yield point	140°F and 14.7 psi	lbf/100 ft ²	11.7	12
10-s gel strength	140°F and 14.7 psi	lbf/100 ft ²	8	10
10-min gel strength	140°F and 14.7 psi	lbf/100 ft ²	13	17
pH	78°F and 14.7 psi	—	11	11

Table IV- 1— Properties of the Ca-bentonite-based drilling fluid and the drilling fluid containing 0.5 wt% of ferric oxide NPs.

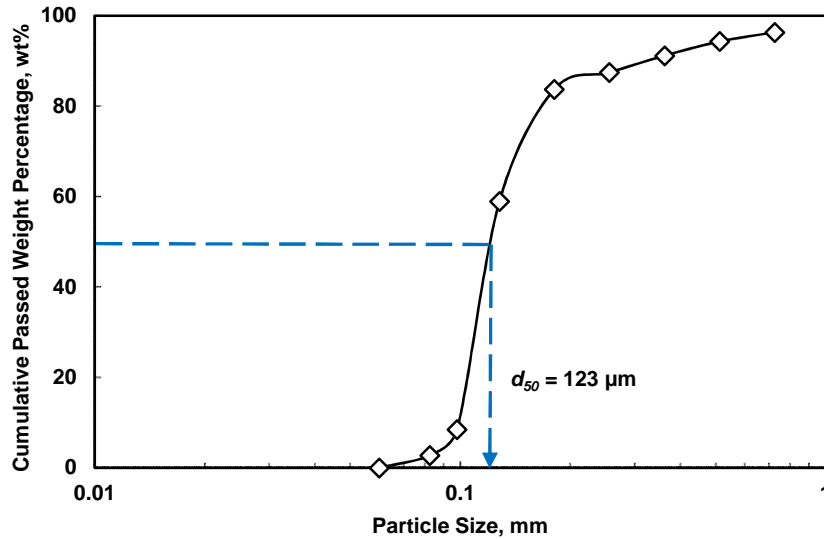


Fig. IV- 1— Particle-size distribution of solids in the drilling fluid.

Filter Press Measurements and Analysis

The HP/HT filter press was used to investigate the filtration properties and generate the filter cakes. The desired differential pressure and temperature were applied. The filtration fluid volume was measured as a function of time for 30 minutes. **Table IV-2** shows a list of the performed filter press experiments and the studied parameters throughout this investigation. The CT scanner was used to investigate the produced filter cakes. CT images were taken through the full cake diameter and analyzed using Imagej™ software. The CT data was analyzed to determine the filter cake thickness and CT number (CTN). Moreover, SEM-EDS was used to analyze the dried filter cakes.

The filter cake permeability was calculated using the model developed by Li et al. (2005), which was found to be the simplest and best way of calculation for this kind of drilling fluid (Elkatatny et al. 2012). The permeability in this model is calculated using Darcy's equation of liquid flow through the porous media. Additionally, the resistance of the filter media (filter disk) for the flow was also included. Calculations in this method mainly depending on the relationship between the cumulative filtrate volume and time. **Eqs. IV-1, IV-2 and IV-3** can be used for these calculations in field units:

$$q = 0.173 k_m \frac{\Delta p_m}{\mu L_m} , \dots\dots\dots (IV-1)$$

$$\Delta p_t = \Delta p_m + \Delta p_c , \dots\dots\dots (IV-2)$$

and

$$q = 0.173 k_c \frac{\Delta p_c}{\mu L_c} , \dots\dots\dots (IV-3)$$

Parameter	NP Concentration, wt%	Temperature, °F	Differential Pressure, psi	Rotation at 100 rpm	Sonication Time, hr	Hydration Time, hr
NP Concentration	0.0	250	300	No	1.0	0.0
	0.3	250	300	No	1.0	0.0
	0.5	250	300	No	1.0	0.0
	1.0	250	300	No	1.0	0.0
Differential Pressure and Temperature	0.5	200	300	No	1.0	0.0
	0.5	300	300	No	1.0	0.0
	0.5	250	200	No	1.0	0.0
	0.5	250	400	No	1.0	0.0
	0.5	350	500	No	1.0	0.0
Dynamic Filtration	0.0	250	500	No	0.0	0.0
	0.0	250	500	Yes	0.0	0.0
	0.5	250	500	No	0.0	0.0
	0.5	250	500	Yes	0.0	0.0
Sonication Time	0.5	250	300	No	0.0	0.0
	0.5	250	300	No	0.5	0.0
Bentonite Hydration	0.0	250	500	No	0.0	16
	0.5	250	500	No	0.0	16

Table IV- 2—The performed filter press experiments and the investigated parameter.

where q = the filtrate rate (ml/in.².s), k_m = permeability of the filter medium (d), k_c = permeability of the filter cake (d), L_m = thickness of the filter medium (in.), L_c = thickness of the filter cake (in.), Δp_t = total pressure drop (psi), Δp_m = pressure drop across the filter medium (psi), Δp_c = pressure drop across the filter cake (psi), and μ = viscosity of the filtrate (cp). The viscosity of the filtrate was measured using a capillary tube viscometer and was determined to be 0.2 cp at 250°F. The value of the filtrate rate q (ml/in.².s) was determined by dividing the slope of the cumulative volume versus time curve on the cross-

sectional area of the filter disk, which is 3.976 in.². The slope of the curve should be determined for the part starting at 430 s when flow through the already formed cake starts (Li et al. 2005).

Effect of Nanoparticle Concentration

The drilling fluid was prepared following the formulation described in chapter II and four different NP concentrations were used (0.0, 0.3, 0.5, and 1.0 wt%). Static filtration experiments were conducted at a differential pressure of 300 psi and a temperature of 250°F (experiments number 1 to 4 in Table IV-2). **Fig. IV-2** shows the cumulative filtrate volume after 30 minutes and the thickness of the generated filter cakes.

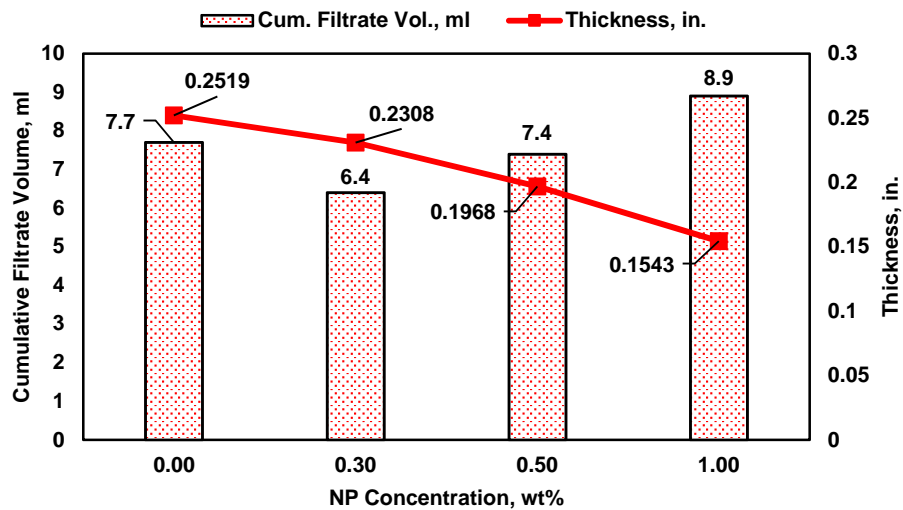


Fig. IV- 2— Cumulative filtrate volume (30 minutes) and filter cake thickness for the filter cakes having different concentrations of ferric oxide NPs formed under static filtration at 250°F and 300 psi differential pressure.

The results showed a decrease in the filter cake thickness with the increase in NP concentration. More specifically, the thickness decreased by 8.4, 21.9, and 38.7% for the filter cakes that contain 0.3, 0.5, 1.0 wt% of NPs, respectively, when compared to the

thickness of the cake that has 0.0 wt% of NPs. Furthermore, the cumulative filtrate volume decreased by 16.9 and 3.9% for the drilling fluids that contain 0.3 and 0.5 wt% of NPs, respectively; however, it increased by 15.6% for the sample that contains 1.0 wt% of NPs compared to the base. These results confirmed what is found in the absence of the drilling fluid additives. It was found that, the 0.5 wt% of ferric oxide NPs is the optimum concentration, which should be used with the 7 wt% Ca-bentonite suspension to obtain the best filter cake characteristics. However, using a higher concentration of NPs resulted in the agglomeration of the excess NPs and thus, less filter cake efficiency.

Fig. IV-3 shows the CT scan images of the filter cakes. The images were taken through the full cake diameter. The filter cakes generally consisted of two layers. The top layer (close to the drilling fluid) had a low CT number (CTN) compared to the bottom layer (close to the formation surface). The average CTN for each layer are shown in **Fig. IV-4**. The CTN were averaged to be 607.60, 735.45, 794.08, and 929.48 for the top layer of the filter cakes that have 0.0, 0.3, 0.5, and 1.0 wt% of NPs, respectively. Moreover, the average CTN for the bottom layer (close to the formation surface) were 790.70, 872.01, 961.28, and 1007.40 for the cakes containing 0.0, 0.3, 0.5, and 1.0 wt% of NPs, respectively. The increase in the average CTN in each layer with the increase in NP concentration indicated that the NPs play a key role in building a different bentonite platelet structure (Barry et al. 2015). Each increase in the CTN by 1 HU represents a 0.1% change in density with respect to the calibration density scale (Wellington and Vinegar 1987; Akin and Kavscek 2003).

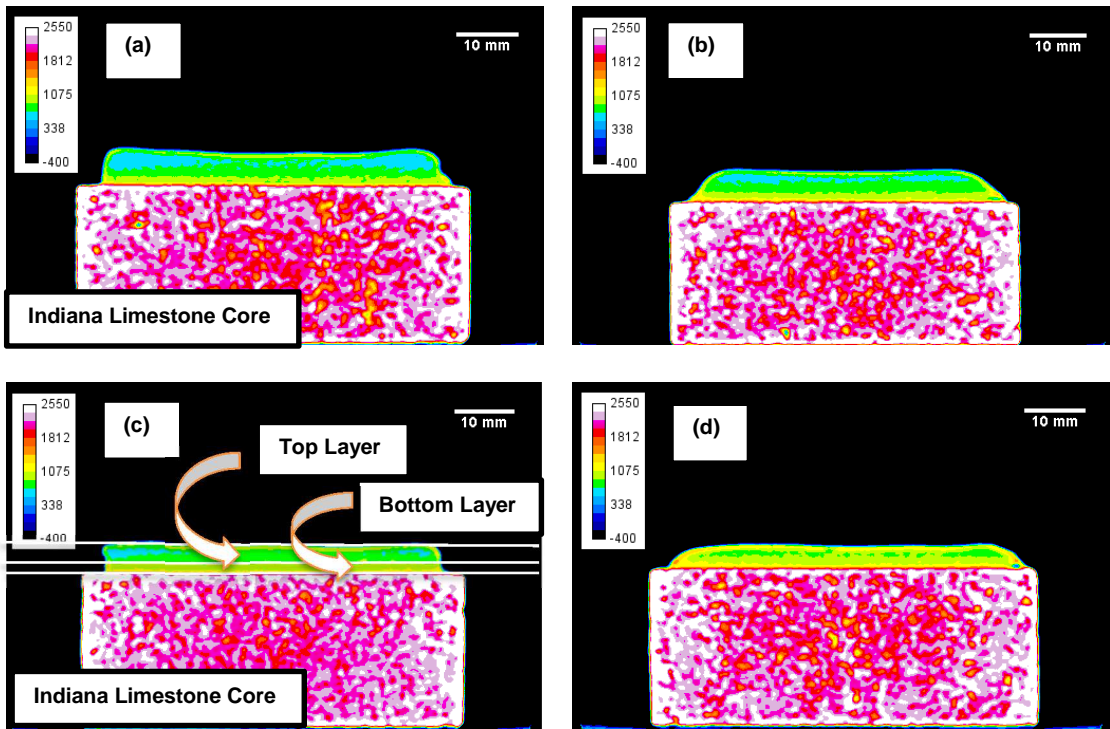


Fig. IV- 3— CT scan images of the filter cakes having different concentrations of ferric oxide NPs formed under static filtration at 250°F and 300 psi differential pressure: (a) with 0.0 wt%, (b) with 0.3 wt%, (c) with 0.5 wt%, and (b) with 1.0 wt% of NPs.

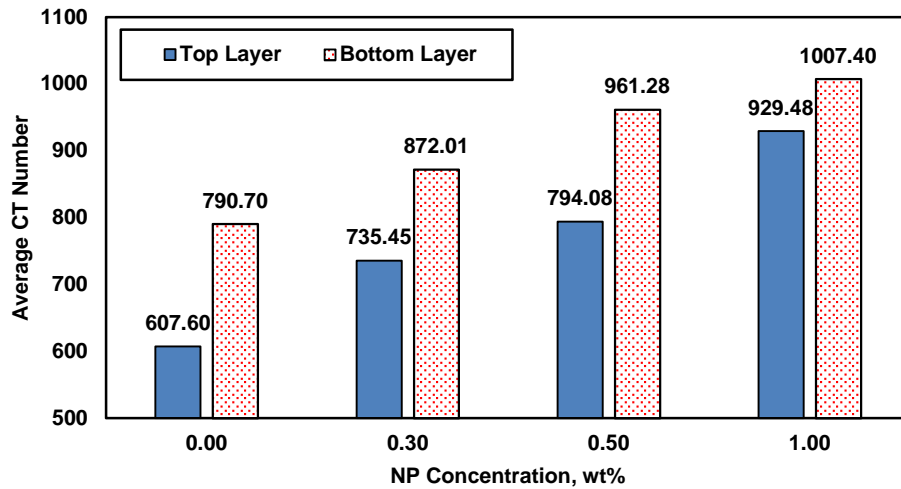


Fig. IV- 4— Average CTNs throughout the filter cakes having different concentrations of ferric oxide NPs generated under static filtration at 250°F and 300 psi differential pressure.

The filter cakes were dried in an oven at 250°F for three hours before running the SEM-EDS analysis. Both sides of the filter cake were analyzed, the top surface (the surface of the top layer) and the bottom surface (the base of the bottom layer). **Fig. IV-5** shows the SEM images of the top surface of the filter cakes that have 0.0 and 0.5 wt% of NPs. Adding 0.5 wt% of NPs to the drilling fluid resulted in generating a less porous structure and smoother surface morphology (Hartman et al. 1988; Chenevert and Huycke 1991; Plank and Gossen 1991).

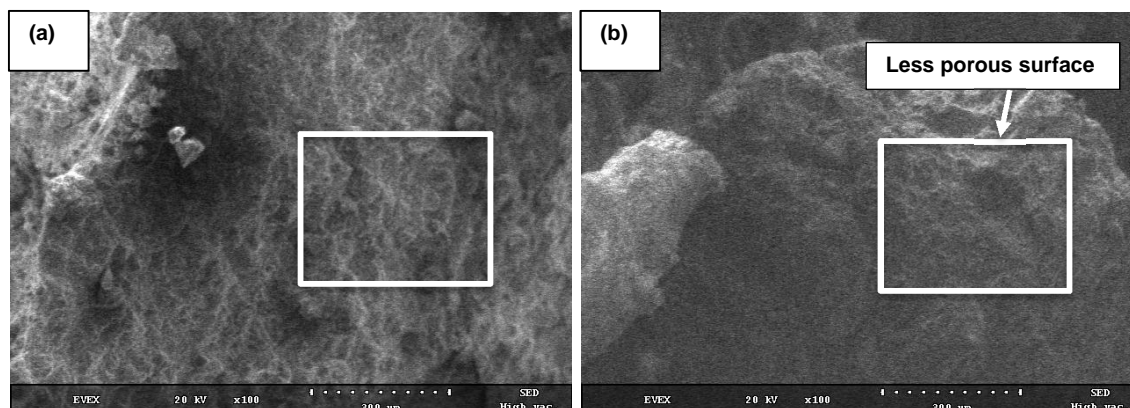


Fig. IV-5—SEM images (X100-300 μm) of the top surface of the dried filter cakes having different concentrations of ferric oxide NPs formed under static filtration at 250°F and 300 psi differential pressure: (a) with 0.0 wt%, and (b) with 0.5 wt% of NPs. The images show that adding 0.5 wt% of NPs to the drilling fluid results in less porous structure.

Fig. IV-6 shows the EDS spectrum analysis of the top surface of the filter cake that has 0.5 wt% of NPs. The EDS counted aluminum (Al) and silicon (Si) because of the used Ca-bentonite, which belongs to the smectite group of clays and is formed by an Al^{3+} octahedral layer sandwiched between two Si^{4+} tetrahedral layers. The calcium (Ca) and manganese (Mn) appeared because of the CaCO_3 and Mn_3O_4 , which were used as bridging and weighting materials. Additionally, these temperatures induced the dissociation of Ca^{2+} cations from the surface of bentonite platelet (Ramos-Tejada et al. 2001; Laribi et al.

2006). The EDS did not count for iron (Fe), which indicated better distribution of ferric oxide NPs in-between the clay platelet in this layer.

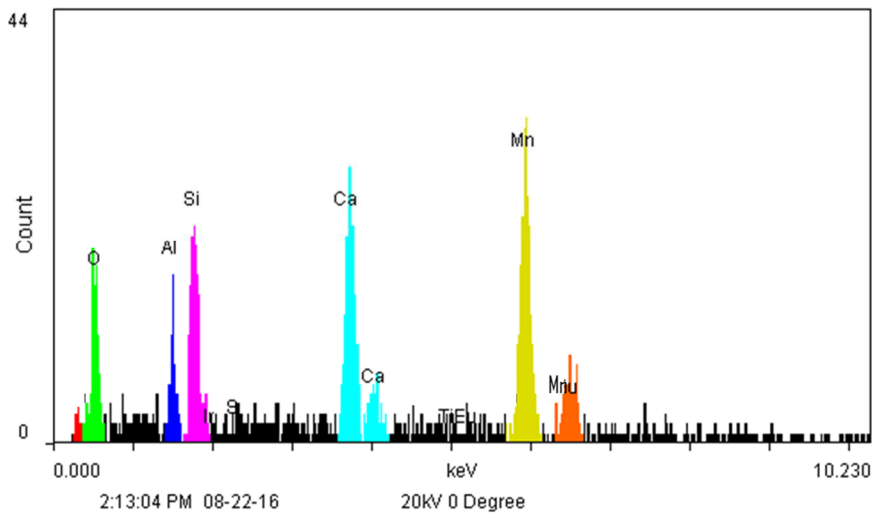


Fig. IV- 6— EDS spectrum analysis of the top surface of the dried filter cake having 0.5 wt% ferric oxide NPs formed under static filtration at 250°F and 300 psi differential pressure.

Fig. IV-7 shows the SEM-EDS of the bottom surface (close to the rock surface) of the same filter cakes. The bottom surface of the filter cake with 0.5 wt% of NPs had a smoother surface morphology and less porous structure (Hartman et al. 1988; Chenevert and Huycke 1991; Plank and Gossen 1991). Furthermore, the EDS spectrum analysis of the bottom surface showed that the Al, Si, Ca, and Mn appeared in this surface. An increase in the concentration of Ca was found when comparing to the elemental analysis of the top surface that has the same NP concentration. Moreover, traces of iron (Fe) appeared in the EDS spectrum of the cake that has 0.5 wt% of NPs (**Fig. IV-8**). This Fe concentration appeared in the EDS was found to increase in the cake containing higher NP concentration. This confirmed the hypothesis that using NP concentration greater than

0.5 wt% will adversely affect the cake characteristics because of the agglomeration of NPs.

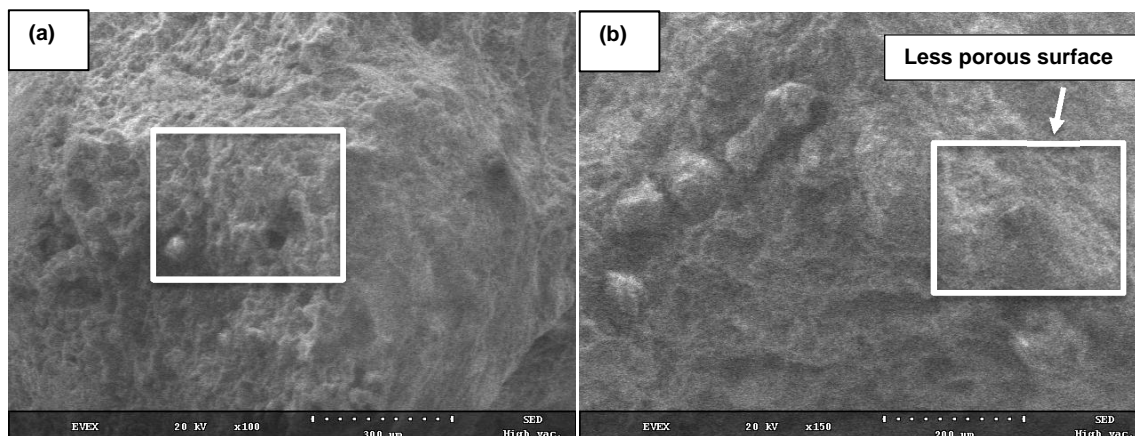


Fig. IV- 7— SEM images of the bottom surface of the dried filter cakes having different ferric oxide NP concentrations formed under static condition at 300 psi differential pressure and 250°F: (a) with 0.0 wt% (X100-300), and (b) with 0.5 wt% of NPs (X150-500 μm). The images show that adding 0.5 wt% of NPs to the drilling fluid results in less porous surface.

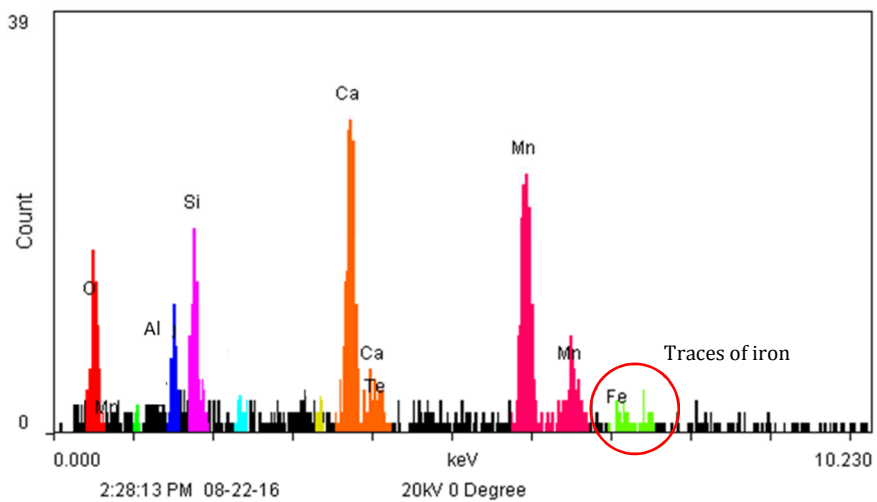


Fig. IV- 8—EDS spectrum analysis of the bottom surface of the dried filter cake having 0.5 wt% ferric oxide NP concentration formed under static condition at 300 psi differential pressure and 250°F. Traces of iron appears in this surface.

Li et al. model (2005) was used to determine the filter cake permeability (**Table IV-3** summarizes the calculations). **Fig. IV-9** shows the cumulative filtrate volume versus time curves, from which the filtrate rate was calculated (for detailed results, see **Appendix D**). A relatively decrease in the filter cake permeability was observed with the increase in NP concentration up to 0.5 wt%. The permeabilities were determined to be 0.598, 0.562, and 0.456 μd for the cakes that have 0.0, 0.3, and 0.5 wt% of NPs, respectively. However, using 1.0 wt% of NPs generated a relatively small increase in the filter cake permeability (0.465 μd) compared to the cake that has 0.5 wt% NPs. This permeability trend gave a reasonable explanation of the filtrate fluid loss profile.

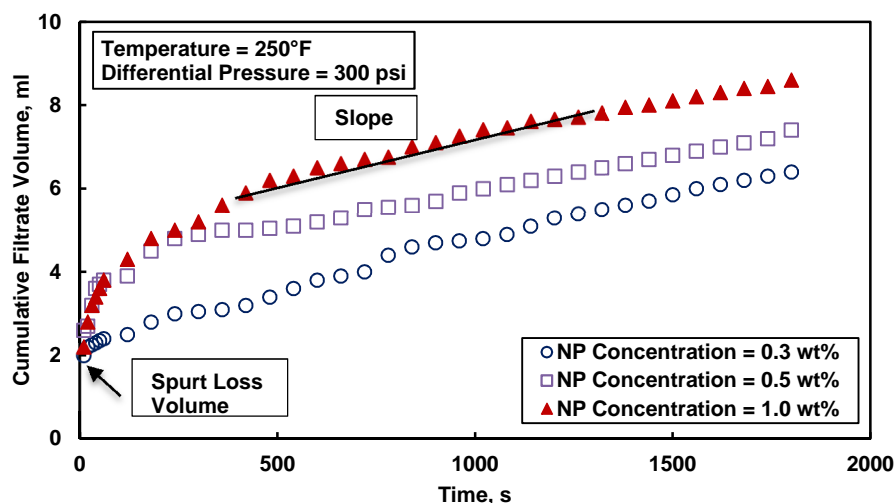


Fig. IV-9—Cumulative filtrate volume as a function of time for drilling fluids containing different concentrations of ferric oxide NPs at 250°F and 300 psi differential pressure.

Effect of Filtration Temperature and Pressure

A series of filter press experiments were conducted using a drilling fluid that has a NP concentration of 0.5 wt% at different temperatures and pressures. The experiments were carried out under static mode at differential pressures of 200, 300, 400, and 500 psi

and temperatures of 200, 250, 300 and 350°F (experiments number 3, and 5 to 9 in Table IV-2). **Table IV-4** summarizes the filter cake characteristics. At a constant pressure of 300 psi, the increase in temperature from 200 to 300°F resulted in an increase in the filter cake thickness and a decrease in the cumulative filtrate volume. The same trends of the filter cake thickness and cumulative filtrate volume were obtained at a constant temperature of 250°F and differential pressures from 200 to 400 psi. The optimum characteristics were found to be 0.197 in. cake thickness and 7.4 ml filtrate volume at 250°F and 300 psi. Furthermore, at 500 psi and 350°F, a filter cake thickness of 0.151 in. and a filtrate volume of 6.9 ml were obtained, which confirmed the applicability of this type of drilling fluid to generate a good-quality filter cake at such harsh conditions.

NP Concentration, wt%	Filtrate Rate, ($\times 10^{-4}$) ml/in. ² .s	Filter Cake Thickness, in.	Δp_m , psi	Δp_c , psi	Filter Cake Permeability, μ d
0.0	6.159	0.2519	0.00356	300	0.598
0.3	6.315	0.2308	0.00365	300	0.562
0.5	4.514	0.1968	0.00425	300	0.456
1.0	7.822	0.1543	0.00453	300	0.465

Table IV- 3—Filter cake permeability calculations for different NP concentrations at 250°F and 300 psi.

The average CTN of both layers in the filter cake at different temperatures and pressures are shown in Table IV-4. The CTN was relatively close in magnitudes for either the top or bottom layer at temperatures of 250, 300, and 350°F and pressures of 300, 400, and 500 psi. However, at the condition of 200°F and 300 psi, the CTN for the top layer was relatively higher compared to that of the top layer at the other conditions of pressure and temperature. Moreover, at 250°F and 200 psi, the CTN for the bottom layer was

relatively low and the CTN for the top layer was relatively high compared to that of the top layers at higher pressures. These results indicating that below 250°F and 200 psi this NPs/Ca-bentonite-based drilling fluid may not performing well.

Temperature, °F	Pressure, psi	Filter Cake Thickness, in.	Cumulative Filtrate Volume, ml	Filter Cake Permeability, μd	CT Number,	
					Top Layer	Bottom Layer
200	300	0.1271	9.0	0.385	964.95	1024.19
250	300	0.1968	7.4	0.343	794.08	961.28
300	300	0.2187	8.6	0.430	781.99	1023.37
250	200	0.1553	9.9	0.460	823.48	836.02
250	400	0.2115	9.5	0.309	770.61	978.64
350	500	0.1514	6.9	0.428	787.88	968.28

Table IV- 4— Filter cake characteristics of the drilling fluid containing 0.5 wt% of ferric oxide NPs at different conditions of pressure and temperature.

Fig. IV-10 shows the cumulative filtrate volume curves versus time (for detailed results, see **Appendix D**). The slope was determined and used to calculate the filter cake permeability. The cake had low permeability at different conditions of pressure and temperature (**Table IV-4**). These results confirmed the applicability of this kind of NPs/Ca-bentonite-based drilling fluid to build-up a filter cake with good characteristics, which can withstand harsh conditions of pressure and temperature.

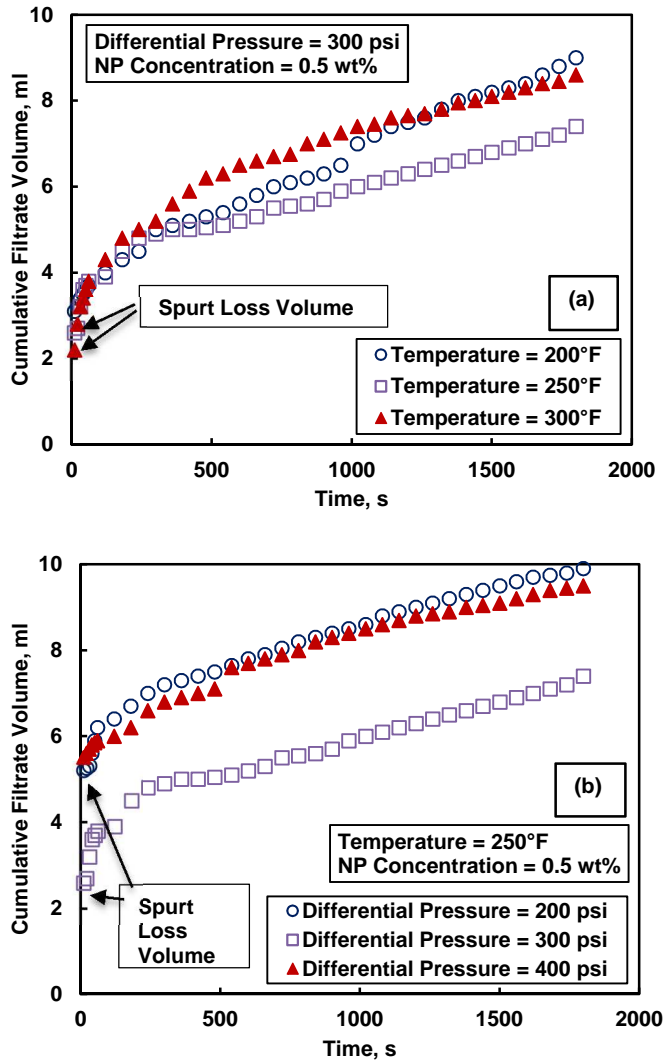


Fig. IV- 10—Cumulative filtrate volume as a function of time for drilling fluids containing 0.5 wt% of ferric oxide NPs at: (a) 300 psi and different temperatures, and (b) 250°F and different pressures.

Effect of Dynamic Filtration

The HP/HT filter press was used under dynamic mode at a rotational speed of 100 rpm to run these experiments. The drilling fluids that have 0.0 and 0.5 wt% of NPs had been investigated at a differential pressure of 500 psi and 250°F (experiments number 11 to 13 in Table IV-2). As a comparison, two other experiments were conducted at the same

conditions under static filtration (experiments number 10 and 12 in Table IV-2). No ultrasonication was used while preparing these drilling fluids.

Table IV-5 shows the characteristics of the filter cake generated under both static and dynamic filtration. For the drilling fluid with no NPs, a decrease in the filter cake thickness by 36.98% and an increase in the cumulative filtrate volume by 81.43% were observed compared to the cake that generated under static conditions. However, the cake thickness decreased by 29% and the filtrate volume increased by 4.5% for the cake having 0.5 wt% of NPs generated at dynamic filtration compared to the one formed at static conditions. Al-Abduwani et al. (2005) reported that under dynamic filtration, the produced filter cake is simultaneously eroded and deposited because of the circulation that affect the solid particles.

NP Concentration wt%	Rotational Speed rpm	Filter Cake Thickness, in.	Cumulative Filtrate Volume, ml	Filter Cake Permeability, μ d	CT Number	
					Top Layer	Bottom Layer
0.0	0	0.338	7.0	0.681	597.83	756.99
0.0	100	0.213	12.7	0.489	649.87	819.85
0.5	0	0.231	8.9	0.417	597.43	778.67
0.5	100	0.164	9.3	0.209	703.48	824.07

Table IV- 5— Filter cake characteristics of the drilling fluids that have 0.0 and 0.5 wt% of ferric oxide NPs at 500 psi and 250°F (effect of dynamic filtration).

The interested part was when comparing the characteristics of the cake that has 0.5 wt% of NPs with the one that has 0.0 wt% NPs under dynamic filtration. Using ferric oxide NPs resulted in a decrease in the cake thickness by 23% and a decrease in the filtrate fluid volume by 26.77%. The filter cake permeability was also calculated and presented

in Table IV-5. Using 0.5 wt% NPs relatively improved the filter cake characteristics at this condition of pressure and temperature under both static and dynamic conditions. **Fig. IV-11** shows the cumulative filtrate volume versus time curves for both drilling fluids (for detailed results, see **Appendix D**).

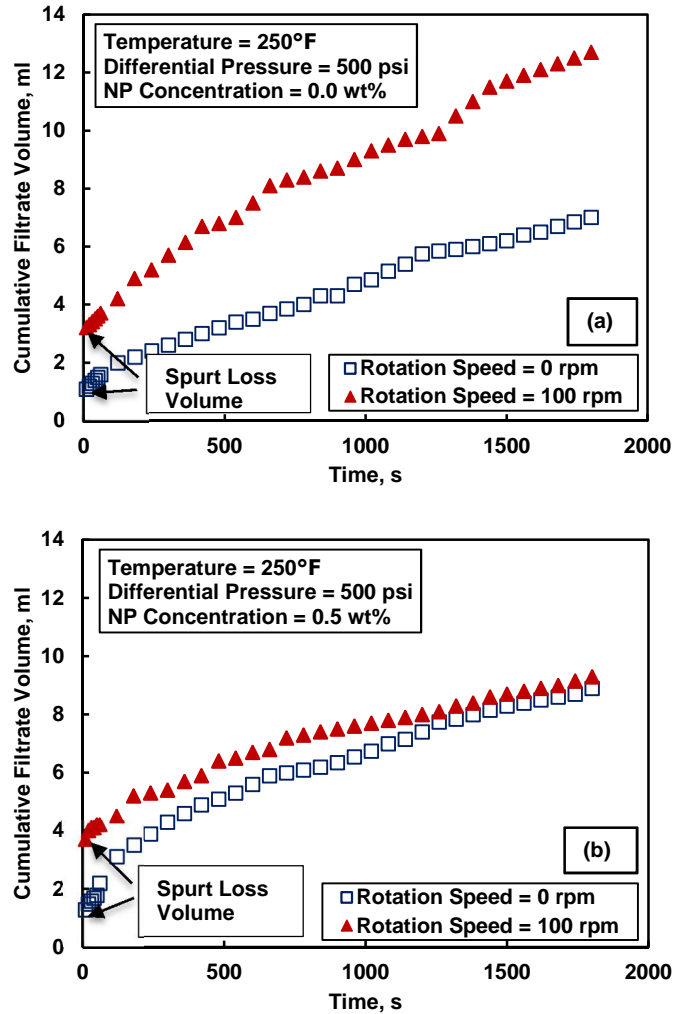


Fig. IV- 11— Cumulative filtrate volume as a function of time for drilling fluids containing different concentrations of ferric oxide NPs under both static and dynamic conditions at 250°F and 500 psi differential pressure: (a) with 0.0 wt%, and (b) with 0.5 wt% of NPs.

Fig. IV-12 shows the SEM images of the bottom surface (close to the rock surface) of the filter cakes generated under dynamic filtration (100 rpm). The filter cake with 0.5

wt% of NPs has a smoother surface morphology and less porous structure compared to the cake with no NPs (Hartman et al. 1988; Chenevert and Huycke 1991; Plank and Gossen 1991). Furthermore, the EDS elemental analysis of this surface did not count for the elemental iron (Fe), which might be because of the better distribution of NPs in the cake due to the circulation of drilling fluid (**Fig. IV-13**).

Effect of Drilling Fluid Preparation Method

All of the drilling fluids used in this research work were prepared following the formulation and procedures mentioned in chapter II unless otherwise stated. Mechanical stirring using the multi mixer and ultrasonication of the NPs/Ca-bentonite suspension for one hour was used before adding the other additives. In the following sections, the effect of two parameters on the drilling fluid preparation have been investigated: (1) the ultrasonication time, and (2) the effect of bentonite hydration.

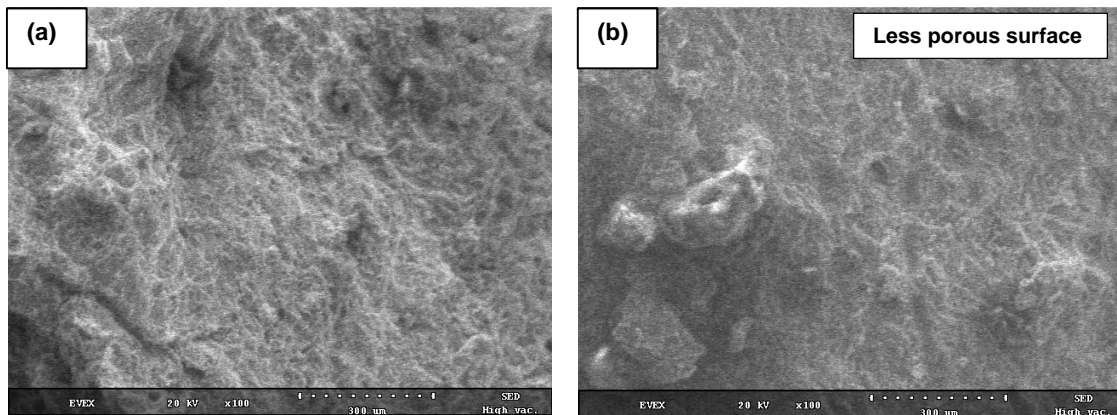


Fig. IV- 12—SEM images (X100-300 μm) of the bottom surface of the dried filter cakes having different concentrations of ferric oxide NPs formed under dynamic filtration (100 rpm) at 250°F and 500 psi differential pressure: (a) with 0.0 wt%, and (b) with 0.5 wt% of NPs. The cake has 0.5 wt% of NPs shows less porous structure.

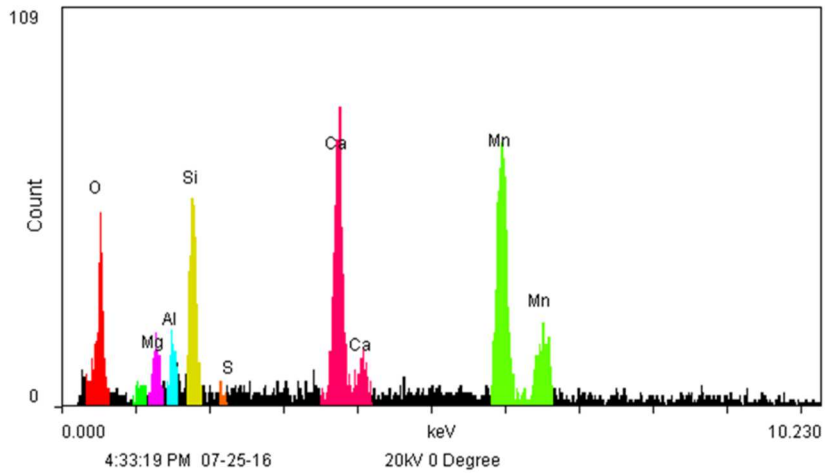


Fig. IV- 13—EDS spectrum analysis of the bottom surface of the dried filter cake having 0.5 wt% ferric oxide NP concentration formed under dynamic filtration (100 rpm) at 250°F and 300 psi differential pressure.

Effect of Ultrasonication

Three different drilling fluids having 0.5 wt% of NPs were prepared using ultrasonication time of: 0.0, 0.5, and 1.0 hour. Then, filter press experiments were conducted at a differential pressure of 300 psi and a temperature of 250°F under static conditions (experiments number 3, 14, and 15 in Table IV-2).

Table IV-6 shows the properties of the filter cakes generated under such conditions. The filter cake of the drilling fluid sonicated for one hour had the optimal properties of 0.197 in. cake thickness, 7.4 ml filtrate volume, and 0.343 μ d filter cake permeability. This showed the importance of ultrasonication of this type of NPs/Ca bentonite-based drilling fluid for one hour to obtain good characteristics. Moreover, the average CTN of the filter cake layers relatively decreased when sonicated, which indicated a better suspension of NPs in the drilling fluid while deposited to form the cake. **Fig. IV-**

14 shows the cumulative filtrate volume plotted against time curves, which were used in the permeability calculation (for detailed results, see **Appendix D**).

Sonication Time, hr	Filter Cake Thickness, in.	Cumulative Filtrate Volume, ml	Filter Cake Permeability, μ d	CT Number	
				Top Layer	Bottom Layer
0.0	0.1611	8.45	0.456	848.02	997.23
0.5	0.2109	9.10	0.629	794.60	960.24
1.0	0.1968	7.40	0.343	794.08	961.28

Table IV- 6— Filter cake characteristics of the drilling fluid having 0.5 wt% of ferric oxide NPs at 300 psi and 250°F and different ultrasonication times.

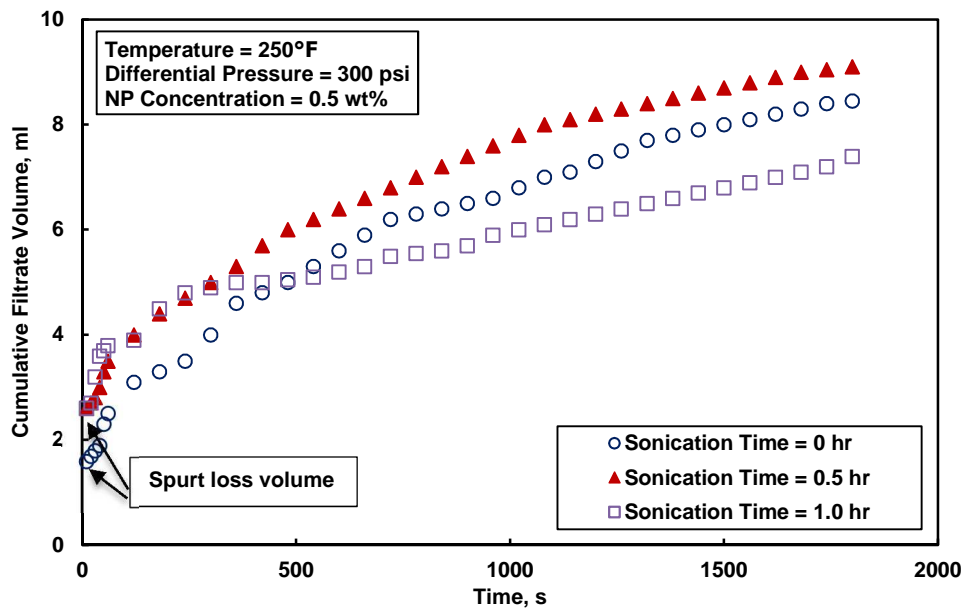


Fig. IV- 14— Cumulative filtrate volume as a function of time for the drilling fluids containing 0.5 wt% ferric oxide NP concentration under static filtration at 250°F and 300 psi differential pressure prepared using different times of ultrasonication (0, 0.5 and 1 hour).

Effect of Bentonite Hydration

In this section, the effect of bentonite hydration on the filter cake characteristics was examined. The bentonite hydration is preferred by the API standards while the

preparation of bentonite suspensions (*API Specifications 13A* 1993; *API 13B-1* 2003). The same procedures mentioned in chapter II were followed except that the ultrasonication was replaced by hydration in a plastic container. The bentonite and the NPs/Ca-bentonite suspensions was sealed in a plastic container and left for 16 hours at room temperature to hydrate. After that, the other drilling fluid additives were added following the aforementioned procedures.

The filtration experiments were conducted under static mode at a differential pressure of 500 psi and a temperature of 250°F (experiments number 16 and 17 in Table IV-2). The results were compared to the experiments number 10 and 12, which were conducted at the same conditions without hydration. **Table IV-7** and **Fig. IV-15** show the filter cake characteristics and the cumulative filtrate volume versus time curve for experiments 16 and 17. The cake generated by the drilling fluid that has 0.5 wt% of NPs (hydrated for 16 hours) has better characteristics compared to the one that has no NPs. A decrease in the filter cake thickness, cumulative filtrate volume, and filter cake permeability by 20.6, 14.3, and 12.8, respectively, was observed. This confirmed the availability of the NPs to generate a good-quality filter cake. Moreover, those cakes had better properties when compared to the cakes generated by the drilling fluids without hydration (experiments 10 and 12). The best cake characteristics were obtained for the filter cake of the drilling fluid that contains 0.5 wt% of NPs, which hydrated for 16 hours. These properties are 0.204 in. thickness, 7.2 ml filtrate volume, and 0.402 μ d filter cake permeability.

Fig. IV-16 shows the SEM image of the top surface (close to the drilling fluid) of the filter cakes generated under static conditions for the drilling fluid that has 0.5 wt% with and without bentonite hydration. The hydration results in a better surface morphology and cake structure (Hartman et al. 1988; Chenevert and Huycke 1991; Plank and Gossen 1991).

NP Concentration	Hydration Time, hr	Filter Cake Thickness, in.	Cumulative Filtrate Volume, ml	Filter Cake Permeability, μ d	CT Number	
					Top Layer	Bottom Layer
0.0	16	0.257	8.4	0.461	568.77	811.41
0.5	16	0.204	7.2	0.402	673.24	802.95

Table IV- 7— Filter cake characteristics of the drilling fluids that have 0.0 and 0.5 wt% of ferric oxide NPs at 500 psi and 250°F (effect of bentonite hydration).

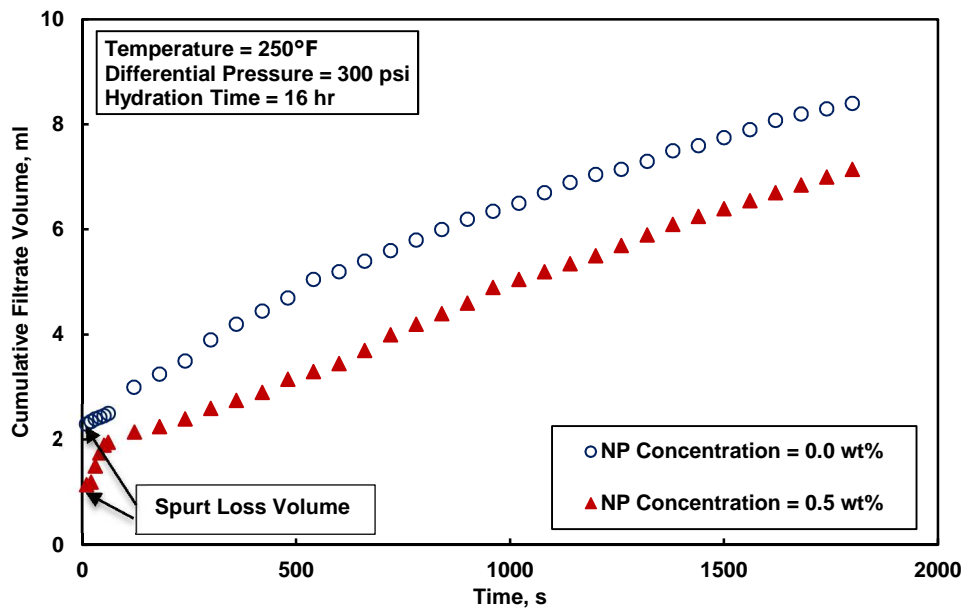


Fig. IV- 15— Cumulative filtrate volume as a function of time for the drilling fluid containing 0.0 and 0.5 wt% ferric oxide NP concentrations under static filtration at 500 psi differential pressure and 250°F prepared using bentonite hydration for 16 hours.

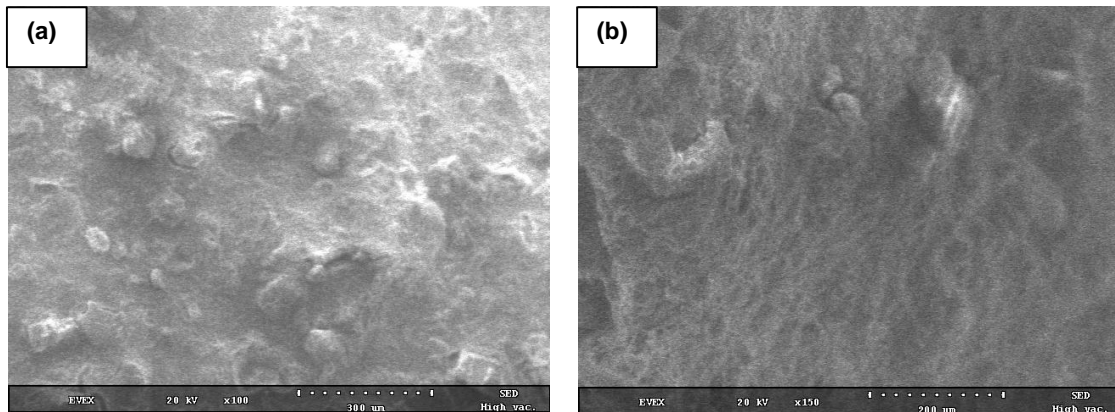


Fig. IV- 16— SEM images of the top surface of the dried filter cakes having 0.5 wt% of ferric oxide NPs formed under static conditions at 250°F and 500 psi differential pressure: (a) with no hydration (X100-300), and (b) with 16 hours of hydration (X150-500 μm).

Conclusions

The effectiveness of using ferric oxide NPs (size less than 50 nm) on the filter cake characteristics and filtration properties of Ca-bentonite-based drilling fluid has been investigated in the presence of polymers and other drilling fluid additives. Based on the results obtained the following conclusions can be drawn:

1. Using ferric oxide NPs improved the filter cake and filtration characteristics of Ca-bentonite-based drilling fluids in the presence of polymer and other additives.
2. The NP concentration less than 1.0 wt% should be used for generating a good-quality cake. The best cake characteristics were obtained at 0.3-0.5 wt% NPs.
3. The NPs/Ca-bentonite-based drilling fluids could withstand downhole conditions up to 500 psi and 350°F. At such conditions, a filter cake with 0.151 in. thickness, 6.9 ml filtrate volume, and 0.428 μd permeability was generated.

4. Adding ferric oxide NPs to the Ca-bentonite-based drilling fluids enhanced their filter cake characteristics under both static and dynamic filtration compared to the base fluid.
5. The ultrasonication of this type of NPs/Ca-bentonite-based drilling fluids for one hour is recommended while preparation. At such preparation method, a filter cake with 0.197 in. thickness, 7.4 ml filtrate volume, and 0.343 μ d permeability was deposited.
6. Bentonite hydration for 16 hours is recommended while preparing this kind of NPs/Ca-bentonite-based drilling fluids. A filter cake with 0.204 in. thickness, 7.2 ml filtrate volume, and 0.402 μ d permeability was generated when the drilling fluid was hydrated before filtration.
7. SEM-EDS analysis confirmed the efficiency of ferric oxide NPs to form a smoother morphology/less porous filter cake because of its ability to form a rigid bentonite-platelet structure in the drilling fluid.

CHAPTER V

CONCLUSIONS AND RECOMMENDATIONS

Different types and sizes of oxide NPs had been investigated for improving the characteristics of Ca-bentonite-based fluids to be used as a fluid for drilling harsh environments. Ferric oxide (of sizes <50 nm), magnetic iron oxide (of average particle size 50 –100 nm), silica (size =12 nm), and zinc oxide NPs (of sizes <100 nm) had been tested throughout this investigation. Based on the experimental results obtained the following conclusions can be drawn:

1. Nanoparticle modified Ca-bentonite can be used a drilling fluid additive instead of Na-bentonite for drilling environments up to 350°F and 500 psi.
2. Adding ferric oxide and magnetic iron oxide NPs at an optimum concentration of 0.5 wt% improved the filter cake characteristics of Ca-bentonite-based fluids at the investigated conditions. However, using silica or zinc oxide NPs reduced the filter cake efficiency of such fluids.
3. A reduction of 43% in the filtrate fluid loss volume and 76.4% in the filter cake permeability was achieved upon the addition of 0.5 wt% of ferric oxide NPs to 7 wt% Ca-bentonite-based fluid compared to that without NPs. The magnetic iron oxide NPs showed the same reduction in the filter loss at the same NP concentration. However it showed a reduction in the filter cake permeability of 35.8% compared to the base and a good achievement in reducing the filter cake thickness.

4. The filter cake of the fluids having iron oxide NPs consisted of two layers as revealed by CT scan analysis. The layer close to the rock surface was the main layer, in which the NPs played a key role in building the filter cake microstructure.
5. Using the optimum NP concentration (0.5 w%) generated a rigid/smooth surface filter cake morphology with less particle agglomeration and low porosity/low permeability structure as indicated by SEM-EDS analysis.
6. A third layer consisting mainly of the agglomerated NPs formed when using higher concentrations of ferric oxide or magnetic iron oxide NPs (2.5 wt%), which reduced the filter cake efficiency (i. e., producing a thick, permeable filter cake with high fluid loss volume).
7. The ferric oxide and magnetic iron oxide NPs promoted better bentonite-platelet microstructure after the dissociation of Ca^{2+} cations from the bentonite at such conditions because of their positively surface charge, which produced a good-quality filter cake.
8. The filter cakes that have optimum concentration of ferric oxide NPs can withstand downhole conditions up to 350°F and 500 psi. Moreover, the effect of temperature on the filter cake characteristics of this type of NPs/Ca-bentonite-based fluids is predominant compared to pressure.
9. Ferric oxide and magnetic iron oxide NPs with positive surface charges were stable in suspensions and building a strong yield structure with Ca-bentonite, which produced fluids with better rheological properties. On the other hand, using silica

NPs that had negative surface charge generated suspensions with higher viscosities and weaker yield structure.

10. Aging at 350°F for 16 hours shows that the rheological properties of Ca-bentonite-based drilling fluid that has ferric oxide NPs remains stable over time with minor loss in the gel structure. On the other hand, aging silica NPs-based fluids under the same conditions showed unstable rheological properties.
11. The Herschel-Bulkley was found to be the best fit model for the experimental data of the tested NPs/Ca-bentonite fluids with R^2 values higher than 0.99 and minimum $\sum Q^2$ values, especially at higher temperatures.
12. The CT scan analysis of the core disks showed a little decrease of the core porosity after the filtration process using the NPs/Ca-bentonite suspensions, which confirming its capability to minimize formation damage.

Ferric oxide NPs had been selected and used for formulating and investigating the filter cake characteristics and filtration properties of a Ca-bentonite-based drilling fluid in the presence of polymers and other drilling fluid additives. Based on the experimental results obtained the following conclusions can be yielded:

1. Ferric oxide NPs improved the filter cake and filtration characteristics of Ca-bentonite-based drilling fluids in the presence of polymer and other additives.
2. A NP concentration of less than 1.0 wt% should be used for generating a good-quality filter cake. The best cake characteristics were obtained at NP concentrations of 0.3-0.5 wt%.

3. The NPs/Ca-bentonite-based drilling fluids could withstand downhole conditions up to 500 psi and 350°F. At such conditions, a filter cake with 0.151 in. thickness, 6.9 ml filtrate volume, and 0.428 μ d permeability was generated.
4. Adding ferric oxide NPs to the Ca-bentonite-based drilling fluids enhanced their filter cake characteristics under both static and dynamic filtration compared to the base fluid.
5. The ultrasonication of this type of NPs/Ca-bentonite-based drilling fluids for one hour is recommended while preparation. At such preparation method, a filter cake with 0.197 in. thickness, 7.4 ml filtrate volume, and 0.343 μ d permeability was deposited.
6. Bentonite hydration for 16 hours is recommended while preparing this kind of NPs/Ca-bentonite-based drilling fluids. A filter cake with 0.204 in. thickness, 7.2 ml filtrate volume, and 0.402 μ d permeability was generated when the drilling fluid was hydrated before filtration.
7. SEM-EDS analysis confirmed the efficiency of ferric oxide NPs to form a smoother morphology/less porous filter cake because of its ability to form a rigid bentonite-platelet structure in the drilling fluid.

This research provides a lab investigation of an improved NPs/Ca-bentonite-based fluid for drilling applications. The ferric oxide and magnetic iron oxide NPs have the potential to promote drilling fluid rheological and filtration characteristics, which provides a high-efficiency drilling practices and less potential to damage the formation. This work

opens a new window on using NPs to enhance the properties Ca-bentonite and formulate higher-efficiency fluids for safer, lower cost drilling applications, and less potential to damage the formation.

REFERENCES

- Abdo, J. and Haneef, M. D. 2012. Nano-Enhanced Drilling Fluids: Pioneering Approach to Overcome Uncompromising Drilling Problems. *J. Energy Resour. Technol* **134** (1): 014501. <http://doi:10.1115/1.4005244>.
- Abdo, J. and Haneef, M. D. 2013. Clay Nanoparticles Modified Drilling Fluids for Drilling of Deep Hydrocarbon Wells. *Appl. Clay Sci.* **86**: 76-82. <http://doi:10.1016/j.clay.2013.10.017>.
- Abrams, A. 1977. Mud Design to Minimize Rock Impairment Due to Particle Invasion. *J Pet Technol* **29** (5): 586-592. SPE-5713-PA. <http://dx.doi.org/10.2118/5713-PA>.
- Aftab, A., Ismail, A. R., Khokhar, S. et al. 2016. Novel Zinc Oxide Nanoparticles Deposited Acrylamide Composite Used for Enhancing the Performance of Water-Based Drilling Fluids at Elevated Temperature Conditions. *J. Pet. Sc. Eng.* **146**: 1142-1157. <https://doi.org/10.1016/j.petrol.2016.08.014>.
- Agarwal, S., Tran, P., Soong, Y. et al. 2011. Flow Behavior of Nanoparticle Stabilized Drilling Fluids and Effect of High Temperature Aging. Presented at the AADE National Technical Conference and Exhibition, Houston, Texas, 12-14 April. AADE-11-NTCE-3.
- Akin, S. and Kovsky, A. R. 2003. Computed Tomography in Petroleum Engineering Research. *Geological Society of London* **215** (1): 23-38. <http://dx.doi:10.1144/GSL.SP.2003.215.01.03>.

- Al-Abduwani, F. A. H., Bedrikovesty, P., Farajzadeh, R. et al. 2005. External Filter Cake Erosion: Mathematical Model and Experimental Study. Presented at the European Formation Damage Conference, Scheveningen, The Netherlands, 25-27 May. SPE-94635-MS. <http://dx.doi.org/10.2118/94635-MS>.
- Alderman, N. J., Gavignet, A., Guillot, D. et al. 1988. High-Temperature, High-Pressure Rheology of Water-Based Muds. Presented at the SPE Annual Technical Conference and Exhibition, Houston, Texas, 2-5 October. SPE-18035-MS. <http://dx.doi.org/10.2118/18035-MS>.
- Alotaibi, M. B., Nasr-El-Din, H. A., and Fletcher, J. J. 2011. Electrokinetics of Limestone and Dolomite Rock Particles. *SPE Res Eval & Eng* **14** (5): 594-603. SPE-148701-PA. <http://dx.doi.org/10.2118/148701-PA>.
- Alsaba, M., Nygaard, R., Hareland, G. et al. 2014. Review of Lost Circulation Materials and Treatments with Updated Classification. Presented at the AADE Fluids Technical Conference and Exhibition, Houston, Texas, 15-16 April. AADE-14-FTCE-25.
- Akhtarmanesh, S., Ameri Shahrabi, M.J., and Atashnezhad, A. 2013. Improvement of Wellbore Stability in Shale Using Nanoparticles. *J Petrol Sci Eng* **112**: 290-295. <http://doi.org/10.1016/j.petrol.2013.11.017>.
- Amaefule, J. O., Kersey, D. G., Norman, D. L. et al. 1988. Advances in Formation Damage Assessment and Control Strategies. Presented at the Annual Technical Meeting of Petroleum Society of CIM and Canadian Gas Processors Association, Calgary, Alberta, 12-16 June. PETSOC-88-39-65. <http://dx.doi.org/10.2118/88-39-65>.

- Amanullah, Md., Al-Arfaj, K., and Al-Abdullatif, Z. 2011. Preliminary Test Results of Nano-Based Drilling Fluids for Oil and Gas Field Application. Presented at the SPE/IADC Conference and Exhibition, Amsterdam, The Netherlands, 1-3 March. SPE/IADC 139534. <http://dx.doi.org/10.2118/139534-MS>.
- Amanullah, Md. and Al-Arfaj, K. 2013. Water-Based Drilling Fluid Composition Having Multifunctional Mud Additive for Reducing Fluid Loss During Drilling. US Patent # 0065798 A1.
- Amarfio, E. M. and Abdulkadir, M. 2015. Effect of Fe₄O₃ Nanoparticles on the Rheological Properties of Water Based Mud. *J. Phys. Sc. App.* **5** (6): 415-422. <https://doi:10.17265/2159-5348/2015.06.005>.
- Amarfio, E. M. and Abdulkadir, M. 2016. Effect of Al₂O₃ Nanoparticles on the Rheological Properties of Water Based Mud. *Int. J. Sc. Eng. App.* **5** (1): 7-11. ISSN-2319-7560 (Online).
- Annis, M. R. 1967. High Temperature Flow Properties of Water-Based Drilling Fluids. *J Pet Technol* **19** (8): 1074–1080. SPE-1698-PA. <http://dx.doi.org/10.2118/1698-PA>.
- Anoop, K., Sadr, R., Al-Jubouri, M. et al. 2014. Rheology of Mineral Oil-SiO₂ Nanofluids at High Pressure and High Temperatures. *Int. J. Therm. Sc.* **77**: 108-115. <https://doi.org/10.1016/j.ijthermalsci.2013.10.016>.
- API Specifications 13A, 18th edition. Specification for Drilling Fluid Materials.* 2010. Washington, DC: API.
- API Specifications 13B-1. Recommended Practice for Field Testing Water-Based Drilling Fluids.* 2003. Washington, DC: API.

- Bageri, B. S., Al-Mutairi, S. H., and Mahmoud, M. 2013. Different Techniques for Characterizing the Filter Cake. Presented at the SPE Unconventional Gas Conference and Exhibition, Muscat, Oman, 28-30 January. SPE-163960-MS. <http://dx.doi.org/10.2118/163960-MS>.
- Baird, J. C. and Walz, J. Y. 2006. The Effects of Added Nanoparticles on Aqueous Kaolinite Suspensions: I. Structural effects. . *J. Colloid Interface Sci.* **297** (1): 161–169. <http://doi:10.1016/j.jcis.2005.10.022>.
- Barry, M. M., Jung, Y., Lee, J. -K. et al. 2015. Fluid Filtration and Rheological Properties of Nanoparticle Additive and Intercalated Clay Hybrid Bentonite Drilling Fluids. *J Petrol Sci Eng* **127**: 338-346. <http://doi:10.1016/j.petrol.2015.01.012>.
- Behari, J. 2010. Principles of Nanoscience: An Overview. *Indian J. Exp. Biol.* **48** (10): 1008–1019.
- Belayneh, M. and Aadnoy, B. S. 2016. Effect of Nano-Silicon Dioxide (SiO₂) on Polymer/Salt Treated Bentonite Drilling Fluid Systems. Presented at the 35th International Conference on Ocean, Offshore and Arctic Engineering, ASME 2016, Busan, South Korea. 19-24 June. OMAE2016-54450. <http://doi:10.1115/OMAE2016-54450>.
- Bourgoyne, A. T., Millheim. K. K., Chenevert, M. E. et al. 1991. *Applied Drilling Engineering*. Second (revised) printing. Richardson, TX: SPE Textbook Series, Vol. 2.
- Bowyer, P. K. and Moine-L, V. 2008. *Bentonite-More than Just Dirt*. Wynboer, a Technical Guide for Wine Producers.

- Cai, J., Chenevert, M. E., Sharma, M. M. et al. 2012. Decreasing Water Invasion into Atoka Shale Using Nanommodified Silica Nanoparticles. *SPE Drill & Compl* **27** (1): 103-112. SPE-146979-PA. <http://dx.doi.org/10.2118/146979-PA>.
- Casillas-Iturate, N. N., Chen, X., Castada, H. et al. 2010. Na⁺ and Ca²⁺ Effect on the Hydration and Orientation of the Phosphate Group of DPPC at Air-Water and Air-Hydrated Silica Interfaces. *J. Phys. Chem.* **114** (29): 9485-9495. <http://doi: 10.1021/jp1022357>.
- Chassin, P., Jounay, C., and Quiquampoix, H. 1986. Measurement of the Surface Free Energy of Calcium-Montmorillonite. *Clay Minerals* **21**: 899-907. http://www.minersoc.org/pages/Archive-CM/Volume_21/21-5-899.pdf.
- Chenevert, M. E. and Huycke, J. 1991. Filter Cake Structure Analysis Using the Scanning Electron Microscope. SPE-22208-MS, unsolicited. *Society of Petroleum Engineers, Richardson, TX*.
- Civan, F. 1994. A Multi-Phase Mud Filtrate Invasion and Wellbore Filter Cake Formation Model. Presented at the International Petroleum Conference and Exhibition of Mexico, Veracruz, Mexico, 10-13 October. SPE-28709-MS. <http://dx.doi.org/10.2118/28709-MS>.
- Civan, F. 1996. A Multi-Purpose Formation Damage Model. Presented at the Formation Damage Control Symposium, Lafayette, Louisiana, 14-15 February. SPE-31101-MS. <http://dx.doi.org/10.2118/31101-MS>.
- Contreras, O., Hareland, G., Husein, M. et al. 2014. Application of In-House Prepared Nanoparticles as Filtration Control Additive to Reduce Formation Damage. Presented

at the International Symposium and Exhibition on Formation Damage Control, Lafayette, Louisiana, 26-28 February. SPE-168116-MS. <http://dx.doi.org/10.2118/168116-MS>.

El-Diasty, A. I. and Aly, A., M. 2015. Understanding the Mechanism of Nanoparticles Applications in Enhanced Oil Recovery. Presented at the SPE North Africa Technical Conference and Exhibition, Cairo, Egypt, 14-16 September. SPE-175806-MS. <https://doi.org/10.2118/175806-MS>.

Elkhatatny, S. M., Mahmoud, M. A., and Nasr-El-Din, H. A. 2012. Characterization of Filter Cake Generated by Water-Based Drilling Fluids Using CT Scan. *SPE Drill & Compl* **27** (2): 282-293. SPE-144098-PA. <http://dx.doi.org/10.2118/144098-PA>.

Elkhatatny, S., Mahmoud, M., and Nasr-El-Din, H., A. 2013. Filter Cake Properties of Water-Based Drilling Fluids Under Static and Dynamic Conditions Using Computed Tomography Scan. *J. Energy Resour. Technol* **135** (4): 042201-9. <http://doi:10.1115/1.4023483>.

Elkhatatny, S., Rostami, A., and Nasr-El-Din, H., A. 2011. Characterization a Self-destructing Filter cake by Using Computer Tomography. Presented at the SPE/IADC Middle East Drilling Technology Conference and Exhibition, Muscat, Oman, 24-26 October. SPE-148124-MS. <https://doi.org/10.2118/148124-MS>.

Foxenberg, W. E., Ali, S. A., Long, T. P. et al. 2008. Field Experience Shows that New Lubricant Reduces Friction and Improves Formation Compatibility and Environmental Impact. Presented at the International Symposium and Exhibition on

Formation Damage Control, Lafayette, Louisiana, 13-15 February. SPE-112483-MS.
<http://dx.doi.org/10.2118/112483-MS>.

Fereydouni, M., Sabbaghi, S., Saboori, R. et al. 2012. Effect of Polyanionic Cellulose Polymer Nanoparticles on Rheological Properties of Drilling Mud. *Int. J. Nanosci. Nanotechnol.* **8** (3): 171-174.
http://ijnnonline.net/article_3902_44daeb1450e7d68c149fe717bd1b8dc4.pdf.

Friedheim, J., Young, S., De Stefano, G. et al. 2012. Nanotechnology for Oilfield Applications – Hype or Reality? Presented at the SPE International Nanotechnology Conference, Noordwijk, The Netherlands, 12-14 June. SPE-157032-MS.
<https://doi.org/10.2118/157032-MS>.

Garcia-Romero, E., Suarez, M. 2010. On the Chemical Composition of Sepiolite and Palygorskite. *Clays Clay Min.* **58** (1): 1-20.
<http://dx.doi.org/10.1346/CCMN.2010.0580101>.

Grandjean, J. 1997. Note: Water Sites at a Clay Interface. *J Colloid Interface Sci.* **185** (2): 554–556. <http://doi:10.1006/jcis.1996.4630>.

Grim, R.E. 1968. *Clay Mineralogy*. Second Edition. New York City: McGraw-Hill Book Company, Inc.

Growcock, F. B., Frederick, T. P., Reece, A. R. et al. 1998. Novel Lubricants for Water-Based Drilling Fluids. Presented at the International Symposium on Oilfield Chemistry, Houston, Texas, 16-19 February. SPE-50710-MS.
<http://dx.doi.org/10.2118/50710-MS>.

- Hartman, A., Ozerler, M., Marx, C. et al. 1988. Analysis of Mudcake Structures Formed Under Simulated Borehole Conditions. *SPE Drill Eng* **3** (4): 885-898. SPE-15413-PA. <http://dx.doi.org/10.2118/15413-PA>.
- Hoerrock, L. L. and Bratcher, G. J. 1998. Dynamic Differential Pressure Effects on Drilling of Permeable Formations. *ASME J. Energy Resour. Technol.* **120** (2): 118-123. <http://doi/10.1115/1.2795021>.
- Hoelscher, K.P., De Stefano, G., Riley, M. et al. 2012. Application of Nanotechnology in Drilling Fluids. Presented at the SPE International Nanotechnology Conference, Noordwijk, The Netherlands, 12-14 June. SPE-157031-MS. <https://doi.org/10.2118/157031-MS>.
- Hoelscher, K.P., Young, S., Friedheim, J. et al. 2013. Nanotechnology Application in Drilling Fluids. Presented at the 11th Offshore Mediterranean Conference and Exhibition, Ravenna, Italy, 20-22 March. OMC-2013-105. <https://www.onepetro.org/conference-paper/OMC-2013-105>.
- Hunter, R. J. 1988. *Zeta Potential in Colloidal Science: Principles and Applications*. Third printing. London: Academic Press.
- Husein, M. M., and Hareland, G. 2014. Drilling Fluids with Nano and Granular Particles and Their Use for Wellbore Strengthening. Patent # WO 2014008598 A1.
- Ismail, A. R., Rashid, N. M., and Jaafar, M. Z. 2014. Effect of Nanomaterial on the Rheology of Drilling Fluids. *J. Appl. Sci.* **14** (11): 1192-1197. <http://doi: 10.3923/jas.2014.1192.1197>.

- Javeri, S. M., Haindade, Z. W., and Jere, C. B. 2011. Mitigation Loss Circulation and Differential Sticking Problems Using Silicon Nanoparticles. Presented at the SPE/IADC Middle East Drilling Technology Conference and Exhibition, Muscat, Oman, 24-26 October. SPE-145840-MS. <http://dx.doi.org/10.2118/145840-MS>.
- Ju, B., Shugao, D., Zhian, L. et al. 2002. A Study of Wettability and Permeability Change Caused by Adsorption of Nanometer Structured Polysilicon on the Surface of Porous Media. Presented at the SPE Asia Pacific Oil and Gas Conference and Exhibition, Melbourne, Australia, 8-10 October. SPE-77938-MS. <https://doi.org/10.2118/77938-MS>.
- Jung, Y., Barry, M., Lee, J. -K. et al. 2011. Effect of Nanoparticle-Additives on the Rheological Properties of Clay-Based Fluids at High Temperature and High Pressure. Presented at the AADE National Technical Conference and Exhibition, Houston, Texas, 12-14 April. AADE-11-NTCE-2.
- Kelessidis, V. C. and Maglione, R. 2008. Yield Stress of Water-Bentonite Dispersions. *Colloids and Surfaces A: Physicochem. Eng. Aspects* **318**: 217-226. <http://doi:10.1016/j.colsurfa.2007.12.050>.
- Kelessidis, V. C. Tsamantaki, C., Michalakis, A. et al. 2007. Greek Lignite as Additives for Controlling Filtration Properties of Water-Bentonite Suspensions at High Temperatures. *Fuel* **86** (7-8): 1112-1121. <http://doi:10.1016/j.fuel.2006.10.009>.
- Kelessidis, V. C. Tsamantaki, C., Pasadakis, N. et al. 2006. Permeability, Porosity and Surface Characteristics of Filter Cakes from Water Bentonite Suspensions. Presented at the 6th International Conference on Advances in Fluid Mechanics, Skiathos, Greece.

WIT Transactions on Engineering Sciences **56** (2007).
[http://doi: 10.2495/MPF070171](http://doi:10.2495/MPF070171).

Kelsall, R. W., Hamley, I. W. and Geoghegan, M. (eds). 2005. *Front Matter, in Nanoscale Science and Technology*. Chichester, UK: John Wiley & Sons, Ltd.
[http://doi: 10.1002/0470020873.fmatter](http://doi:10.1002/0470020873.fmatter).

Keren, R. 1988. Rheology of Aqueous Suspension of Sodium/Calcium Montmorillonite. *Soil Sci. Soc. Am. J.* **52** (4): 924-928. [http://doi: 10.2136/sssaj1988.03615995005200040004x](http://doi:10.2136/sssaj1988.03615995005200040004x).

Kosynkin, D. V., Ceriotti, G., Wilson, K. C. et al. 2012. Graphene Oxide as a High-Performance Fluid-Loss-Control Additive in Water-Based Drilling Fluids. *ACS Appl. Mater. Interfaces* **4** (1): 222-227. <http://pubs.acs.org/doi/abs/10.1021/am2012799>.

Laribi, S., Fleureau, J. -M., Grossiord, J. -L. et al. 2006. Effect of pH on the Rheological Behavior of Pure and Interstratified Smectite. *Clays Clay Min.* **54** (1): 29-37.
<http://doi:10.1346/CCMN.2006.0540104>.

Li, D. and He, W. 2015. Journey into Filter Cakes: A Microstructural Study. Paper presented at the International Petroleum Technology Conference, Doha, Qatar, 6-9 December. IPTC-18246-MS. <http://dx.doi.org/10.2523/IPTC-18246-MS>.

Li, M. -C., Wu, Q., Song, K. et al. 2015a. Cellulose Nanocrystals and Polyanionic Cellulose as Additives in Bentonite Water-Based Drilling Fluids: Rheological Modeling and Filtration Mechanisms. *Ind. Eng. Chem. Res.* **55** (1):133-143.
<https://doi:10.1021/acs.iecr.5b03510>.

- Li, M. -C., Wu, Q., Song, K. et al. 2015b. Cellulose Nanoparticles as Modifiers for Rheology and Fluid Loss in Bentonite Water-Based Fluids. *ACS Appl. Mater. Interfaces*. **7** (8): 5006-5016. <https://doi: 10.1021/acsami.5b00498>.
- Li, S., Osisanya, S., and Haroun, M. 2016. Development of New Smart Drilling Fluids Using Nano-materials for Unconventional Reservoirs. Presented at the Abu Dhabi International Petroleum Exhibition & Conference, Abu Dhabi, UAE, 7-10 November. SPE-183509-MS. <https://doi.org/10.2118/183509-MS>.
- Li, W., Kiser, C., and Richard, Q. 2005. Development of a Filter Cake Permeability Test Methodology. Paper presented at the American Filtration and Separation Society International Topical Conference and Exposition, Ann Arbor, Michigan, USA, 19-22 September.
- Lu, A., -H., Salabas, E. L., and Schuth, F. 2007. Magnetic Nanoparticles: Synthesis, Protection, Functionalization, and Application. *Angew. Chem. Int. Ed.* **46** (8): 1222–1244. <http://doi: 10.1002/anie.200602866>.
- Luckham, P. F. and Rossi, S. 1999. The Colloidal and Rheological Properties of Bentonite Suspensions. *Adv Colloid Interface Sci* **82** (1-3): 43–92. [http://doi:10.1016/S0001-8686\(99\)00005-6](http://doi:10.1016/S0001-8686(99)00005-6).
- Manea, M. 2012. Design of Drilling Fluids Using Nano Scale Polymer Additives. *Rev. Roum. Chim.* **57** (3): 197-202. http://revroum.lew.ro/wp-content/uploads/2012/RRCh_3_2012/Art%2005.pdf.
- Mao, H., Qiu, Z., Shen, Z. et al. 2015. Novel Hydrophobic Associated Polymer Based Nano-Silica Composite with Core-Shell Structure for Intelligent Drilling Fluid Under

- Ultra-High Temperature and Ultra-High Pressure. *Progress in Natural Science: Materials International* **25** (1): 90-93. <https://doi.org/10.1016/j.pnsc.2015.01.013>.
- Marcus, Y. 1991. Thermodynamics of Solvation of Ions. Part 5. – Gibbs Free Energy of Hydration at 298.15 K. *J. Chem. Soc., Faraday Trans.* **87** (18): 2995-2999. <http://doi:10.1039/FT9918702995>.
- Mas, M., Tapin, T., Macrquez, R. et al. 1999. A New High-Temperature Oil-Based Drilling Fluid. Presented at the Latin American and Caribbean Conference, Caracas, Venezuela, 21-23 April. SPE-53941-MS. <http://dx.doi.org/10.2118/53941-MS>.
- Michaelides, E. E. 2014. *Nanofluidics: Thermodynamics and Transport Properties*. New York: Springer Cham Heidelberg.
- Missana, T. and Adell, A. 2000. On the Applicability of DLVO Theory to the Prediction of Clay Colloids Stability. *J. Colloid Interf. Sci.* **230** (1): 150–156. <http://doi:10.1006/jcis.2000.7003>.
- Nasser, J., Jesil, A., Mohiuddin, T. et al. 2013. Experimental Investigation of Drilling Fluid Performance as Nanoparticles. *World Journal of Nano Science and Engineering* **3** (3): 57-61. <http://doi:10.4236/wjnse.2013.33008>.
- Nwaoji, C. O., Hareland, G., Husein, M. et al. 2013. Wellbore Strengthening-Nano-Particle Drilling Fluid Experimental design Using Hydraulic Fracture Apparatus. Presented at the SPE/IADC Drilling Conference and Exhibition, Amsterdam, The Netherlands, 5-7 march. SPE-163434-MS. <https://doi.org/10.2118/163434-MS>.

- Parizad, A. and Shahbazi, K. 2016. Experimental Investigation of the Effects of SnO₂ Nanoparticles and KCl salt on a Water Base Drilling Fluid Properties. *Can. J. Chem. Eng.* **94** (10): 1924-1938. <http://doi: 10.1002/cjce.22575>.
- Plank, J. P. and Gossen, F. A. 1991. Visualization of Fluid-Loss Polymers in Drilling-Mud Filter Cakes. *SPE Drill Eng* **06** (3): 203-208. SPE-19534-PA. <http://dx.doi.org/10.2118/19534-PA>.
- Ponmani, S., William, J.K.M., Samuel, R. et al. 2014. Formation and Characterization of Thermal and Electrical Properties of CuO and ZnO Nanofluids in Xanthan Gum. *Colloids and Surfaces A: Physicochem. Eng. Aspects* **443**: 37-43. <http://doi.org/10.1016/j.colsurfa.2013.10.048>.
- Ramos-Tejada, M., Arroyo, F., Perea, R. et al. 2001. Scaling behavior of the Rheological Properties of Montmorillonite Suspensions: Correlation between Interparticle Interaction and Degree of Flocculation. *J. Colloid Interface Sci.* **235** (2): 251-259. <http://doi:10.1006/jcis.2000.7370>.
- Ravi, K., Patil, R.C., Patil, S.P., et al. 2011. Lost Circulation Compositions and Associated Methods. US Patent # 20110162845.
- Riddick, T. M. 1986. *Control of Stability through Zeta Potential*. New York: Zeta-Meter Inc., Vol. 1.
- Sadeghalvaad, M. and Sabbaghi, S. 2015. The Effect of the TiO₂/Polyacrylamide Nanocomposite on Water-Based Drilling Fluid Properties. *Powder Technology* **272**: 113-119. <https://doi.org/10.1016/j.powtec.2014.11.032>.

- Salih, A. H., Elshehabi, T. A., Bilgesu, H. I. 2016. Impact of Nanomaterials on the Rheological and Filtration Properties of Water-Based Drilling Fluids. Presented at the SPE Eastern Regional Meeting, Canton, Ohio, USA, 13-15 September. SPE-184067-MS. <https://doi.org/10.2118/184067-MS>.
- Sensoy, T., Chenevert, M. E. and Sharma, M. M. 2009. Minimizing Water Invasion in Shale Using Nanoparticles. Presented at the SPE Annual Technical Conference and Exhibition, New Orleans, Louisiana, USA, 4-7 October. SPE-124429-MS. <https://doi.org/10.2118/124429-MS>.
- Sharma, M. M., Zhang, R., Chenevert, M. E. et al. 2012. A New Family of Nanoparticle Based Drilling Fluids. Presented at the SPE Annual Technical Conference and Exhibition, San Antonio, Texas, 8-10 October. SPE-160045-MS. <https://doi.org/10.2118/160045-MS>.
- Shin, Y., Lee, D., Lee, K. et al. 2008. Surface Properties of Silica Nanoparticles Modified with Polymers for Polymer Nanocomposite Applications. *J IND ENG CHEM* **14** (4): 515–519. <http://doi.org/10.1016/j.jiec.2008.02.002>.
- Srivatsa, J. T. and Ziaja, M. B. 2011. An Experimental Investigation on Use of Nanoparticles as Fluid Loss Additives in a Surfactant-Polymer Based Drilling Fluid. Presented at the International Technology Conference, Bangkok, Thailand, 7-9 February. IPTC-14952-MS. <https://doi.org/10.2523/IPTC-14952-MS>.
- Szabo, T., Bakandritsos, A., Tzitzios, V., et al. 2007. Magnetic Iron Oxide/Clay Composites: Effect of the Layer Silicate Support on the Microstructure and Phase

- Formation of Magnetic Nanoparticles. *Nanotechnology* **18**: 285602-285610. <http://doi:10.1088/0957-4484/18/28/285602>.
- Taha, N. M. and Lee, S. 2015. Nano Graphene Application Improving Drilling Fluids Performance. Presented at the International Technology Conference (IPTC), Doha, Qatar, 6-9 December. IPTC-18539-MS. <https://doi.org/10.2523/IPTC-18539-MS>.
- Tohver, V., Samy, J. E., Braem, A. et al. 2001. Nanoparticle Holes: A New Colloid Stabilization Mechanism. *Proc. Natl. Acad. Sci.* **98** (16): 8950-8954. <http://doi:10.1073/pnas.151063098>.
- Tombácz, E., Csanaky, C., Illés, E. 2001. Polydisperse Fractal Aggregate Formation in Clay Mineral and Iron Oxide Suspensions, pH and Ionic Strength Dependence. *Colloid Polym Sci* **279**: 484-492. <http://doi:10.1007/s003960100480>.
- Veblen, D. R., Guthrie Jr, G. D., Livi, K. J. T. et al. 1990. High Resolution Transmission Electron Microscopy and Electron Diffraction of Mixed-Layer Illite/Smectite: Experimental Results. *Clays Clay Min.* **38** (1): 1-13. <http://dx.doi.org/10.1346/CCMN.1990.0380101>.
- Wang, N., Hsu, C., Zhu, L. et al. 2013. Influence of Metal Oxide Nanoparticles Concentration on Their Zeta Potential. *J Colloid Interface Sci.* **407**: 22–28. <http://doi.org/10.1016/j.jcis.2013.05.058>.
- Wellington, S. L. and Vinegar, H. J. 1987. X-Ray Computerized Tomography. *J Pet Technol* **39** (08): 885-898. SPE-16983-PA. <http://dx.doi.org/10.2118/16983-PA>.
- William, J.K.M., Ponmani, S., Samuel, R. et al. 2014. Effect of CuO and ZnO Nanofluids in Xanthan Gum on Thermal, Electrical and High Pressure Rheology of Water-Based

Drilling Fluids. *J Petrol Sci Eng* **117**:15-27.

<http://doi.org/10.1016/j.petrol.2014.03.005>.

Xu, G., Zhang, J., and Song, G. 2003. Effect of Complexation on the Zeta Potential of Silica Powder. *Powder Technology* **134** (3): 218–222. [http://doi.org/10.1016/S0032-5910\(03\)00172-4](http://doi.org/10.1016/S0032-5910(03)00172-4).

Yalcin, T., Alemdar, A., Ece, O. I. et al. 2002. The Viscosity and Zeta Potential of Bentonite Dispersions in Presence of Anionic Surfactants. *Mater. Lett.* **57** (2): 420–424. [http://doi:10.1016/S0167-577X\(02\)00803-0](http://doi:10.1016/S0167-577X(02)00803-0).

Zakaria, M. F., Husein, M., and Hareland, G. 2012. Novel Nanoparticle-Based Drilling Fluid with Improved Characteristics. Presented at the Oilfield Nanotechnology Conference and Exhibition, Noordwijk, The Netherlands, 12-14 June. SPE-156992-MS. <http://dx.doi.org/10.2118/156992-MS>.

APPENDIX A

DEHYDRATION OF CA-BENTONITE SUSPENSIONS

Introduction

The purpose of this appendix is to present in detail the images that show the dehydration, at 212°F (100°C) and ambient pressure, of the 7 wt% Ca-bentonite suspension in deionized water. The examined samples were prepared by following the American Petroleum Institute Standards (*API Specifications 13A* 1993; *API 13B-1* 2003). The fluid was formulated using a bentonite concentration of 7 wt% mixed in 600 ml of deionized water for 20 minutes under mechanical stirring. In this case, a sample of 100 ml were used directly after preparing (without sealing in plastic containers for bentonite to hydrate). The sample was put in a water bath at 212°F (100°C) and the following set of images were taken, which show the physical change in the Ca-bentonite sample as a function of time.



Fig. A- 1—Base Fluid in a water bath at 212°F (100°C) at time zero.



Fig. A- 2—Base Fluid in a water bath at 212°F (100°C) after 30 minutes.



Fig. A- 3—Base Fluid in a water bath at 212°F (100°C) after 60 minutes.

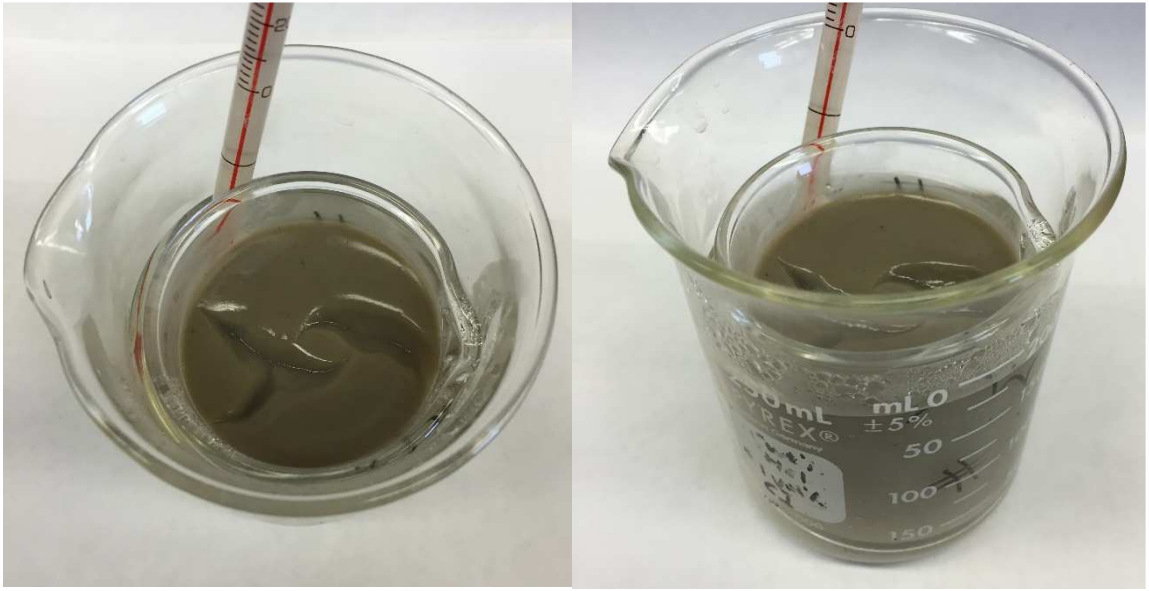


Fig. A- 4—Base Fluid in a water bath at 212°F (100°C) after 90 minutes.



Fig. A- 5—Base Fluid in a water bath at 212°F (100°C) after 120 minutes.

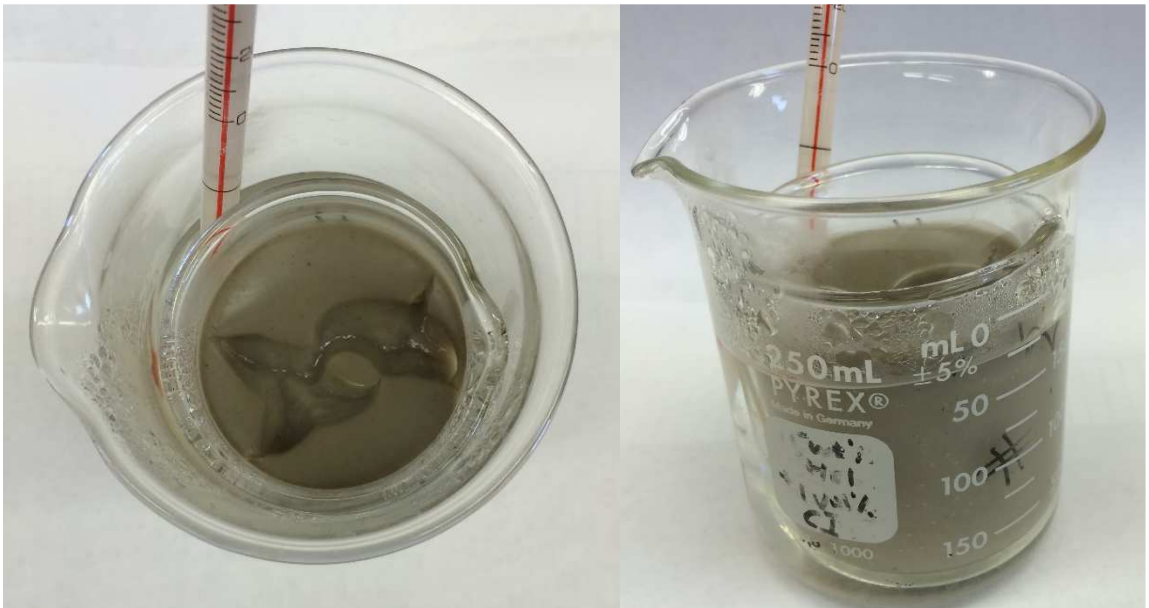


Fig. A- 6—Base Fluid in a water bath at 212°F (100°C) after 150 minutes.



Fig. A- 7—Base Fluid left for 16 hours after thermal aging in a water bath at 212°F (100°C) for 150 minutes.



Fig. A- 8—Base Fluid left for 24 hours at ambient pressure and temperature (no water bath).

APPENDIX B

DETAILED RHEOLOGICAL MEASUREMENT RESULTS

Introduction

The purpose of this appendix is to present the detailed results of the rheological measurement in chapter III. The rheological measurements are conducted on the 7 wt% Ca-bentonite-based suspensions having different concentrations of NPs at various temperatures (120, 140, 160, 180, and 200°F) and ambient pressure. The fluctuations in the data may be due to a possible evaporation of water from the base fluid at atmospheric pressure. The resulted shear stress versus shear rate data was fitted to the non-Newtonian rheological models (Bingham Plastic and Herschel-Bulkley). These models can be described as (**Eqs. III-1**, and **III-2**):

Bingham Plastic model:

$$\tau = \tau_o + \mu_p \dot{\gamma} \quad , \dots\dots\dots (III-1)$$

where τ is the shear stress (lbf/100 ft²), τ_o is the yield stress (lbf/100 ft²), μ_p is the plastic viscosity (cp), and $\dot{\gamma}$ is the shear rate (s⁻¹).

Herschel-Bulkley model:

$$\tau = \tau_o + K \dot{\gamma}^n \quad , \dots\dots\dots (III-2)$$

where K is the consistency index (lbf. sⁿ/100 ft²), and n is the flow behavior index (dimensionless).

Temperature	Bingham Plastic Model				Herschel-Bulkley Model				
	τ_o	μ_p	R^2	$\sum Q^2$	τ_o	k	n	R^2	$\sum Q^2$
(°F)	(lbf/100 ft ²)	(cp)		(lbf/100 ft ²) ²	(lbf/100 ft ²)	(lbf. s ⁿ /100 ft ²)			(lbf/100 ft ²) ²
120	9.64	8.00	0.9966	1.7547	9.25	0.0331	0.9046	0.9947	2.8112
140	10.41	7.08	0.9961	1.6646	10.26	0.0228	0.9389	0.9949	2.0196
160	12.75	6.11	0.9942	1.6235	12.31	0.0278	0.8923	0.9984	0.5174
180	14.32	6.21	0.9953	1.4850	14.36	0.0120	1.0105	0.9997	0.0826
200	14.96	4.84	0.9944	1.0835	14.88	0.0145	0.9486	0.9979	0.4083

Table B- 1— Bingham Plastic and Herschel-Bulkley model constants of the base fluid at different temperatures.

Temperature	Apparent Viscosity (cp)		
	(°F)	1021.381 s ⁻¹	510.6905 s ⁻¹
120	12.52	17.07	22.08
140	11.96	16.84	22.13
160	12.09	17.98	24.23
180	12.92	19.65	26.24
200	11.85	18.44	26.14

Table B- 2— Apparent viscosity of the base fluid at different temperatures and shear rates.

Shear rate	Shear Stress (lb/100 ft ²)				
	(s ⁻¹)	120°F	140°F	160°F	180°F
1021.38	26.70	25.52	25.79	27.57	25.27
510.69	18.21	17.96	19.18	20.96	19.67
340.46	15.70	15.73	17.23	18.66	18.59
170.23	12.15	12.81	14.48	16.53	16.55
102.14	11.35	12.02	14.13	15.45	16.05
51.07	10.49	10.89	13.40	14.84	15.47
10.21	9.58	10.55	12.53	14.59	15.06
5.11	10.93	11.70	13.94	15.57	15.92

Table B- 3— Rheograms of the base fluid at different temperatures.

Temperature	Bingham Plastic Model				Herschel-Bulkley Model				
	τ_o	μ_p	R^2	$\sum Q^2$	τ_o	k	n	R^2	$\sum Q^2$
(°F)	(lb/100 ft ²)	(cp)		(lb/100 ft ²) ²	(lb/100 ft ²)	(lb. s ⁿ /100 ft ²)			(lb/100 ft ²) ²
120	16.36	8.90	0.9977	1.5315	15.55	0.0628	0.8303	0.9968	2.2210
140	18.55	7.29	0.9950	2.0324	17.21	0.0706	0.7907	0.9945	3.0057
160	20.09	6.61	0.9931	2.2420	19.70	0.0334	0.8764	0.9936	2.5098
180	20.66	6.24	0.9961	1.1418	20.18	0.0277	0.8964	0.9985	0.5145
200	21.16	6.51	0.9974	0.8486	21.04	0.0165	0.9736	0.9987	0.4398

Table B- 4— Bingham Plastic and Herschel-Bulkley model constants fitted for the fluid containing 0.5 wt% of ferric oxide NPs at different temperatures.

Temperature	Apparent Viscosity (cp)		
	(°F)	1021.381 s ⁻¹	510.6905 s ⁻¹
120	16.56	24.35	34.12
140	15.99	24.67	33.39
160	16.02	24.77	35.75
180	15.93	25.46	35.29
200	16.43	25.98	36.27

Table B- 5— Apparent viscosity of the fluid containing 0.5 wt% of ferric oxide NPs at different temperatures and shear rates.

Shear rate	Shear Stress (lb/100 ft ²)				
	(s ⁻¹)	120°F	140°F	160°F	180°F
1021.38	35.33	34.11	34.18	33.97	35.05
510.69	25.97	26.32	26.42	27.15	27.71
340.46	23.50	23.74	25.45	25.10	25.79
170.23	20.10	21.30	21.76	22.53	23.53
102.14	18.01	19.77	21.63	22.07	22.52
51.07	16.97	19.35	20.39	21.38	21.38
10.21	16.27	17.65	20.17	20.39	21.39
5.11	16.97	19.51	20.96	21.63	21.90

Table B- 6— Rheograms of the fluid containing 0.5 wt% of ferric oxide NPs at different temperatures and shear rates.

NP Concent. (wt%)	Bingham Plastic Model				Herschel-Bulkley Model				
	τ_o	μ_p	R^2	$\sum Q^2$	τ_o	k	n	R^2	$\sum Q^2$
	(lbf/100 ft ²)	(cp)		(lbf/100 ft ²) ²	(lbf/100 ft ²)	(lbf. s ⁿ /100 ft ²)			(lbf/100 ft ²) ²
0.0	9.64	8.00	0.9966	1.7547	9.25	0.0331	0.9046	0.9947	2.8112
0.5	16.36	8.90	0.9977	1.5315	15.55	0.0628	0.8303	0.9968	2.2210
1.5	17.75	9.40	0.9992	0.9089	16.93	0.0321	0.9349	0.7817	722.05
2.5	21.65	11.72	0.9995	2.3054	20.87	0.0378	0.9419	0.9995	1.8826

Table B- 7— Bingham Plastic and Herschel-Bulkley model constants fitted for the fluid containing 0.5 wt% of ferric oxide NPs at 120°F and different NP concentrations.

NP Concent. (wt%)	Bingham Plastic Model				Herschel-Bulkley Model				
	τ_o	μ_p	R^2	$\sum Q^2$	τ_o	k	n	R^2	$\sum Q^2$
	(lbf/100 ft ²)	(cp)		(lbf/100 ft ²) ²	(lbf/100 ft ²)	(lbf. s ⁿ /100 ft ²)			(lbf/100 ft ²) ²
0.0	10.41	7.08	0.9961	1.6661	10.28	0.0218	0.9450	0.9951	1.9551
0.5	18.55	7.29	0.9950	2.0324	17.63	0.0357	0.8855	0.9937	3.5443
1.5	19.39	8.99	0.9992	0.5874	19.39	0.0188	1.0002	0.7410	883.44
2.5	23.87	10.13	0.9998	0.8209	23.78	0.0257	0.9728	0.9998	0.9446

Table B- 8— Bingham Plastic and Herschel-Bulkley model constants fitted for the fluid containing 0.5 wt% of ferric oxide NPs at 140°F and different NP concentrations.

Temperature	Bingham Plastic Model				Herschel-Bulkley Model				
	τ_o	μ_p	R^2	$\sum Q^2$	τ_o	k	n	R^2	$\sum Q^2$
(°F)	(lbf/100 ft ²)	(cp)		(lbf/100 ft ²) ²	(lbf/100 ft ²)	(lbf. s ⁿ /100 ft ²)			(lbf/100 ft ²) ²
120	3.49	9.59	0.9934	5.0166	2.95	0.0627	0.8289	0.9984	1.1188
140	4.18	9.63	0.9933	4.6674	3.71	0.0718	0.8130	0.9975	2.0959
160	5.26	9.63	0.9929	5.4799	5.16	0.0489	0.8608	0.9974	2.2486
180	6.86	9.86	0.9924	6.0933	6.60	0.0343	0.9199	0.9951	3.8995
200	9.35	9.91	0.9959	4.5486	9.48	0.0177	1.0221	0.9956	5.1903

Table B- 9— Bingham Plastic and Herschel-Bulkley model constants fitted for the fluid containing 0.5 wt% of silica NPs at different temperatures.

Temperature	Apparent Viscosity (cp)			
	(°F)	1021.381 s ⁻¹	510.6905 s ⁻¹	340.4603 s ⁻¹
120	12.86	15.22	21.93	
140	11.72	11.34	11.15	
160	57.76	194.18	502.59	
180	30.55	42.26	67.23	
200	16.07	15.24	14.80	

Table B- 10—Apparent viscosity of the fluid containing 0.5 wt% of silica NPs at different temperatures and shear rates.

Shear rate	Shear Stress (lb/100 ft ²)				
	120°F	140°F	160°F	180°F	200°F
1021.38	22.52	23.77	24.23	26.70	30.49
510.69	13.71	14.45	15.52	17.37	20.12
340.46	10.83	11.94	12.91	14.79	17.09
170.23	7.80	8.39	9.29	10.86	12.88
102.14	6.06	6.86	7.80	9.02	11.03
51.07	4.49	5.15	6.16	7.17	9.43
10.21	2.47	2.99	4.14	5.33	7.87
5.11	3.20	4.28	5.36	6.96	9.57

Table B- 11—Rheograms of the fluid containing 0.5 wt% of silica NPs at different temperatures and shear rates.

Temperature	Bingham Plastic Model				Herschel-Bulkley Model				
	τ_o	μ_p	R^2	$\sum Q^2$	τ_o	k	n	R^2	$\sum Q^2$
	(°F)	(lb/100 ft ²)	(cp)	(lb/100 ft ²) ²	(lb/100 ft ²)	(lb. s ⁿ /100 ft ²)			(lb/100 ft ²) ²
120	3.99	17.76	0.9808	109.03	4.15	0.2586	0.7192	0.9991	2.6967
140	8.72	18.52	0.9779	57.991	4.89	0.47616	0.6356	0.9976	6.4152
160	7.69	16.29	0.9747	50.328	8.45	0.0631	0.8907	0.9827	27.033
180	10.21	26.71	0.9764	173.67	6.93	0.5559	0.6446	0.9986	6.8195
200	13.60	27.13	0.9824	131.78	11.84	0.3134	0.7315	0.9968	13.836

Table B- 12— Bingham Plastic and Herschel-Bulkley model constants fitted for the fluid containing 1.5 wt% of silica NPs at different temperatures.

Temperature	Apparent Viscosity (cp)			
	(°F)	1021.381 s ⁻¹	510.6905 s ⁻¹	340.4603 s ⁻¹
120		19.63	24.15	29.91
140		20.54	26.69	34.81
160		18.11	23.49	31.04
180		25.93	36.45	45.33
200		28.89	39.88	52.18

Table B- 13—Apparent viscosity of the fluid containing 1.5 wt% of silica NPs at different temperatures and shear rates.

Shear rate	Shear Stress (lb/100 ft ²)					
	(s ⁻¹)	120°F	140°F	160°F	180°F	200°F
1021.38		41.88	43.82	38.64	55.31	61.65
510.69		25.76	28.47	25.06	38.88	42.54
340.46		21.27	24.75	22.07	32.23	37.11
170.23		14.62	18.41	16.57	22.21	26.87
102.14		11.56	13.12	14.20	17.89	20.89
51.07		8.08	10.69	9.36	13.06	16.05
10.21		4.66	5.47	5.36	7.73	13.26
5.11		5.05	6.23	6.40	8.53	12.84

Table B- 14—Rheograms of the fluid containing 1.5 wt% of silica NPs at different temperatures and shear rates.

Temperature	Bingham Plastic Model				Herschel-Bulkley Model				
	τ_o	μ_p	R^2	$\sum Q^2$	τ_o	k	n	R^2	$\sum Q^2$
	(°F)	(lb/100 ft ²)	(cp)	(lb/100 ft ²) ²	(lb/100 ft ²)	(lb. s ⁿ /100 ft ²)			(lb/100 ft ²) ²
120	12.97	39.67	0.9825	255.05	6.64	0.76	0.6685	0.9988	12.533
140	13.06	39.42	0.9846	289.70	9.15	0.72	0.6665	0.9992	7.1081
160	18.99	37.77	0.9891	220.62	16.92	0.35	0.7628	0.9989	9.7751
180	24.68	37.44	0.9866	251.60	18.57	0.71	0.6611	0.9994	4.7979
200	29.45	35.58	0.9786	303.56	25.22	0.68	0.6558	0.9989	9.8033

Table B- 15— Bingham Plastic and Herschel-Bulkley model constants fitted for the fluid containing 2.5 wt% of silica NPs at different temperatures.

Temperature	Apparent Viscosity (cp)		
	(°F)	1021.381 s ⁻¹	510.6905 s ⁻¹
120	39.77	51.83	61.93
140	38.27	51.66	62.71
160	40.04	55.58	68.09
180	41.95	60.57	75.09
200	41.86	63.18	81.36

Table B- 16—Apparent viscosity of the fluid containing 2.5 wt% of silica NPs at different temperatures and shear rates.

Shear rate	Shear Stress (lb/100 ft ²)				
	(s ⁻¹)	120°F	140°F	160°F	180°F
1021.38	84.83	81.63	85.42	89.49	89.29
510.69	55.28	55.10	59.28	64.61	67.39
340.46	44.03	44.59	48.42	53.40	57.85
170.23	31.12	32.23	35.40	38.88	45.01
102.14	26.66	23.88	28.51	33.03	39.30
51.07	17.20	17.09	23.02	28.67	33.24
10.21	9.29	12.32	18.27	21.65	26.23
5.11	8.91	12.25	18.58	22.76	27.20

Table B- 17—Rheograms of the fluid containing 2.5 wt% of silica NPs at different temperatures and shear rates.

Temperature	Bingham Plastic Model				Herschel-Bulkley Model				
	τ_o	μ_p	R^2	$\sum Q^2$	τ_o	k	n	R^2	$\sum Q^2$
	(°F)	(lb/100 ft ²)	(cp)	(lb/100 ft ²) ²	(lb/100 ft ²)	(lb. s ⁿ /100 ft ²)			(lb/100 ft ²) ²
120	7.21	10.43	0.9947	6.4146	5.31	0.1010	0.7903	0.9985	1.4973
140	8.32	11.58	0.9893	14.278	6.16	0.1643	0.7226	0.9981	1.8480
160	9.01	12.77	0.9902	13.689	7.36	0.1693	0.7272	0.9990	1.5024
180	11.49	10.94	0.9932	6.8780	10.38	0.1411	0.7440	0.9959	5.8067
200	16.01	11.13	0.9921	9.8226	13.22	0.1959	0.7081	0.9975	3.6249

Table B- 18— Bingham Plastic and Herschel-Bulkley model constants fitted for the fluid containing 0.5 wt% of ferric oxide NPs + 0.5 wt% of silica NPs at different temperatures.

Temperature	Apparent Viscosity (cp)			
	(°F)	1021.381 s ⁻¹	510.6905 s ⁻¹	340.4603 s ⁻¹
120		13.80	17.53	21.67
140		14.39	19.39	19.39
160		15.84	21.21	26.88
180		16.33	21.87	21.87
200		18.60	26.14	34.95

Table B- 19—Apparent viscosity of the fluid containing 0.5 wt% of ferric oxide NPs + 0.5 wt% of silica NPs at different temperatures and shear rates.

Shear rate	Shear Stress (lb/100 ft ²)					
	(s ⁻¹)	120°F	140°F	160°F	180°F	200°F
1021.38		29.45	30.70	33.80	34.84	39.68
510.69		18.69	20.68	22.63	23.32	27.88
340.46		15.42	17.23	19.11	21.37	24.85
170.23		11.17	12.57	14.38	15.28	20.68
102.14		9.22	10.86	12.25	14.79	18.45
51.07		8.32	9.54	10.37	12.67	17.20
10.21		5.36	5.99	7.21	10.50	13.64
5.11		6.20	7.14	7.95	11.49	14.83

Table B- 20—Rheograms of the fluid containing 0.5 wt% of ferric oxide NPs + 0.5 wt% of silica NPs at different temperatures and shear rates.

Temperature	Bingham Plastic Model				Herschel-Bulkley Model				
	τ_o	μ_p	R^2	$\sum Q^2$	τ_o	k	n	R^2	$\sum Q^2$
(°F)	(lb/100 ft ²)	(cp)		(lb/100 ft ²) ²	(lb/100 ft ²)	(lb. s ⁿ /100 ft ²)			(lb/100 ft ²) ²
120	20.49	6.93	0.9959	1.6714	20.56	0.0112	1.0407	0.9969	1.4756
140	21.92	6.81	0.9912	3.3216	21.85	0.0317	0.8849	0.9858	6.2719
160	24.09	6.82	0.9977	0.9584	24.08	0.0159	0.9844	0.9973	1.1423
180	25.88	6.39	0.9959	1.2419	25.35	0.0302	0.8500	0.9955	13.528
200	27.19	6.33	0.9908	3.0319	26.52	0.0740	0.7513	0.3092	0.7672

Table B- 21— Bingham Plastic and Herschel-Bulkley model constants fitted for the fluid containing 0.5 wt% of ferric oxide NPs (using 15 min. ultrasonication) at different temperatures.

Temperature	Apparent Viscosity (cp)			
	(°F)	1021.381 s ⁻¹	510.6905 s ⁻¹	340.4603 s ⁻¹
120	16.73	25.29	35.74	
140	17.08	26.08	26.08	
160	18.11	28.75	40.63	
180	18.52	30.19	30.19	
200	18.75	30.22	44.84	

Table B- 22—Apparent viscosity of the fluid containing 0.5 wt% of ferric oxide NPs (using 15 min. ultrasonication) at different temperatures and shear rates.

Shear rate	Shear Stress (lb/100 ft ²)				
	120°F	140°F	160°F	180°F	200°F
1021.38	35.68	36.45	38.64	39.51	40.00
510.69	26.98	27.81	30.67	32.20	33.95
340.46	25.41	26.11	28.32	30.42	32.42
170.23	22.14	24.07	26.64	28.94	30.60
102.14	21.96	24.26	25.77	27.27	29.20
51.07	21.23	22.96	24.84	26.24	27.87
10.21	20.81	22.30	24.07	25.58	26.87
5.11	20.58	21.99	24.16	26.24	27.08

Table B- 23—Rheograms of the fluid containing 0.5 wt% of ferric oxide NPs (using 15 min. ultrasonication) at different temperatures and shear rates.

Temperature	Bingham Plastic Model				Herschel-Bulkley Model				
	τ_o	μ_p	R^2	$\sum Q^2$	τ_o	k	n	R^2	$\sum Q^2$
(°F)	(lb/100 ft ²)	(cp)		(lb/100 ft ²) ²	(lb/100 ft ²)	(lb. s ⁿ /100 ft ²)			(lb/100 ft ²) ²
120	19.67	22.48	0.9917	33.028	17.93	0.1673	0.8138	0.9977	10.375
140	25.53	22.05	0.9927	27.074	23.36	0.2099	0.7804	0.9985	6.4759
160	26.73	27.25	0.9968	12.143	24.74	0.1001	0.8910	0.9979	7.0505
180	27.80	12.54	0.9840	19.666	26.66	0.0849	0.8362	0.9825	20.808
200	16.43	12.04	0.9910	10.816	14.80	0.1132	0.7917	0.5201	6.0592

Table B- 24— Bingham Plastic and Herschel-Bulkley model constants for the base fluid at different temperatures measured after aging for 16 hours at 350°F.

Temperature	Apparent Viscosity (cp)			
	(°F)	1021.381 s ⁻¹	510.6905 s ⁻¹	340.4603 s ⁻¹
120		30.45	40.93	53.85
140		32.89	45.98	45.98
160		34.37	45.72	61.53
180		25.57	35.60	35.60
200		19.74	27.41	36.91

Table B- 25—Apparent viscosity of the base fluid at different temperatures and shear rates measured after aging for 16 hours at 350°F.

Shear rate	Shear Stress (lb/100 ft ²)					
	(s ⁻¹)	120°F	140°F	160°F	180°F	200°F
1021.38		64.95	70.18	73.31	54.55	42.12
510.69		43.65	49.05	48.77	37.98	29.24
340.46		38.29	43.93	43.76	38.81	26.25
170.23		28.40	34.32	34.50	32.89	20.78
102.14		25.34	31.12	31.75	31.29	20.75
51.07		22.07	27.88	28.72	29.14	17.72
10.21		16.26	22.87	24.44	26.32	14.34
5.11		18.34	24.19	27.64	26.98	15.73

Table B- 26—Rheograms of the base fluid at different temperatures and shear rates measured after aging for 16 hours at 350°F.

Temperature	Bingham Plastic Model				Herschel-Bulkley Model				
	τ_o	μ_p	R^2	$\sum Q^2$	τ_o	k	n	R^2	$\sum Q^2$
	(°F)	(lb/100 ft ²)	(cp)	(lb/100 ft ²) ²	(lb/100 ft ²)	(lb. s ⁿ /100 ft ²)			(lb/100 ft ²) ²
120	11.93	27.15	0.9810	120.31	16.56	0.01268	1.1792	0.9653	186.42
140	15.24	26.21	0.9839	90.95	13.89	0.14704	0.8491	0.9933	30.49
160	17.37	26.83	0.9884	70.99	17.06	0.08283	0.9281	0.9924	39.73
180	23.52	25.53	0.9809	95.62	26.92	0.03328	1.0417	0.9795	88.765
200	27.71	25.55	0.9878	66.72	27.46	0.12868	0.8603	0.9938	23.56

Table B- 27— Bingham Plastic and Herschel-Bulkley model constants for the fluid containing 0.5 wt% of ferric oxide NPs at different temperatures measured after aging for 16 hours at 350°F.

Temperature	Apparent Viscosity (cp)			
	(°F)	1021.381 s ⁻¹	510.6905 s ⁻¹	340.4603 s ⁻¹
120	28.75	38.35	49.00	
140	30.27	40.50	40.50	
160	32.10	43.11	55.76	
180	33.89	47.58	47.58	
200	36.08	51.53	68.93	

Table B- 28—Apparent viscosity of the fluid containing 0.5 wt% of ferric oxide NPs at different temperatures and shear rates measured after aging for 16 hours at 350°F.

Shear rate	Shear Stress (lb/100 ft ²)				
	(s ⁻¹)	120°F	140°F	160°F	180°F
1021.38	61.40	64.57	68.47	72.30	76.96
510.69	40.90	43.20	45.98	50.75	54.96
340.46	34.84	36.34	39.65	44.17	49.01
170.23	24.78	27.71	29.55	36.48	40.79
102.14	20.02	22.94	25.18	31.68	35.56
51.07	14.83	18.03	20.22	26.25	29.73
10.21	8.74	11.54	14.94	19.31	25.58
5.11	9.71	12.50	15.98	20.31	27.99

Table B- 29—Rheograms of the fluid containing 0.5 wt% of ferric oxide NPs at different temperatures and shear rates measured after aging for 16 hours at 350°F.

Temperature	Bingham Plastic Model				Herschel-Bulkley Model				
	τ_o	μ_p	R^2	$\sum Q^2$	τ_o	k	n	R^2	$\sum Q^2$
	(°F)	(lb/100 ft ²)	(cp)	(lb/100 ft ²) ²	(lb/100 ft ²)	(lb. s ⁿ /100 ft ²)			(lb/100 ft ²) ²
120	10.12	34.08	0.9827	177.78	14.51	0.09613	0.9243	0.9881	185.71
140	14.75	32.58	0.9938	75.97	10.91	0.30332	0.7771	0.9995	3.55
160	18.54	27.25	0.9975	16.22	18.30	0.08893	0.9383	0.9985	9.63
180	20.64	27.25	0.9968	24.91	20.46	0.06018	0.9924	0.9967	23.86
200	21.97	27.04	0.9943	41.49	19.57	0.17674	0.8412	1.5628	7.71

Table B- 30— Bingham Plastic and Herschel-Bulkley model constants for fluid containing 0.5 wt% of Silica NPs at different temperatures measured after aging for 16 hours at 350°F.

Temperature	Apparent Viscosity (cp)			
	(°F)	1021.381 s ⁻¹	510.6905 s ⁻¹	340.4603 s ⁻¹
120		34.04	43.57	53.85
140		36.13	46.41	46.41
160		36.36	48.20	58.01
180		36.93	50.09	50.09
200		37.34	50.65	63.29

Table B- 31—Apparent viscosity of the fluid containing 0.5 wt% of ferric oxide NPs at different temperatures and shear rates measured after aging for 16 hours at 350°F.

Shear rate	Shear Stress (lb/100 ft ²)					
	(s ⁻¹)	120°F	140°F	160°F	180°F	200°F
1021.38		72.61	77.07	77.55	78.77	79.64
510.69		46.47	49.50	51.41	53.43	54.02
340.46		37.29	38.74	41.25	43.16	45.01
170.23		25.14	26.80	28.68	30.60	32.41
102.14		21.38	22.94	25.24	25.81	26.35
51.07		13.75	18.03	20.81	23.05	24.90
10.21		6.44	11.54	19.07	20.58	21.38
5.11		5.88	12.50	18.85	20.94	18.71

Table B- 32—Rheograms (shear stress versus shear rate) of the fluid containing 0.5 wt% of ferric oxide NPs at different temperatures and shear rates measured after aging for 16 hours at 350°F.

APPENDIX C

DETAILED FLUID LOSS RESULTS OF NPS/CA-BENTONITE
SUSPENSIONS

Introduction

The purpose of this appendix is to present the detailed results of the filter press measurement of the fluid loss volumes as a function of time for the data in chapter III. The measurements of the NPs/Ca-bentonite suspensions were investigated using an OFITE HP/HT filter press (**Fig. II-10**). The setup includes a 500 ml cell which was modified to use 2.5-in. in diameter and 1-in. in thickness cores instead of filter papers, cell caps, valve stems, heating element, and a nitrogen-gas line. The suspensions were put in the cell, and the cell was then put in the heating jacket. A differential pressure from 300 to 500 psi and a temperature range of 175 to 250°F were used. Furthermore, the fluid loss volume was measured as a function of time for 30 minutes, as per API standards.

Time (min)	Cumulative Filtrate Volume (ml)						
	Base (1)	Base (2)	Base (3)	0.3 wt% Ferric Oxide NPs	0.5 wt% Ferric Oxide NPs	1.5 wt% Ferric Oxide NPs	2.5 wt% Ferric Oxide NPs
1	7.2	8.3	8.2	1.65	1.4	2.75	4.2
2	7.6	8.5	8.4	1.7	1.6	2.8	4.6
3	8	8.7	8.6	1.8	2	3.3	4.8
4	8.2	8.9	8.8	1.85	2.4	3.7	6
5	8.5	9.1	9	1.9	3.6	4	6.3
6	8.7	9.3	9.1	2	4	4.5	6.7
7	9	9.5	9.3	2.1	4.2	5	6.9
8	9.2	9.7	9.5	2.2	4.4	5.5	7
9	9.4	9.8	9.7	2.3	4.6	6	7.4
10	9.6	9.9	9.9	2.4	4.8	6.3	7.6
11	9.8	10.1	10	2.6	5	6.5	7.8
12	10	10.2	10.1	2.8	5.15	6.7	8.1
13	10.1	10.3	10.2	3	5.25	6.8	8.4
14	10.2	10.4	10.3	3.5	5.35	7	8.8
15	10.4	10.5	10.4	4.4	5.5	7.1	9
16	10.6	10.6	10.5	5	5.7	7.2	9.4
17	10.8	10.7	10.6	5.8	5.8	7.4	9.8
18	10.9	10.8	10.7	6	5.9	7.6	10.2
19	11	10.9	10.8	6.2	6	7.8	10.4
20	11.1	11	10.9	7.2	6.1	8	10.6
21	11.2	11.1	11	7.5	6.2	8.1	10.8
22	11.25	11.2	11.1	8	6.3	8.2	11
23	11.35	11.3	11.2	8.5	6.4	8.3	11.4
24	11.45	11.4	11.3	9	6.5	8.4	11.6
25	11.55	11.5	11.4	9.3	6.6	8.5	11.8
26	11.6	11.6	11.5	9.5	6.7	8.6	11.8
27	11.7	11.7	11.6	9.7	6.75	8.7	11.8
28	11.8	11.8	11.7	9.8	6.8	8.8	11.8
29	11.9	11.9	11.8	9.9	6.85	8.9	11.8
30	12	12	11.9	10	6.9	9	11.9

Table C- 1—Detailed fluid loss volumes for the base fluid and samples containing different concentrations of ferric oxide NPs at 250°F and 300 psi.

Time (min)	Cumulative Filtrate Volume (ml) - 0.5 wt% Ferric Oxide NPs						
	175°F, 300 psi	200°F, 300 psi	250°F, 300 psi	300°F, 300 psi	250°F, 200 psi	250°F, 400 psi	350°F, 500 psi
1	6.2	3	1.4	3.3	5.3	2.5	2
2	6.6	3.2	1.6	3.4	5.33	3.2	2.2
3	7.2	3.8	2	3.5	5.37	3.3	2.24
4	7.4	3.9	2.4	3.55	5.4	3.5	2.28
5	7.7	4	3.6	3.6	5.48	3.7	2.3
6	8	4.1	4	4	5.55	4	2.32
7	8.2	4.2	4.2	4.4	5.6	4.6	2.35
8	8.7	4.5	4.4	4.8	6.6	5.2	2.37
9	9	4.8	4.6	5	7.5	5.5	2.39
10	9.2	5.2	4.8	5.3	7.8	5.9	2.4
11	9.4	5.6	5	5.6	8.1	6.4	2.42
12	9.5	5.9	5.15	6	8.8	6.6	2.44
13	9.6	6	5.25	6	9.3	6.7	2.46
14	9.7	6.4	5.35	6	9.5	7.2	2.48
15	9.9	6.5	5.5	6	9.65	7.6	2.5
16	10.1	6.7	5.7	6	9.8	8.2	2.6
17	10.3	6.9	5.8	6	9.9	8.3	2.7
18	10.4	7.1	5.9	6	10	8.3	2.75
19	10.5	7.4	6	6	10.4	8.4	2.8
20	10.7	7.7	6.1	6	10.6	8.4	2.85
21	10.9	8	6.2	6	10.8	8.5	2.87
22	11.1	8.3	6.3	6	11	8.5	2.89
23	11.3	8.5	6.4	6	11.2	8.6	2.94
24	11.5	8.8	6.5	6	11.6	8.7	2.97
25	11.6	9	6.6	6	12	8.8	3
26	11.8	9.3	6.7	6	12.2	8.9	3.1
27	12.1	9.7	6.75	6.2	12.5	9	3.15
28	12.2	10.4	6.8	6.27	12.7	9.1	3.2
29	12.3	11	6.85	6.35	12.9	9.4	3.25
30	12.4	11.8	6.9	6.4	13	9.6	3.3

Table C- 2— Detailed fluid loss volumes for the samples containing 0.5 wt% of ferric oxide NPs at a different pressures and temperatures.

Time (min)	Cumulative Filtrate Volume (ml)						
	0.5 wt% Silica NPs	1.5 wt% Silica NPs	2.5 wt% Silica NPs	0.5 wt% Fe ₃ O ₄ NPs	1.5 wt% Fe ₃ O ₄ NPs	2.5 wt% Fe ₃ O ₄ NPs	0.5 wt% Zinc Oxide NPs
1	3.5	3.4	3.8	2	2	1.7	4
2	3.6	4.8	5	2.3	2.4	2.4	4.3
3	4	5.8	6.3	2.9	3	2.9	4.4
4	4.4	6.6	7.2	3.3	3.5	3.3	4.6
5	4.8	7.5	7.9	3.8	4	3.9	4.8
6	5	8.3	8.4	4.2	4.5	4.5	5.1
7	5.6	9.1	8.6	4.8	4.9	5.1	6
8	6.2	9.8	8.9	5.2	5.3	5.6	6.4
9	6.6	10.3	9.1	5.5	5.8	5.9	7
10	7	11	9.3	5.9	6.1	6.1	8
11	8	11.6	9.4	6.2	6.3	6.3	8.9
12	8.8	12.1	9.5	6.4	6.4	6.4	9
13	9.5	12.4	9.6	6.7	6.5	6.5	9.05
14	10.2	13.1	9.7	6.9	6.7	6.8	9.4
15	11.1	13.4	9.8	7.2	6.85	6.9	10
16	11.6	13.8	9.9	7.4	7	7	10.5
17	11.9	14.3	10	7.6	7.1	7.2	11.4
18	12.4	14.9	10.1	7.8	7.3	7.3	11.5
19	12.6	15.3	10.3	7.9	7.4	7.4	11.6
20	12.8	15.5	10.5	8.05	7.5	7.6	11.8
21	13	16	10.6	8.2	7.7	7.8	12
22	13.1	16.4	10.7	8.35	7.8	8	12.1
23	13.2	16.7	10.8	8.5	7.9	8.1	12.3
24	13.3	17	10.9	8.6	8.05	8.2	12.5
25	13.4	17.4	10.95	8.75	8.3	8.3	12.6
26	13.5	17.7	11	8.85	8.45	8.5	12.7
27	13.6	18.1	11.05	8.95	8.6	8.6	12.8
28	13.6	18.3	11.1	9.05	8.7	8.7	12.9
29	13.6	18.6	11.2	9.15	8.8	8.8	13.1
30	13.6	18.9	11.3	9.25	9	9	13.2

Table C- 3— Detailed fluid loss volumes for the samples containing silica, magnetic iron oxide, and zinc oxide NPs at 250°F and 300 psi.

Time (min)	Cumulative Filtrate Volume (ml)						
	Base (4) (Dyn., 100 rpm)	Base (5) (Dyn., 100 rpm)	0.5 wt% Ferric Oxide NPs (Dyn., 100 rpm)	Base (6) (15 min Ultrasonic.)	Base (7) (15 min Ultrasonic.)	0.5 wt% Ferric Oxide NPs (15 min Ultrasonic.)	0.5 wt% Silica NPs (15 min Ultrasonic.)
1	3.2	3.3	2	1.75	3.8	2.3	5.2
2	4	4.4	3.5	2.4	4.2	2.35	5.3
3	5.2	5.2	5.1	3	4.8	2.4	5.7
4	6.3	5.9	5.2	3.8	5	2.5	6.2
5	7	6.4	5.4	4.9	5.1	3.2	6.8
6	7.5	6.8	6.5	6.2	5.8	3.22	7.3
7	7.7	7.3	7	6.9	6.6	3.25	7.6
8	7.9	7.6	7.2	7.15	6.9	3.28	8.4
9	8	7.85	7.3	7.2	7.1	3.3	9
10	8.1	8.1	7.4	7.4	7.3	3.35	10
11	8.2	8.35	7.45	7.5	7.6	3.4	10.8
12	8.3	8.55	7.5	7.6	7.65	3.4	11.3
13	8.45	8.75	7.55	7.75	7.7	3.45	11.4
14	8.5	8.9	7.6	7.85	8.4	3.45	11.5
15	8.55	9	8.2	8	8.4	3.5	11.6
16	8.65	9.1	9.2	8.15	8.4	3.5	11.8
17	8.75	9.2	10	8.25	8.6	3.55	12.2
18	8.9	9.3	10.15	8.35	8.7	3.55	12.5
19	9.1	9.4	10.3	8.45	9	3.55	12.8
20	9.2	9.5	10.4	8.55	9.1	3.6	13.2
21	9.3	9.6	10.7	8.65	9.2	3.6	13.3
22	9.4	9.75	10.9	8.75	9.3	3.6	13.5
23	9.45	9.85	11	8.85	9.4	3.6	13.8
24	9.55	9.9	11.2	9	9.5	3.65	14.5
25	9.65	10.05	11.5	9.05	9.6	3.65	14.6
26	9.75	10.15	11.7	9.15	9.6	3.65	14.7
27	9.85	10.2	11.8	9.2	9.6	3.65	14.7
28	9.9	10.3	12	9.25	9.7	3.65	14.7
29	10	10.35	12.2	9.3	9.8	3.7	14.7
30	10.1	10.4	12.4	9.5	10	3.7	15

Table C- 4— Detailed fluid loss volumes for the base fluid and samples containing 0.5 wt% of ferric oxide and silica NPs at 250°F and 300 psi when using dynamic filtration (100 rpm) or ultrasonication for 15 minutes while preparation.

APPENDIX D

DETAILED FLUID LOSS RESULTS OF FULLY FORMULATED

DRILLING FLUID

Introduction

The purpose of this appendix is to present the detailed results of the filter press measurement of the fluid loss volumes as a function of time for the data in chapter IV. The measurements of the Ca-bentonite based drilling fluid (fully formulated) were investigated using an OFITE HP/HT filter press (**Fig. II-10**). The setup includes a 500 ml cell which was modified to use 2.5-in. in diameter and 1-in. in thickness cores instead of filter papers, cell caps, valve stems, heating element, and a nitrogen-gas line. The drilling fluids were put in the cell, and the cell was then put in the heating jacket. A differential pressure from 300 to 500 psi and a temperature range of 175 to 250°F were used. Furthermore, the fluid loss volume was measured as a function of time for 30 minutes, as per API standards.

Time (min)	Cumulative Filtrate Volume (ml)			
	Base (1)	0.3 wt% Ferric Oxide NPs	0.5 wt% Ferric Oxide NPs	1.5 wt% Ferric Oxide NPs
1	2.35	2.4	3.8	3.7
2	2.85	2.5	3.9	4
3	3.5	2.8	4.5	4.6
4	3.8	3	4.8	4.7
5	4	3.05	4.9	4.8
6	4.15	3.1	5	5
7	4.65	3.2	5	5.2
8	4.75	3.4	5.05	5.4
9	4.85	3.6	5.1	5.6
10	5	3.8	5.2	5.8
11	5.15	3.9	5.3	6.2
12	5.25	4	5.5	6.6
13	5.4	4.4	5.55	6.8
14	5.55	4.6	5.6	6.9
15	5.7	4.7	5.7	7
16	6.2	4.75	5.9	7.2
17	6.3	4.8	6	7.4
18	6.35	4.9	6.1	7.5
19	6.35	5.1	6.2	7.6
20	6.4	5.3	6.3	7.7
21	6.4	5.4	6.4	7.8
22	6.6	5.5	6.5	8
23	6.7	5.6	6.6	8.1
24	6.9	5.7	6.7	8.2
25	7.3	5.85	6.8	8.3
26	7.35	6	6.9	8.4
27	7.4	6.1	7	8.5
28	7.45	6.2	7.1	8.6
29	7.55	6.3	7.2	8.7
30	7.77	6.4	7.4	8.9

Table D- 1—Detailed fluid loss volumes for the Ca-bentonite-based drilling fluid and fluids containing different concentrations of ferric oxide NPs at 250°F and 300 psi (No hydration, 1 hour of ultrasonication, and static filtration).

Time (min)	Cumulative Filtrate Volume (ml) - 0.5 wt% Ferric Oxide NPs						
	200°F, 300 psi	250°F, 300 psi	300°F, 300 psi	350°F, 300 psi	250°F, 200 psi	250°F, 400 psi	350°F, 500 psi
1	3.7	3.8	3.8	4.9	6.2	5.9	3.1
2	4	3.9	4.3	5.5	6.4	6	3.4
3	4.3	4.5	4.8	5.8	6.7	6.2	3.5
4	4.5	4.8	5	6	7	6.6	3.6
5	5	4.9	5.2	6.1	7.2	6.8	3.7
6	5.1	5	5.6	6.2	7.3	6.9	3.8
7	5.2	5	5.9	6.3	7.4	7	4
8	5.3	5.05	6.2	6.4	7.5	7.1	4.2
9	5.4	5.1	6.3	6.5	7.65	7.6	4.4
10	5.6	5.2	6.5	6.6	7.8	7.7	4.5
11	5.8	5.3	6.6	6.7	7.9	7.8	4.6
12	6	5.5	6.7	6.8	8.05	7.9	4.8
13	6.1	5.55	6.75	7	8.2	8	5
14	6.2	5.6	7	7.1	8.3	8.2	5.1
15	6.3	5.7	7.1	7.2	8.4	8.3	5.2
16	6.5	5.9	7.25	7.3	8.5	8.4	5.3
17	7	6	7.4	7.4	8.6	8.5	5.5
18	7.2	6.1	7.45	7.5	8.8	8.6	5.6
19	7.4	6.2	7.6	7.6	8.9	8.7	5.7
20	7.5	6.3	7.65	7.7	9	8.8	5.8
21	7.6	6.4	7.7	7.8	9.1	8.85	5.9
22	7.8	6.5	7.8	7.9	9.2	8.9	6
23	8	6.6	7.95	8	9.3	9	6.1
24	8.1	6.7	8	8.1	9.4	9.05	6.2
25	8.2	6.8	8.1	8.2	9.5	9.1	6.4
26	8.3	6.9	8.2	8.3	9.6	9.2	6.5
27	8.4	7	8.3	8.4	9.7	9.3	6.6
28	8.6	7.1	8.4	8.5	9.75	9.4	6.7
29	8.8	7.2	8.45	8.6	9.8	9.45	6.8
30	9	7.4	8.6	8.7	9.9	9.5	6.9

Table D- 2— Detailed fluid loss volumes for the Ca-bentonite-based drilling fluid containing 0.5 wt% of ferric oxide NPs at different pressures and temperatures (No hydration, 1 hour of ultrasonication, and static filtration).

Time (min)	Cumulative Filtrate Volume (ml)			
	Base (No Ultrasonic.)	0.5 wt% Ferric Oxide NPs (No Ultrasonic.)	0.5 wt% Ferric Oxide NPs (30 min. Ultrasonic.)	0.5 wt% Ferric Oxide NPs (60 min Ultrasonic.)
1	2.35	2.5	3.5	3.8
2	2.85	3.1	4	3.9
3	3.5	3.3	4.4	4.5
4	3.8	3.5	4.7	4.8
5	4	4	5	4.9
6	4.15	4.6	5.3	5
7	4.65	4.8	5.7	5
8	4.75	5	6	5.05
9	4.85	5.3	6.2	5.1
10	5	5.6	6.4	5.2
11	5.15	5.9	6.6	5.3
12	5.25	6.2	6.8	5.5
13	5.4	6.3	7	5.55
14	5.55	6.4	7.2	5.6
15	5.7	6.5	7.4	5.7
16	6.2	6.6	7.6	5.9
17	6.3	6.8	7.8	6
18	6.35	7	8	6.1
19	6.35	7.1	8.1	6.2
20	6.4	7.3	8.2	6.3
21	6.4	7.5	8.3	6.4
22	6.6	7.7	8.4	6.5
23	6.7	7.8	8.5	6.6
24	6.9	7.9	8.6	6.7
25	7.3	8	8.7	6.8
26	7.35	8.1	8.8	6.9
27	7.4	8.2	8.9	7
28	7.45	8.3	9	7.1
29	7.55	8.4	9.05	7.2
30	7.77	8.45	9.1	7.4

Table D- 3— Detailed fluid loss volumes for the Ca-bentonite-based drilling fluid containing no NPs and 0.5 wt % of ferric oxide NPs at 250°F and 300 psi using different ultrasonication times while preparation (No hydration and static filtration).

Time (min)	Cumulative Filtrate Volume (ml)					
	Base (3) (No Hyd., No Ultrasonic., Static filtration)	Base (4) (16 hrs Hyd., No Ultrasonic., Static filtration)	Base (5) (No Hyd., No Ultrasonic., Dyn.100 rpm)	0.5 wt% Ferric Oxide NPs (No Hyd., No Ultrasonic., Static filtration)	0.5 wt% Ferric Oxide NPs (16 hrs Hyd., No Ultrasonic., Static filtration)	0.5 wt% Ferric Oxide NPs (No Hyd., No Ultrasonic., Dyn. 100 rpm)
1	1.6	2.5	3.7	2.2	1.95	4.2
2	2	3	4.2	3.1	2.15	4.5
3	2.2	3.25	4.9	3.5	2.25	5.2
4	2.4	3.5	5.2	3.9	2.4	5.3
5	2.6	3.9	5.7	4.3	2.6	5.4
6	2.8	4.2	6.15	4.6	2.75	5.7
7	3	4.45	6.7	4.9	2.9	5.9
8	3.2	4.7	6.8	5.1	3.15	6.4
9	3.4	5.05	7	5.3	3.3	6.5
10	3.5	5.2	7.5	5.6	3.45	6.7
11	3.7	5.4	8.1	5.9	3.7	6.8
12	3.85	5.6	8.3	6	4	7.2
13	4	5.8	8.4	6.1	4.2	7.3
14	4.3	6	8.6	6.2	4.4	7.4
15	4.3	6.2	8.7	6.35	4.6	7.5
16	4.7	6.35	9	6.55	4.9	7.6
17	4.85	6.5	9.3	6.75	5.05	7.7
18	5.15	6.7	9.5	7	5.2	7.8
19	5.4	6.9	9.7	7.15	5.35	7.9
20	5.75	7.05	9.8	7.4	5.5	8
21	5.85	7.15	9.9	7.75	5.7	8.1
22	5.9	7.3	10.5	7.85	5.9	8.3
23	6	7.5	11	8	6.1	8.4
24	6.1	7.6	11.5	8.15	6.25	8.6
25	6.2	7.75	11.7	8.3	6.4	8.7
26	6.4	7.9	11.9	8.4	6.55	8.8
27	6.5	8.08	12.1	8.5	6.7	8.9
28	6.7	8.2	12.3	8.6	6.85	9
29	6.85	8.3	12.5	8.7	7	9.15
30	7	8.4	12.7	8.9	7.15	9.3

Table D- 4— Detailed fluid loss volumes for the Ca-bentonite-based drilling fluid and fluids containing 0.5 wt% of ferric oxide at 250°F and 500 psi when using 16 hours of hydration while preparation or dynamic filtration (100 rpm).